STUDY OF CHEMICAL COMPOSITION, STRUCTURAL AND THERMOELECTRIC PROPERTIES OF FLEXIBLE Bi-Te THIN FILMS DEPOSITED BY MAGNETRON SPUTTERING TECHNIQUE

PILAIPON NUTHONGKUM

A THESIS SUBMITTED IN PARTIAL FULFILLMENT OF THE REQUIREMENT FOR
THE DEGREE OF DOCTOR OF PHILOSOPHY IN APPLIED PHYSICS
DEPARTMENT OF PHYSICS FACULTY OF SCIENCE
KING MONGKUT'S INSTITUTE OF TECHNOLOGY LADKRABANG
2019

KMITL-2019-SC-D-030-063

STUDY OF CHEMICAL COMPOSITION, STRUCTURAL AND THERMOELECTRIC PROPERTIES OF FLEXIBLE Bi-Te THIN FILMS DEPOSITED BY MAGNETRON SPUTTERING TECHNIQUE

การศึกษาองค์ประกอบทางเคมี โครงสร้าง และสมบัติเทอร์โมอิเล็กทริกของฟิล์มบางบิสมัสเทลลูไรด์บิดงอได้เคลือบโดยเทคนิคแมกนีตรอนสปัตเตอริง

PILAIPON NUTHONGKUM
พิไลพร หนูทองคำ

วิทยานิพนธ์นี้เป็นส่วนหนึ่งของการศึกษาตามหลักสูตร
ปรัชญาดุษฎีบัณฑิต สาขาวิชาฟิสิกส์ประยุกต์
ภาควิชาฟิสิกส์ คณะวิทยาศาสตร์
สถาบันเทคโนโลยีพระจอมเกล้าเจ้าคุณทหารลาดกระบัง
พ.ศ. 2562

KMITL-2019-SC-D-030-063

หัวข้อวิทยานิพนธ์	การศึกษาองค์ประกอบทางเคมี โครงสร้าง และสมบัติเทอร์โมอิเล็กทริกของฟิล์มบางบิสมัสเทลลูไรด์บิดงอได้เคลือบโดยเทคนิคแมกนีตรอนสปัตเตอริง
ชื่อนักศึกษา	พิไลพร หนูทองคำ
รหัสประจำตัว	58605015
ปริญญา	ปรัชญาดุษฎีบัณฑิต (ฟิสิกส์ประยุกต์)
ภาควิชา	ฟิสิกส์
คณะ	วิทยาศาสตร์
พ.ศ.	2562
อาจารย์ที่ปรึกษาวิทยานิพนธ์	ผู้ช่วยศาสตราจารย์ ดร.อาภาภรณ์ สกุลการะเวก

บทคัดย่อ

วิทยานิพนธ์ฉบับนี้ ได้เตรียมฟิล์มบางบิสมัสเทลลูไรด์แบบบิดงอได้ ด้วยเทคนิคแมกนีตรอนสปัตเตอริง โดยใช้เป้าสปัตเตอร์ริง (sputtering target) เป็นบิสมัสเทลลูไรด์ (Bi_2Te_3) โดยใช้พอลิไอมายด์ (polyimide) เป็นวัสดุฐานรอง วัตถุประสงค์ของวิทยานิพนธ์นี้คือเพื่อทำความเข้าใจกับปัจจัยที่ส่งผลกระทบต่อกระบวนการสปัตเตอร์ริงที่สำคัญต่อกระบวนการสปัตเตอร์ริง ได้แก่ อัตราการไหลของก๊าซ Ar หรือความดันสปัตเตอร์ริง (sputtering pressures) การให้อุณหภูมิแก่วัสดุฐานรองก่อนการสปัตเตอร์ริง (pre-heating temperature) และอุณหภูมิการอบ (annealing temperature) ซึ่งส่งผลต่อสมบัติเทอร์โมอิเล็กทริกของฟิล์มบางบิสมัสเทลลูไรด์ จากนั้นทำการวิเคราะห์องค์ประกอบทางเคมีของฟิล์มบางด้วยเครื่องวิเคราะห์ธาตุเชิงพลังงาน (EDS) การวิเคราะห์โครงสร้างผลึกและสัณฐานวิทยาพื้นผิวของฟิล์มบางได้วิเคราะห์ด้วยการเลี้ยวเบนของรังสีเอกซ์ (XRD) และศึกษาลักษณะทางสัณฐานวิทยาด้วยกล้องจุลทรรศน์อิเล็กตรอนแบบส่องกราด (FE-SEM) ตามลำดับ คุณสมบัติทางไฟฟ้ารวมถึงความเข้มข้นของตัวพาและความคล่องตัวนั้นวัดด้วยวิธีการวัดปรากฏการณ์ฮอลล์ (Hall effect measurements) สัมประสิทธิ์ซีเบคและค่าการนำไฟฟ้าถูกวัดพร้อมกันด้วยเครื่อง ZEM-3 จากการศึกษาพบว่าความดันสปัตเตอร์ริงส่งผลต่อองค์ประกอบทางเคมีและโครงสร้างผลึกของฟิล์มบาง Bi-Te กระบวนการหลอมส่งผลให้ฟิล์มบาง Bi-Te มีอัตราส่วน Bi:Te เท่ากับ 2:3 และช่วยปรับปรุงคุณภาพผลึกให้ดีขึ้น แต่จากผลการทดลองความเป็นผลึกของฟิล์มที่ได้ต่ำ ซึ่งส่งผลให้ฟิล์มที่ได้มีสมบัติเทอร์โมอิเล็กทริกที่ต่ำไปด้วย และสุดท้ายการให้อุณหภูมิแก่วัสดุฐานรองก่อนการสปัตเตอร์ริงส่งผลกระทบอย่างมีนัยสำคัญต่อองค์ประกอบทางเคมีของฟิล์มบาง Bi-Te นอกจากนี้ยังพบว่าความเป็นผลึกของฟิล์มได้รับการปรับปรุงดีที่สุดเมื่อใช้เทคนิคดีซีแมกนีตรอนสปัตเตอร์ริง (DC magnetron sputtering technique) ซึ่งให้ค่าสมบัติเทอร์โมอิเล็กทริกดี

ที่สุดเท่ากับ3.5×10^{-3} W / m.K^2 ที่ความดันสปัตเตอร์ริงที่ 1.4 Pa และให้อุณหภูมิแก่วัสดุฐานรองก่อนการสปัตเตอร์ริงที่ 285 °C

คำสำคัญ : ฟิล์มบางบิดงอได้, แมกนีตรอนสปัตเตอริง, สมบัติเทอร์โมอิเล็กทริก

Thesis Title	Study of chemical composition, structural and thermoelectric properties of flexible Bi-Te thin films deposited by magnetron sputtering technique
Student Name	Pilaipon Nuthongkum
Student ID	58605015
Degree	Doctor of Philosophy (Applied Physics)
Department	Physics
Faculty	Science
Year	2019
Thesis Advisor	Asst. Prof. Dr. Aparporn Sakulkalavek

Abstract

In this thesis, flexible Bi_xTe_y thin films were prepared by RF magnetron sputtering using a Bi_2Te_3 target on polyimide substrate. The purpose of this thesis is to understand the key parameters of maximizing thermoelectric power factor in Bi-Te thin films by an in-depth investigating on the chemical composition, structural and thermoelectric properties of thin films. Study of the effects of sputtering parameters, including the Ar gas flow rate (sputtering pressures) and pre-heating temperature and the annealing temperature on chemical composition of [Bi]:[Te]. The [Bi]:[Te] ratio of thin film was determined by energy dispersive spectrometry (EDS). The characterization of the crystal structure and surface morphology of thin film was analyzed by x-ray diffraction (XRD) and a field emission scanning electron microscope (FE-SEM), respectively. Electrical transport properties, including carrier concentration and mobility, were measured by Hall effect measurements. Seebeck coefficients and electrical conductivities were simultaneously measured by a direct current (DC) four-terminal method (ZEM-3). It was found that the effects of various sputtering pressures were significant for controlling compositions and improving thermoelectric properties of Bi-Te thin films. Annealing process, it was indicated that the crystalline quality of the films was enhanced after annealing but the crystalline size of the thin film is of little value, which affects to decrease thermoelectric properties. And it was found that the pre-heat treatment significantly affected the composition of thin films. In addition,

it was shown that crystallinity was enhanced in the DC sputtered coatings at a high pre-heating temperature. The highest power factor of 3.5×10^{-3} W/m.K^2 at 285°C.

Keywords: Flexible thin films, Magnetron sputtering, Thermoelectric properties

Acknowledgements

First and foremost, I would like to express my sincere appreciation to my advisor Asst. Prof. Dr. Aparporn Sakulkalavek for her guidance and encouragement throughout my research. I would like to thank Asst. Prof. Dr. Rachsak Sakdanupha for his research instruments and suggestion for the improvement of this study.

Special thanks to Asst.Prof. Dr. Chittra Kedkaew, Assoc.Prof. Dr. Wisanu Pecharapa, Assoc.Prof. Dr. Chesta Ruttanapun, and Asst.Prof. Dr. Prathan Buranasiri, for kindly serving as my thesis committee and providing valuable suggestions that improved the quality of this study.

Special thanks to Professor Dr. Pichet Limsuwan who helps comments and proofreading several chapters of this manuscript.

I would like to thank the lab group members and all those helped me to stay focused on completing the thesis and who have provided me with the encouragement to continue when the going got tough.

I am grateful to my parents for their support throughout my education and their love and care. Finally, special thanks are due to Rajabhat Rajanagarindra University for their financial support and sponsorship.

Pilaipon Nuthongkum

Table of Contents

Page

Page

List of Tables

List of Figures

Page

Page

Chapter 1
Introduction

1.1 Research Motivation

Thermoelectric generator (TEG) is proposed as a solid-state energy harvester from waste heat sources. TEG produces the electrical power from a temperature difference applied across the device. Over the last decade, the human body has been considered as a heat source for the wearable TEGs. It may become an attraction for an alternative power generation technique. The energy conversion of wearable TEGs has been demonstrated in order of microwatt range or less. The amount of generator electrical power being produced from TEG depends on material properties (ZT) and a temperature difference between two sides of the module. The thermoelectric figure of merit (ZT), used to characterize the performance of a thermoelectric material, is defined as $ZT = S^2\sigma T/\kappa$, where S is the Seebeck coefficient, σ is electrical conductivity, κ is thermal conductivity and T is temperature. A large value of ZT means higher thermoelectric conversion efficiency, which requires a high power factor ($P = S^2\sigma$) along with low thermal conductivity [2]. The usefulness of thermoelectric material is determined by the two factors device efficiency and power factor.

Bismuth telluride (Bi_2Te_3) is one of the most interesting thermoelectric materials that have been used widely due to high ZT value, and high performance at room temperature. The ZT value can be made to increase when improvements are made to low-dimensional materials due to the influences of quantum confinement effect and phonon scattering on nanostructured materials [3,4]. The thin film is one of low dimensional materials. In addition, thin film thermoelectric devices provide the possibility of using flexible substrates and can be applied to diverse fields [5].

Bi_2Te_3 thin films have been prepared using different deposition methods, such as magnetron sputtering [3,4,13,14,15], co-evaporation [9,10] and pulsed laser deposition [11,12]. Magnetron sputtering method was selected due to the possibility of large-scale fabrication of high-quality films. The good thermoelectric properties of Bi_2Te_3 thin films must have a stoichiometric composition. However, it was difficult to control the stoichiometry of Bi-Te films by magnetron sputtering technique because tellurium (Te) exhibits lower sputtering yield than bismuth (Bi), therefore it is difficult

to obtain stoichiometric Bi_2Te_3 thin films. Most of the research works have been used co- sputtering and adjusted sputtering powers of Bi and Te targets to control compositions [4-7]. Only fill a small number of works on the control ratio of [Bi] and [Te] using a Bi_2Te_3 target have been reported. In this work, Bi-Te thin films were deposited using a Bi_2Te_3 target by RF and DC magnetron sputtering methods.

Sputtering process can be operated by RF or DC power supplies depends on the electrical conductivity of the target materials. The uses of DC power supplies in plasma systems sputtering requires electrically conductive target materials while RF power supplies can be used for both conductive and non-conductive target materials [13]. Bi_2Te_3 target is conductive materials (semiconductor materials), which can be sputtered with DC and RF power supplies.

The stoichiometry of Bi_2Te_3 thin films can be prepared by controlling various sputtering parameters, such as post-annealing process [3,4,14,15], working pressure [11,13], temperature of substrate [11,13], sputtering power [14,15] and pre-heating of substrate [17]. It was indicated that controlling various sputtering parameters is essential in fabricating Bi-Te thin film deposited using magnetron sputtering.

An alternative for a study of the effects of the chemical composition of [Bi]:[Te] in various sputtering parameters of Bi-Te thin films is response surface methodology (RSM). RSM is a statistical design method using mathematical and statistical methods for designing experiments, building models, evaluating the effects of several factors and finding the optimum conditions for target responses [2,17-18]. This approach can result in having to do fewer experiments, which therefore reduces the cost, and it has advantages, making possible improved statistical interpretation of the results, and it requires less time for analysis [2].

In this work, Bi-Te thin films were deposited on flexible substrates using a Bi_2Te_3 target. Magnetron sputtering technique was used. Study of the effects of sputtering parameters, including the Ar gas flow rate (sputtering pressures) and pre-heating temperature and the annealing temperature on chemical composition of [Bi]:[Te]. RSM was used for a statistical study of the effects of deposition parameters, including the Ar gas flow rate and the annealing temperature on the response (Te content). Finally, the purpose of this thesis is to understand the key parameters of maximizing thermoelectric power factor in Bi-Te thin films by an in-depth investigating on the chemical composition, structural and thermoelectric properties of thin films.

1.2 Objectives of the study

1) To study the synthesis of Bi-Te thin films deposited by RF magnetron sputtering process and investigation on the effect of sputtering pressures on chemical composition, structural and thermoelectric properties of Bi-Te thin films on flexible substrates.
2) To study the synthesis of Bi-Te thin films deposited by RF magnetron sputtering process and investigation on the effect of sputtering pressures and annealing temperature on chemical composition, structural and thermoelectric properties of Bi-Te thin films on flexible substrates.
3) To study the influence of pre-heating temperature on chemical composition, structural and thermoelectric properties of Bi-Te thin films on flexible substrates prepared by RF and DC magnetron sputtering.
4) To assess and understand the key parameters and conditions that the best of thermoelectric properties on Bi-Te thin films deposited by magnetron sputtering.

1.3 Scope of the study

The scope of this thesis is as follows:

1) Synthesis of Bi-Te thin films via magnetron sputtering process and investigation on the effects of sputtering parameters such as sputtering pressures (0.6–1.6 Pa), annealing temperature (250–320°C) and pre-heating temperature (150–400°C) on the chemical composition, structural and thermoelectric properties of Bi-Te thin films.
2) Characterization chemical composition, surface morphology and structure of the deposited Bi-Te thin films by following techniques:
    2.1) Energy dispersive spectrometry (EDS)
    2.2) Field emission scanning electron microscope (FE-SEM)
    3.3) X-ray diffractometer (XRD)
3) Measure transport properties, including carrier concentration and mobility of Bi-Te thin films by Hall effect measurements.
4) Measure Seebeck coefficients and electrical conductivities by a direct current (DC) four-terminal method (ZEM-3).

1.4 Expected Results

1) Flexible Bi-Te thin films were obtained by magnetron sputtering technique using a Bi_2Te_3 target.
2) The effects of various sputtering parameters such as sputtering pressures, annealing temperature and pre-heating temperature significant for controlling compositions and improving thermoelectric properties of Bi-Te thin films were studied and classified.
3) The relevant key parameters on chemical composition, structural and thermoelectric properties of Bi-Te thin films has been clearly understood.
4) The best of deposition conditions can be achieved for stoichiometric Bi_2Te_3 thin films.

1.5 Arrangement of document

This thesis is organized into five chapters. In Chapter 1, we explain the important background that motivates the present work and the purpose of the study. In Chapter 2, we explained about the fundamental of thermoelectric, the effects of low-dimensional materials and basics of the thin film deposition process. The last, the literature reviews and analyzed techniques will be presented in chapter 2. The tools and framework for the research methods in this study are discussed in Chapter 3. In Chapter 4 we show measured results and discussions for parameters affect the power factor of Bi-Te thin films. Finally, in Chapter 5, the conclusion of this thesis is given.

Chapter 2
Theory and Literature Reviews

This chapter is intended to give the reader an understanding of thermoelectric effects, thermoelectric transport properties, low-dimensional systems, thermoelectric coefficients in low-dimensional materials, bismuth telluride, thin film deposition process, statistical design method for designing experiments, characterization techniques and Literature Reviews.

2.1 Thermoelectric effects

The fundamental thermoelectric effect (TE) involving the interaction and conversion between heat and electricity in solids. There are two main thermoelectric effects named as Seebeck effect and Peltier effect.

One of the most fundamental TE phenomena is the Seebeck effect, discovered by Thomas Johann Seebeck in 1821. The Seebeck effect is defined by a voltage difference (ΔV), develops in response to the applied temperature gradient (ΔT). Mathematics can be expressed as

$$S = \frac{\Delta V}{\Delta T} \tag{2.1}$$

The Seebeck effect is related to an intrinsic property of the materials, called the Seebeck coefficient (S). The units of the Seebeck coefficient is V/K in SI units. Generally, the Seebeck coefficient of semiconductor is higher than the metal material. In semiconductors, the Seebeck coefficient is negative for n-type and positive for p-type [2].

From Figure 2.1 (a), the small electric current will flow in a closed circuit composed of two dissimilar materials when their junctions are maintained at different temperatures. Which causes charge carriers in the material to diffuse from the hot side to the cold side based on the Fermi-Dirac distribution function lead to an increase in the thermoelectric voltage. However, if both electron and hole move in the same direction, we do not get the current. Thermoelectric devices are thus made by two types (n-type and p-type) of the semiconductor.

The second thermoelectric effect, the reversal of Seebeck effect is known as the Peltier effect, discovered by Jean Charles Athanase Peltier in 1834. The electric current flows across a junction of two dissimilar materials effect to heat gradient in the circuit, as shown in Fig.2.1 (b). Heat is released or absorbed depending on the direction of the current. This effect is due largely to the difference in Fermi energies of the two materials. The Peltier coefficient can be expressed as [1,2]:

$$\prod = \frac{Q}{I} \tag{2.2}$$

where Q is the total heat absorption (or dissipation) at each junction, I is the current passing through the junction and $\prod$ is called the Peltier coefficient. The unit of the Peltier coefficient is $W/A \; or \; V$ in SI units.

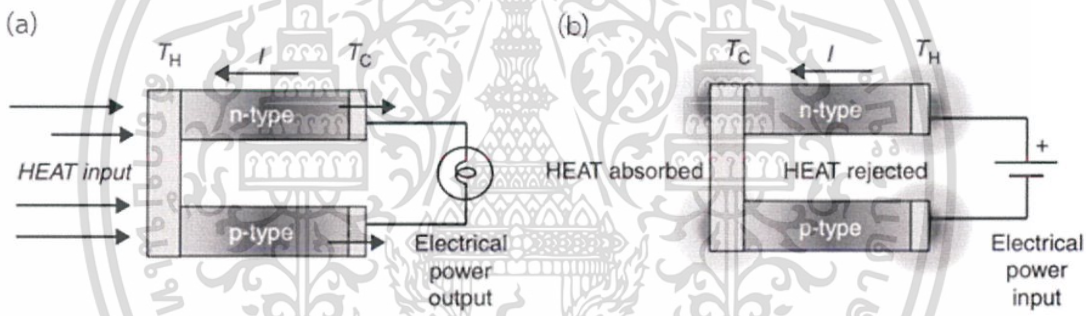

Figure 2.1 Schematic diagrams of thermoelectric devices (a) power generation (Seebeck effect) and (b) refrigeration (Peltier effect) [4].

The Seebeck and the Peltier coefficient are related by the Kelvin relationship. The relevant equation is shows as

$$\prod = S\,T \tag{2.3}$$

The usefulness of material in thermoelectric systems is determined by the two factors device efficiency and power factor. The potential of thermoelectric devices is determined in large part by a measure of the dimensionless Figure of Merit, can be expressed as

$$zT = \frac{S^2\sigma}{\kappa}T \tag{2.4}$$

where S is the Seebeck coefficient, σ is electrical conductivity, κ is thermal conductivity and T is absolute temperature.

When $zT > 1$, then the thermoelectric material can be considered as the best thermoelectric material. Previous research has reported the evolution of the thermoelectric efficiency, which is characterized by figure-of-merit (zT) value, as shown in Fig.2.2. It is important to note that zT value can be made to increase when improvements are made to low-dimensional thermoelectric materials.

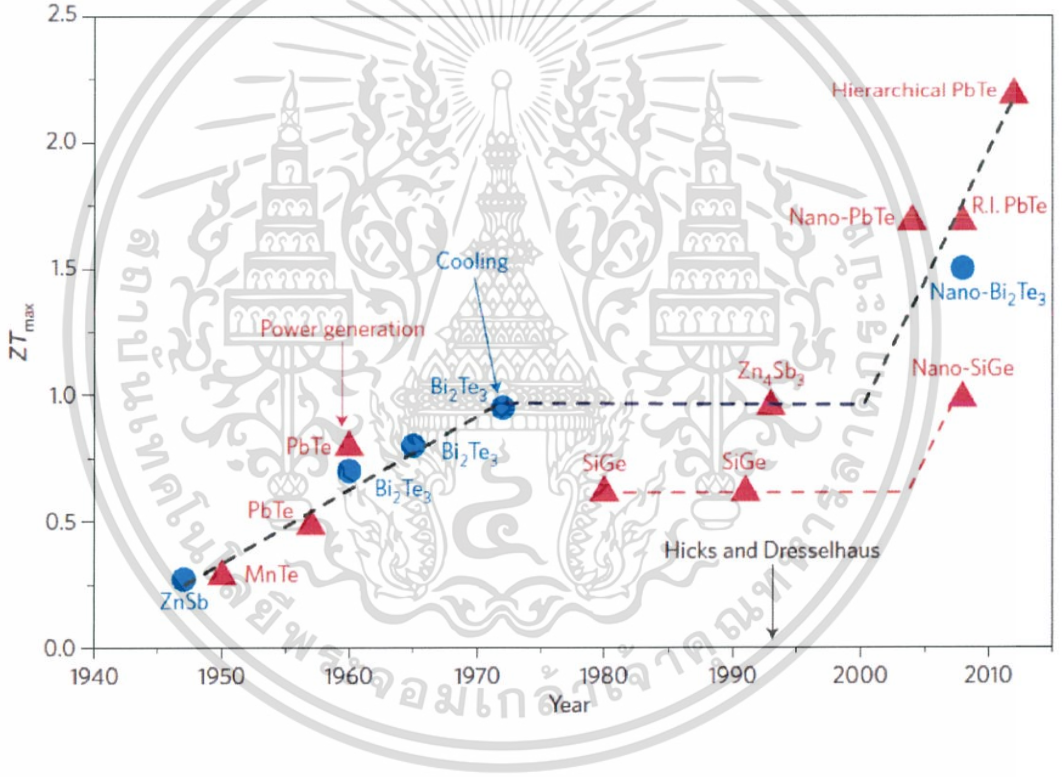

Figure 2.2 Evolution of the maximum ZT over time [19].

The power factor is a property of material that describes its ability to generate more energy from a given temperature difference. It can be expressed as

$$PF = S^2\sigma \tag{2.5}$$

A large value of zT means higher thermoelectric conversion efficiency, which requires a high power factor (PF) along with low thermal conductivity (κ). The power factor is optimized in narrow-gap semiconducting materials as a function of carrier concentration (about 10^{19} carriers/cm^3) , as shown in Fig.2.3. As the carrier concentration increases, both electrical conductivity and electronic thermal conductivity increase since there are more carriers to transport electron charges and heat energy, through the Wiedemann–Franz relationship.

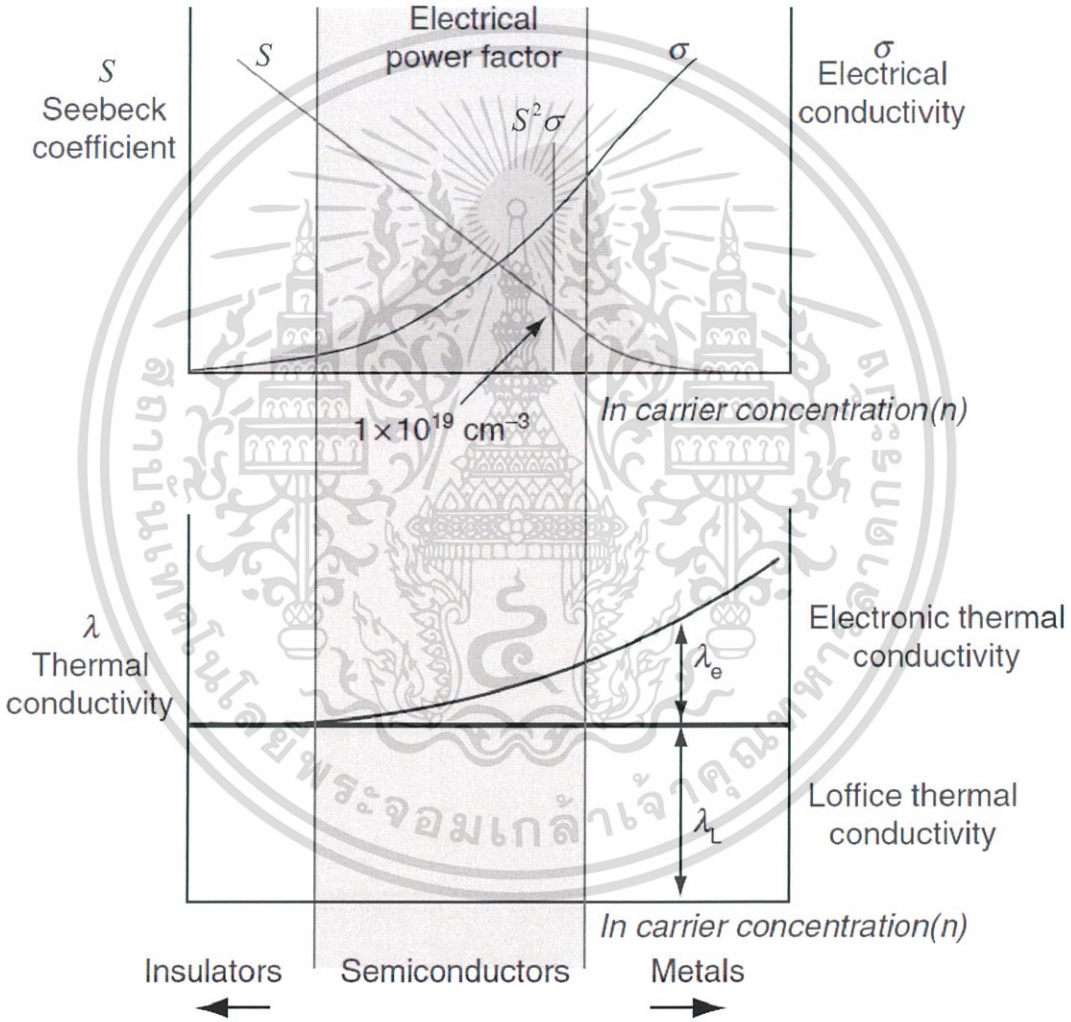

Figure 2.3 Schematic dependence of electrical conductivity, Seebeck coefficient, power factor, and thermal conductivity on concentration of free carriers [22].

The electrical conductivity is a reflection of the charge carrier concentration and all three parameters which occur in the figure-of-merit are functions of carrier

concentration. It has always been challenging for researchers to enhance the high ZT value of the material. Preparation of low-dimensional materials may be dedicated to reducing thermal conductivity due to can be increased boundary scattering in the nanostructures. Evidently, the figure-of-merit optimizes at carrier concentrations which correspond to semiconductor materials. Consequently, semiconductors are the materials most researched for thermoelectric applications [22]. The success in reducing thermal conductivity thus leads to the next challenge in increasing the thermoelectric power factor.

2.2 Thermoelectric transport properties

The physics of transport properties in materials is a key component in understanding the thermoelectric phenomena. Starting from the most fundamental concept of electrical and thermal transport in materials. It is important in the development of the thermoelectric device [5,6,7]. The analogy between electrical and thermal quantities is well known, as illustrated in Table 2.1

Table 2.1 Correspondence between thermal and electrical quantities [5].

	Thermal	Electrical
Quantity	Heat	Charge
Potential	Temperature	Potential
Current Type	Thermal current density	Electrical current density
Driving Force	Temperature difference	Potential difference

2.2.1 Electrical transport

Electrical conductivity is the ability of a material to carry the transport of charge carrier. The types of charge carriers in a conductor, which are electrons (n) or holes (p). Electrons are providing n-type conduction and the holes are providing p-type conduction [3,8-14]. The charge carriers transport mechanism is due to the thermal energy and involved the scattering mechanism of the carriers.

In a semiconductor, the electrical conductivity and drift mobilities can be related to relaxation time as equations (2.7), (2.8) and (2.9).

$$\sigma = ne\mu_e + pe\mu_h \tag{2.7}$$

$$\mu_e = \frac{e\tau_e}{m_e^*} \tag{2.8}$$

$$\mu_h = \frac{e\tau_h}{m_h^*} \tag{2.9}$$

where σ is electrical conductivity (S/m), n and p are the density of carriers (C). μ_e and μ_h are the mobilities of carriers $(m^2/V \cdot s)$, m_e^* and m_h^* is the effective mass of carriers, τ_e and τ_h are a charge-carriers relaxation time which depends on the charge carrier scattering [8-11,14].

The electrical conductivity of a material is determined by convolutions of carrier concentration and carrier mobility. The scattering mechanisms influence the carrier mobility, is mainly due to impurities and lattice scattering. In a semiconductor, the carrier concentration and carrier mobility are temperature dependent [8]. The mobility due to these scattering mechanisms is illustrated in Fig.2.4.

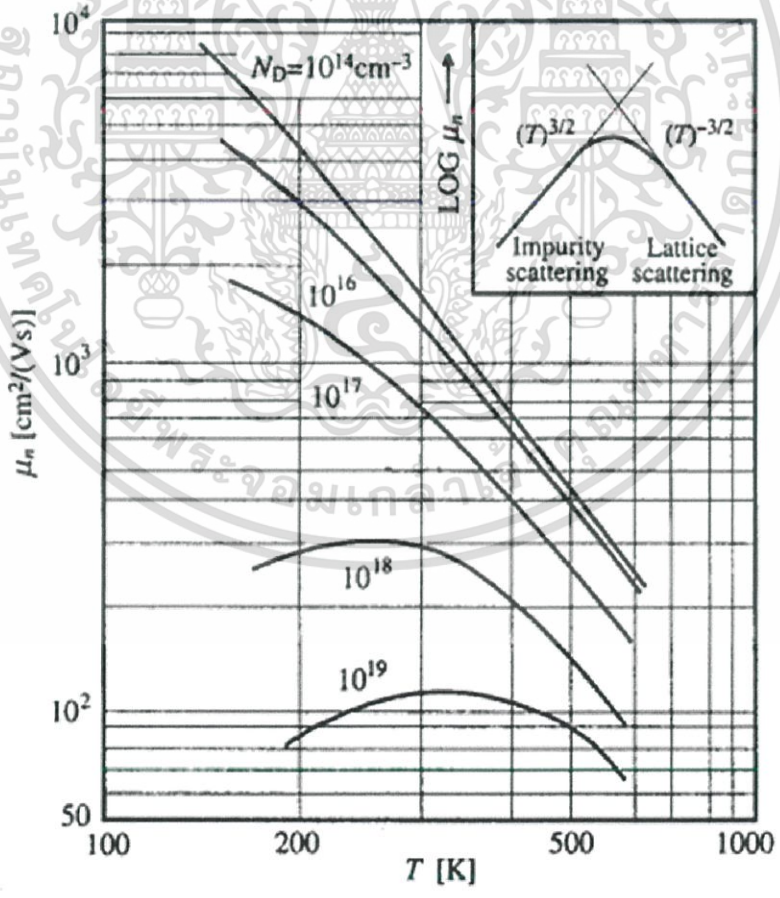

Figure 2.4 Temperature dependence of mobilities due to lattice and impurity scattering in n-type Si for different electron concentration [20].

2.2.1.1 The temperature dependence of the carrier mobility, at lower Debye temperatures ($T = \theta_D$). A passing charge carrier will be deflected by the Coulomb force between the carrier and the ionized impurity. This is known as impurity scattering, is caused by crystal defects such as ionized donor, acceptor impurities dislocations, grain boundaries, vacancies, surfaces, or any other deviation from a perfectly periodic lattice [10-9,dree]. The amount of scattering depends on the interaction time and the number of impurities. As a result, Impurity scatting is significant with lower temperatures ($T = \theta_D$), the charge carriers are moving slower and interact with the impurity for a longer time, and the carrier mobility increases due to scattering from ionized impurities [8-14], is defined as:

$$\mu_I = \frac{T^{3/2}}{N_I} \tag{2.10}$$

where N_I is the density of ionized impurities.

2.2.1.2 The temperature dependence of the carrier mobility, at temperatures above Debye temperatures ($T > \theta_D$). Lattice scattering is mainly due to thermal vibrations of the lattice and generates acoustic waves in the crystal, which are termed phonons. The motion of phonon can interaction with an electron (or hole) in the crystal. This is known as Lattice scattering. Since the density of phonons increases with temperature increasing, and thus increased electron scattering [8-13], which tends to reduce carrier mobility, is defined as:

$$\mu_L \propto T^{-3/2} \tag{2.10}$$

2.2.2 Thermal conductivity

Thermal conductivity is the ability of a material to transfer heat under the effect of a temperature gradient across different points. The total thermal conductivity consists of electronic transporting heat and phonons traveling through the lattice, can be written as [1-3]:

$$\kappa = \kappa_e + \kappa_l \tag{2.7}$$

where κ is thermal conductivity $(W \cdot m^{-1} \cdot K^{-1})$

The electronic thermal conductivity (κ_e) results from charge carriers (electron or hole) transporting heat, and is the ratio of the electronic transporting heat to the electrical conductivity of a metal is proportional to the temperature through the Wiedemann-Franz law [1,dre].

$$\frac{\kappa_e}{\sigma} = LT \tag{2.8}$$

where L is approximately constant called "Lorenz number". At low temperatures, the Lorenz number of the free electron is defined as:

$$L = \frac{\pi^2 k_B^2}{3e^2} = 2.45 \times 10^{-8} W \cdot \Omega \cdot K^{-2} \tag{2.8}$$

From equation 2.8, it was found that high electrical conductivity materials have high electronic thermal conductivity as well. However, the electronic thermal conductivity has less influence on thermal conductivity and can be neglected at low temperature.

In semiconductors, thermal transport is dominated by the lattice contribution. The thermal vibrations of the lattice are quantized and created the energy of quanta of which are phonons [4]. The lattice thermal conductivity (κ_l) results from phonons traveling through the lattice. From simple considerations based on kinetic theory of gases is [1,4]:

$$\kappa_l = \frac{1}{3} C_v v_s \Lambda_{ph} \tag{2.10}$$

where C_v is the specific heat at constant volume, v_s is the speed of sound and Λ_{ph} is the phonon mean free path.

The phonon means free path depends on phonon scattering mechanisms. In 1959 Joseph Callaway developed a model to calculate the lattice thermal conductivity with phonon transport model, which is based on the relaxation time. The

lattice thermal conductivity, using the Callaway formalism [2,4,6-7,20,21], can be written as

$$\kappa_l = \frac{k_B}{2\pi^2 v_s}\left(\frac{k_B T}{\mathsf{h}}\right)^3 \int_0^{\frac{\theta_D}{T}} \tau_c \frac{x^4 e^x}{\left(e^x - 1\right)^2} dx \qquad (2.11)$$

where θ_D is Debye temperature, h is the reduced Planck constant with $\mathsf{h} = \frac{h}{2\pi}$, x is the dimensionless parameter with $x = \frac{h\omega}{2\pi k_B T}$, ω is phonon frequency and τ_C is the combined phonon relaxation time.

The relation between the phonon scattering mechanisms and the combined phonon relaxation time can be obtained according to Matthiessen's rule [2,4,6-7,10], can be written as

$$\frac{1}{\tau_C} = \frac{1}{\tau_U} + \frac{1}{\tau_D} + \frac{1}{\tau_B} + \frac{1}{\tau_{EP}} \qquad (2.12)$$

where τ_C^{-1} is the total probability of scattering, τ_U^{-1} is the probability for Umklapp scattering, τ_D^{-1} is the probability for point defect scattering, τ_B^{-1} is the probability for boundary scattering and τ_{EP}^{-1} is the probability for electron-phonon scattering.

The major of phonon scattering mechanisms are Umklapp scattering, point defect scattering, boundary scattering and electron-phonon scattering, which are briefly discussed in the following subsections.

2.2.2.1 Umklapp Scattering

The Umklapp scattering is three-phonon scattering due to the absorption or emission of one phonon by other phonons [T3,dree,6]. The Umklapp scattering is dominated at high temperatures (T ? θ_D), is given by

$$\tau_U^{-1} = B\omega^2 T \exp\left(-\frac{\theta_D}{3T}\right) \qquad (2.13)$$

2.2.2.2 Point defect phonon scattering

A point defect includes a variety of vacancies, dislocations, uncharged impurity sites and different isotopes of the host constituents. A defect with dimensions much smaller than the phonon wavelength can be considered as a point defect. Point defect phonon scattering. The Point defect phonon scattering is caused by the difference in mass and bonding between the atoms. The Point defect phonon scattering is given by

$$\tau_D^{-1} = A\omega^4 \tag{2.14}$$

2.2.2.3 Boundary scattering

The boundary scattering is important at low temperatures where the phonon density is low. Boundary scattering becomes more significant as the crystallite size decreases. The Boundary scattering can be written in terms of grain size of thin films and film thickness as

$$\tau_B^{-1} = \frac{v_s}{d_1} + \frac{v_s}{d_2} \tag{2.15}$$

2.2.2.4 Carrier phonon scattering

The carrier phonon scattering is effective at scattering low energy which the wavelength phonon is high. Carrier phonon scattering can be increased when the material is heavily doped and charge carriers are created. The carrier phonon scattering is given by

$$\tau_{EP}^{-1} = C\omega \tag{2.16}$$

The relaxation time fitting parameters A, B, and C depends on the type of materials. The parameters A, B, and C of Sb_2Te_3 and Bi_2Te_3 is shown in table 2.2.

Table 2.2 Callaway model parameters for Sb_2Te_3 and Bi_2Te_3 [7].

Property	Units	Symbol	Bi_2Te_3	Sb_2Te_3
Primitive per unit cells	(m^3)	N	5.95×10^{27}	6.40×10^{27}
Phonon sound velocity	(m/s)	v_s	3,058	2,888
Lattice thermal conductivity (at 300 K)	(W/m/K)	κ_{ph}	1.5	1.5
Debye cutoff frequency	(rad/s)	ω_0	2.16×10^{13}	2.09×10^{13}
Defect scattering	(s^3)	A	1.3×10^{-42}	1.2×10^{-41}
Umklapp scattering	(s/K)	B	120	120
Carrier phonon scattering	(K)	C	1.1×10^{-18}	4.4×10^{-19}

2.3 Low-dimensional systems

The low-dimensional systems (LDSs) have characterized by compressing of electrons and holes inside the highly limited space of nanometric size resulting from quantum confinement. LDSs with nanometric structures can be classified into three types such as (1) two-dimensional systems (2D) have one dimension of nanometer size (quantum well e.g., thin film, superlattice), (2) one-dimensional systems (1D) have two dimensions of nanometer size (quantum wire e.g., nano-wire or nano-tube) and (3) zero-dimensional systems (0D) have all three dimensions of nanometer size (quantum dot e.g., nanoparticle, cluster, colloid).

The phenomenological dimensionality of nanometer materials is called the quantum size effect. The basic type of quantum confined structure is shown in Table 2.3.

Table 2.3 Classification of quantum confined structures.

Structure	Quantum confinement	Number of free dimension
Bulk (3D)	0	3
Quantum well (2D)	1	2
Quantum wire (1D)	2	1
Quantum dot (0D)	3	0

Quantum effects arise in systems which confine carriers when the physical size of the confinement potential is comparable to the de Broglie wavelength of the electrons or holes. The Fermi energy is commonly referred to as the topmost filled energy level at absolute zero and the corresponding Fermi wavelength is the de Broglie wavelength of the electrons present near the Fermi energy level.

In bulk materials (3D), the charge carriers are free to move in three directions which the carriers exhibit continuous energy spectrum. The energy of an electron is

$$E_{3D}(k) = \frac{\hbar^2 k_x^2}{2m_x^*} + \frac{\hbar^2 k_y^2}{2m_y^*} + \frac{\hbar^2 k_z^2}{2m_z^*} \tag{2.17}$$

where m_x^*, m_y^*, m_z^* and k_x, k_y, k_z are the carrier effective mass and wave vectors in x, y and z directions. The wave vector (k) is inversely proportional to the electron wavelength in k - space.

In two-dimensional systems (2D), quantum wells are formed. The charge carriers are free to move in two directions and confined in the other one direction. When the length along one of these directions becomes comparable to Fermi wavelength, the corresponding momentum is quantized. For example, if the length along the z-axis becomes comparable to the Fermi wavelength. The energy of an electron is

$$E_{2D}(k) = \left(\frac{\hbar^2 k_x^2}{2m_x^*} + \frac{\hbar^2 k_y^2}{2m_y^*} \right) + E_{nz} \tag{2.18}$$

The quantized energy E_{nz} results from the calculation of the wave function in quantum well with an infinite quantum-well potential of barriers and a finite width of the well (L_z). The energy levels in the x and y directions form a continuous, and for the z-direction discrete energy. The quantization energy is expressed by

$$E_{nz} = \frac{\hbar^2 k_z^2}{2m_z^*}, \quad k_z = \frac{n_z \pi}{L_z} \tag{2.19}$$

where k_z is wavenumber in the *z*-direction and n is quantum number. Then the total energy can be written as

$$E_{2D}(k_{xy}, n_z) = \left(\frac{\hbar^2 k_x^2}{2m_x^*} + \frac{\hbar^2 k_y^2}{2m_y^*} \right) + \frac{\hbar^2 n_z^2 \pi^2}{2m_z^* L_z^2}, \; n_z = 1,2,3,... \quad (2.20)$$

In one-dimensional systems (1D), quantum wires are formed. The charge carriers are free to move in one direction and confined in the other two directions. Assuming that the confinement occurs in the yz-plane, the total energy of an electron is

$$E_{1D}(k) = \left(\frac{\hbar^2 k_x^2}{2m_x^*} \right) + \frac{\hbar^2 n_y^2 \pi^2}{2m_y^* L_y^2} + \frac{\hbar^2 n_z^2 \pi^2}{2m_z^* L_z^2}, \; n_y, n_z = 1,2,3,... \quad (2.21)$$

with L_y and L_z describing the wire dimensions in the transverse plane $(L_z, L_y << L_x)$

In zero-dimensional systems (0D), quantum dots are formed. The charge carriers are confined in their motion in all three directions.

$$E_{0D}(k) = \frac{\hbar^2 n^2 \pi^2}{2d^2} \left(\frac{1}{m_x^*} + \frac{1}{m_y^*} + \frac{1}{m_z^*} \right), \; n = 1,2,3,... \quad (2.22)$$

The Fermi energy is a concept of the density of electronic states, or simply the density of states (DOS). Generally, Most properties of semiconductors, including optical, thermodynamic and transport properties, depending on the density of states. The DOS is essential for determining the carrier concentrations and energy distributions of carriers within a semiconductor. The DOS of semiconductor structure plotted against energy is depicted in Figure 2.5. The DOS is defined essentially the number of different states at a particular energy level that electrons are allowed to occupy, with in k-space. Mathematically, it is derived as

$$D(E) = \frac{dN}{dE} \quad (2.23)$$

where $D(E)$ is the DOS as a function of energy, N is the number of different states and E is the energy of different states.

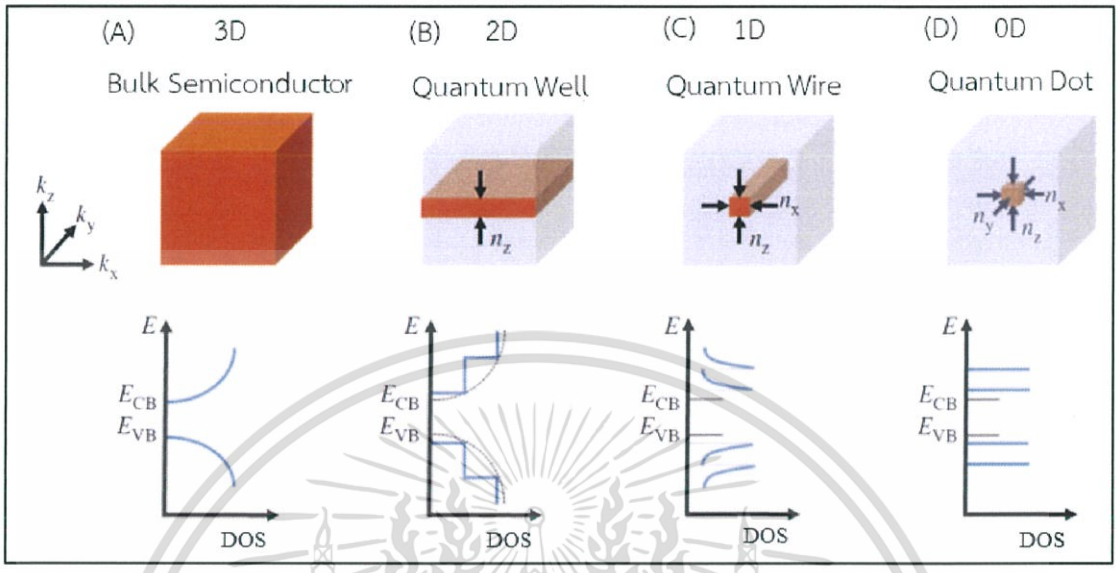

Figure 2.5. Electronic density of states for (A) a bulk semiconductor, (B) a 2D quantum well, (C) a 1D nanowire or nanotube and (D) a 0D quantum dot.

In the case of 3D semiconductor, the calculation of the DOS yields is given by

$$D_{3D}(E) = \frac{1}{V}\frac{dN}{dE} = \frac{1}{2\pi^2}\left(\frac{2m^*}{\hbar^2}\right)^{3/2} \cdot \sqrt{E} \qquad (2.24)$$

where $m^* = (m_x^* m_y^* m_z^*)^{1/3}$, which is called the effective mass for the DOS. The DOS then for the 3-D, or bulk material, shown in Fig.2.5 (A), has the parabolic relationship follow $\sqrt{E}$.

In the case of 2D quantum well structure, as sketched in Fig.2.5 (B). The carriers are still free to move in the directions parallel to the quantum well plane (surface of the film). The quantization of the carriers occurs in the perpendicular direction to the quantum well plane, which the thickness of the well is inverse proportional to the confinement energy $(L_z << L_x; L_y)$. Moreover, for decreasing the width of the wall caused the quantized energy increases of carriers.

The effect of quantization also in influences the density of states, as the density of states changes from a continuous dependence to a step-like dependence. The calculation of the DOS yields for each allowable k_{xy} series is

$$D_{2D}(E) = \frac{1}{A}\frac{dN}{dE} = \frac{1}{A}\left(\frac{dN}{dk_{xy}}\right)\left(\frac{dk_{xy}}{dE}\right) = \frac{m^*}{\pi\,\hbar^2} \qquad (2.25)$$

In the case of 1D quantum wire structure, as sketched in Fig.2.5 (C). The calculation of the DOS yields is given by

$$D_{1D}(E) = \frac{1}{L_z}\frac{dN}{dE} = \frac{1}{L_z}\left(\frac{dN}{dk_z}\right)\left(\frac{dk_z}{dE}\right) = \frac{1}{\pi}\left(\frac{m_z^*}{\hbar^2}\right)^{1/2} E^{-1/2} \qquad (2.26)$$

The DOS for such an ideal quantum wire, has a characteristic singularity follow $E^{-1/2}$.

In the case of 0D quantum dot structure, the calculation of the DOS yields is a series of δ -function peaks, is given by

$$D_{0D}(E) = \sum_n 2\delta(E - E_n) \qquad (2.27)$$

The quantum dot is restricted in three spatial dimensions, there is no k-space that could be filled with electrons. Therefore, each quantum state at the energy is occupied by only two electrons. For this reason, the DOS function is described by a series of δ -functions. The DOS for such an ideal quantum dot, as sketched in Fig.2.5 (D).

2.4 Thermoelectric coefficients in low-dimensional materials

High-Performance thermoelectric material is usually evaluated by two main parameters power factor (PF) and thermoelectric figure-of-merit (ZT). A most of research reported the possibility of improved ZT when moving from higher to lower dimensional materials using the change in the shape of DOS. The DOS is modulated as a result of this quantization. A sharp increase of the DOS near the Fermi energy

could lead to substantial enhancement in the Seebeck coefficient. The Seebeck coefficient can be approximated as

$$S(T) = \frac{\pi^2 k_B^2 T}{3e}\left[\frac{d\left[\ln(\sigma(E))\right]}{dE}\right]_{E=E_F} \tag{2.28}$$

where k_B is the Boltzmann constant, e is the electron charge. The Seebeck coefficient is proportional to the energy derivative of the differential conductivity, $\sigma(E)$. The total electrical conductivity (σ) can be calculated using the integral of $\sigma(E)$ over the entire energy range, moderated by the Fermi distribution function, as expressed

$$\sigma = \int_E \sigma(E)\, dE \tag{2.29}$$

Thus, The Seebeck coefficient depends on the energy derivative of energy-dependent electrical conductivity $\sigma = n(E)\cdot e\cdot \mu(E)$ taken at Fermi energy (E_F). Here, $n(E) = D(E)\cdot f(E)$ is the carrier density at the energy level (E) considered, $D(E)$ is the density of states, $f(E)$ is the Fermi–Dirac distribution and $\mu(E)$ is the carrier mobility. According to the Mott expression, The Seebeck coefficient can rewrite expansion in the form $D(E)$ and $f(E)$ as

$$\begin{aligned} S(T) &= \frac{\pi^2 k_B^2 T}{3e}\left[\frac{1}{n}\frac{d\ n(E)}{dE} + \frac{1}{\mu}\frac{d\ \mu(E)}{dE}\right]_{E=E_F} \\ &= \frac{\pi^2 k_B^2 T}{3e}\left[\frac{1}{n}\left(D(E)\frac{d\ f(E)}{dE} + f(E)\frac{d\ D(E)}{dE}\right) + \frac{1}{\mu}\frac{d\ \mu(E)}{dE}\right]_{E=E_F} \end{aligned} \tag{2.30}$$

Which shows that the Seebeck coefficient could be enhanced by two mechanisms as.

1) Increased energy dependence of carrier concentration, which is a function of the DOS (for instance, by a local increase in DOS).

2) Increased energy dependence of mobility, for instance, by a scattering mechanism that strongly depends on the energy of the charge carriers.

For low-dimensional materials, enhancement in the Seebeck coefficient mainly comes from the first mechanism. Thus, if we control the Fermi level so as to locate it near a sharp peak of the DOS, we can enhance the Seebeck coefficient dramatically without reducing electrical conductivity too much. For 2D quantum well, as the well thickness decreases, the spacing among subbands enlarges and correspondingly the magnitude of DOS at each subband increases. The more quantization of energy subbands and the better carrier confinement will be. The quantum confinement effect on carriers led to the enhancement in power factor for quantum well as mentioned above.

2.5 Bismuth Telluride

Bismuth telluride is one of the most interesting thermoelectric materials with a high ZT and it is known to have an excellent thermoelectric performance at room temperature [2]. Z. Zeng et al reported bismuth telluride bulk alloys have a high ZT about 1.14 at room temperature [14]. The ZT value can be made to increase when improvements are made to low-dimensional thermoelectric materials [3]. Bismuth telluride is a narrow gap layered semiconductor with band gap of 0.15 eV.

Bismuth telluride has a severalty of different crystals structures depend on a stoichiometric composition of materials. Bismuth telluride has general formula $(Bi_{1-x})_2Te_3$. The crystal structure of the most common is BiTe phase and Bi_2Te_3 phase [15] as shown in Figure 2.6. Bismuth telluride (Bi_2Te_3) thin films normally require a stoichiometric ratio of [Bi] and [Te] for achieving the best thermoelectric performance [3].

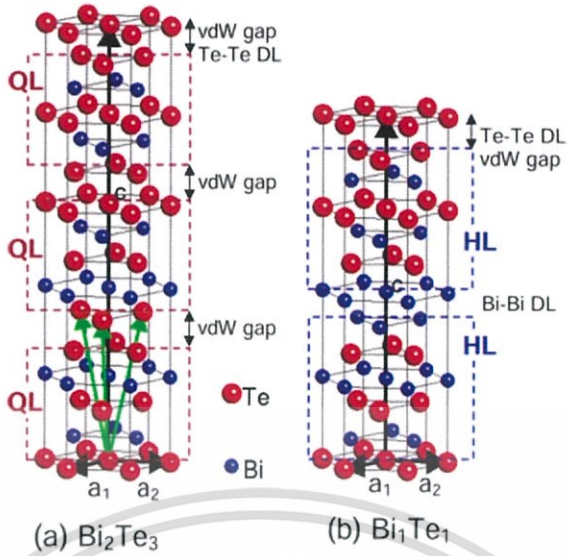

Figure 2.6 Hexagonal unit cell of (a) Bi_2Te_3 and (b) BiTe with the base vectors indicated by the black arrows [15].

Bismuth telluride has been crystallized in a tetradymite–type structure.For Bi_2Te_3, the stacking sequence of lattice planes results in the formation of three groups consisting of 5 atom layers (quintuple layer, QL) with the sequence Te^1–Bi–Te^2–Bi–Te^1 stacking along the c-axis. [15,16,17]. The bonding inside the quintuple layer is described as mixed ionic-covalent bonds (Te^1-Bi and Bi-Te^2), while Te-Te bonds between quintuple layers are of only weak van der Waals bonding as shown in Figure 2.6 (a) [15,16]. The unit cell of Bi_2Te_3 is rhombohedral in space group $R\bar{3}m$, which the lattice parameters of Bi_2Te_3 in terms of the hexagonal axes are $a_H = 4.383\,\text{Å}$, $c_H = 30.487\,\text{Å}$ [15].

For BiTe, the stacking sequence of lattice planes results in the formation of two groups consisting of 6 atom layers (hextuple layer, HL) with the sequence Te^1–Bi^1–Te^2–Bi^2–Te^3–Bi^3–Bi^3–Te^3–Bi^2–Te^2–Bi^1–Te^1 stacking along the c-axis. [15,16,17]. The bonding inside the hextuple layer is described as mixed ionic-covalent bonds, while Te-Te bonds between hextuple layers are of only weak van der Waals bonding as shown in Figure 2.6 (b) [15,16]. The unit cell of BiTe is rhombohedral in space group $R\bar{3}m$, which the lattice parameters of BiTe in terms of the hexagonal axes are $a_H = 4.402\,\text{Å}$, $c_H = 24.202\,\text{Å}$ [15].

2.6 Thin film deposition process

The thermoelectric conversion efficiency of thermoelectric materials is called ZT value, which ZT value can be made to increase when improvements are made to low-dimensional thermoelectric materials. Thermoelectric thin film is one of the most important low-dimensional thermoelectric materials. The general properties of the thin films, such as composition, crystal phase, and orientation, thickness, and microstructure, are controlled by the deposition conditions. Thermoelectric thin film has been created using different deposition methods, such as co-evaporation, pulsed laser deposition, and RF magnetron sputtering.

2.6.1 Classification of deposition processes

The vapor deposition method is one of the most common technique and widely used in deposit thin films. Vapor deposition technique can be classified into two categories.

2.6.1.1 Chemical Vapor Deposition (CVD)

Chemical vapor deposition (CVD) is a chemical process used to deposit films on or near the vicinity of a heated substrate surface in the chamber from the reaction of vapor-phase precursors. In general, the CVD process involves the following key steps (1) The volatile precursors in the gaseous are introduced into a reaction chamber; (2) Gas phase reactions of precursors occur in the reaction zone; (3) Mass transport of gaseous precursors to the substrate surface; (4) Absorption of gaseous precursors onto the substrate surface; (5) Surface diffusion to growth sites, nucleation and surface chemical reactions leading to growth of the film; (6) Desorption and mass transport of remaining fragments of the decomposition away from the deposition chamber [23-25], as shown in Figure 2.7.

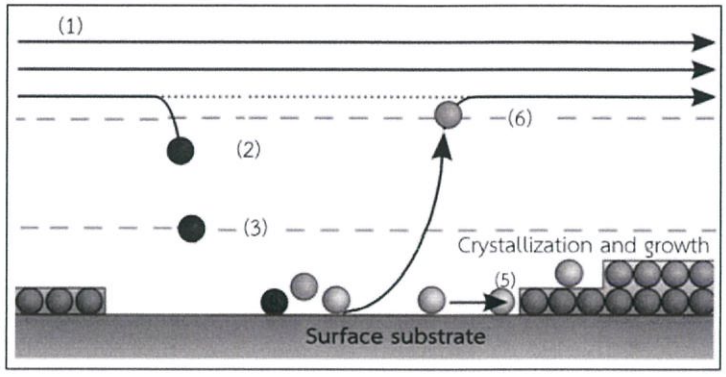

Figure 2.7 Schematic illustration of the key CVD steps [24,25].

Although the CVD coating technique can be coated on a variety of materials with high purity, it is also an extremely complex chemical process. Typically, the chemical reactions occur at temperatures ranging from 200-1600°C, which is higher than the PVD process and may be affected to some substrate material.

2.6.1.2 Physical Vapor Deposition (PVD)

Physical vapor deposition (PVD) is a vaporization coating process that requires a transfer of solid material from the source to the surface of a substrate. The main difference between CVD and PVD process is that in CVD, the target material is in gas or liquid form, but in PVD, the target material is in solid form.

In this work, PVD process was selected due to it can be used all types of inorganic materials and some types of organic materials. Further, this process is environmentally friendly compared to many other and the possibility of large-scale fabrication of high-quality films, which the process can be used in the surface coatings industries.

PVD technique can be classified into two main categories: (1) Evaporation technique and (2) sputtering technique. Evaporation involving thermal evaporation techniques and sputtering techniques involving ionic sputtering methods. The difference between sputtering technique and evaporation technique, is that evaporation technique is shown certain disadvantages. In particular, the target of material is alloys and refractory metals cause problems because of differences in alloy constituent vapor pressures and their high melting points which effects on growth a film. Sputtering technique was selected due to the possibility of large-scale fabrication of high-purity films and extremely high adhesion of films.

2.6.2 Sputtering Process

The basic of the sputtering process is as follows. The sputtering target is bombarded by energetic ions from glow discharge plasma consists of ions, electrons and neutral species in a quasi-neutral electrical state. The energetic ions are accelerated by a negative voltage applied to the cathode, as shown in Eq. 2.31. Typically, the most commonly used incident gas ions are inert gas ions such as Ar^+, Kr^+, Xe^+.

$$Ar + e^- \rightarrow Ar^+ + 2e^- \tag{2.31}$$

The results from interactions between the energetic inert gas ions and surface atoms on the target will eject atoms of the sputtering target by momentum transfer in the near-surface region of the target. The ejection depth of the target atoms is approximate 10 Å. During the interchange of momentum can be described two main mechanisms, an elastic or a nuclear collisions and an inelastic or an electronic collisions [26-29]. The result of elastic nuclear collisions, the sputtered atoms from the target can be ejected. If the transferred energy to the target atoms is enough to overcome the surface binding energy of target atoms. Inelastic electronic collisions are a collision of the ions with the electron and results in excitation and ionization of constituent electrons in the atom.

Thus, the interactions of the incident ions with the target surface are not only the sputtered atoms but also causes the generation of secondary electrons and reflected ion and neutrals [26-30]. Bombarding ions may be implanted into the target material with or without the ejection of the target atoms. The secondary electrons are repelled away from the target due to the application of a negative potential on the target. The secondary electrons are repelled away from the target and are needed to maintain the glow discharge plasma process. The sputtering process is illustrated in Figure 2.6. The sputtered atoms from the target directly coated onto the surface of the substrate, thus forming a thin film.

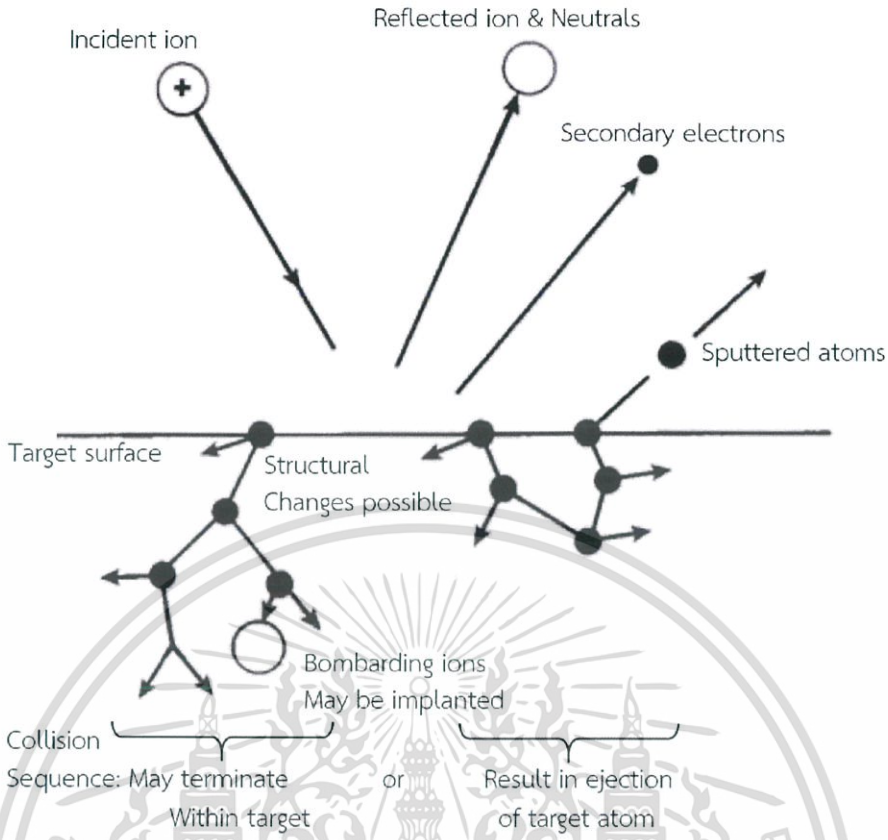

Figure 2.8 Schematic illustration of sputtering process.

2.6.3 Sputtering Yield

As a result of collisions between the incident ions with the target surface, kinetic energy is transferred to the target atom result in the ejection of surface and near-surface atoms also referred to as knock-on sputtering. The average number of ejected atoms from the surface of a target surface per number of incident ions is called sputtering yield. It is a significant measure of the efficiency of the sputtering process [26,29,31]. For energetic ions from 100 to 1000 eV, the sputtering yield can be calculated in eq. 2.32.

$$Y = \frac{3\alpha}{4\pi^2} \frac{4M_i M_t}{(M_i + M_t)^2} \frac{E}{U} \qquad (2.32)$$

where α is a dimensionless parameter depending on the mass ratio M_t/M_i, M_i and M_t is the atomic masses of the incident ion and the target atom (in amu), E the

energy of the incident ion and U is the binding energy of the surface atom of the target.

The sputtering yield is strongly dependent on the energy of the incident ions, target materials and angle of incidence, can also be understood from equation (2.1). Sputter yields increase as the mass of incident ion increases due to a process of momentum transfer [31] and also tend to increase as the kinetic energy of incident ions above the threshold energy. This tendency decrease when it reaches around 10 keV because the incident ions lose beneath the surface of the target material and much of their energy is dissipated [29,31]. Sputter yields vary with the atomic number of the target material and angles of incident ions. The maximum sputtering yield occurs between angles of incident ions about 75- 85° depending on the target material [29].

2.6.4 Glow discharge

Glow discharges are essential in order to master the sputter deposition system since virtually all of the energetic incident particles originate in the plasma. Plasma is defined as a gas which partially consists of ions, atoms, and electrons. The characteristic glow is given by the relaxation of the atoms excited by the electrons accelerated toward the anode. There are two means of operation to create plasma.

2.6.4.1 Direct current (DC) diode discharge

In DC diode discharge utilizes a DC voltage power supply. A negative voltage is applied to the target of material as the cathode. Similarly, the substrate holder and the entire vacuum chamber are grounded as an anode to drive the sputtering process [22,23]. For DC power supply, the target of material is located in this main discharge and is the plasma generation region. Ions are extracted from the plasma and accelerated toward the negative target [22]. Generally, the cathode in DC discharge must be an electrical conductor due to an insulating surface will develop a surface charge that will prevent ion bombardment of the surface. This condition implies that dc sputtering is must be used with electrically conductive target materials.

An advantage of DC sputtering is that the plasma can be established uniformly over a large area and easy to control to deposit. On the other hand, a disadvantage of DC sputtering configuration is that it cannot be utilized for insulators. When the ions bombard an insulating cathode a charge is built upon the cathode surface and reduces the field between the electrodes. As a result, the plasma ceases to exist.

2.6.4.2 Radio frequency (RF) diode discharge

The commonly applied radio frequency is 13.56 MHz for RF sputtering. In RF diode discharge utilizes an alternating current (AC) voltage power supply. The target of material as the cathode is linked to the RF generator via a series a blocking capacitor. The blocking capacitor is placed in the circuit to develop the all-important DC self-bias. This method prevents the charge build-up on the target surface by frequently neutralizing the surface with electrons or ions. Therefore, RF sputtering can be used with electrically conductive or insulating target materials, to avoid charge accumulation on the target.

An advantage of the alternating field has a second benefit as well. When the field is changed, the electrons which have not yet reached the anode will be accelerated toward the "new" anode and hence, increase the probability of a collision with an atom. This implies a higher density of ions and higher sputtering rate.

RF-sputtering offers advantages over DC; in particular sputtering of an electrically insulating target becomes possible. The DC powered magnetron plasma can be operated in the range of 10-100 mTorr which RF powered magnetron plasma can be operated at a lower pressure of less than 1 mTorr. The result is fewer gas collisions affects to equaling more efficient line of sight deposition of the coating material.

2.6.4.3 Discharge in a Magnetic Field

Magnetrons can be powered by a variety of methods. Generally used with among power supply from direct current (DC) and radio frequencies (RF). During the sputtering process, a magnetic field can be used by putting a magnet to the top of the cathode to trap secondary electrons close to the target. The electrons follow helical paths around the magnetic field lines enhancing more collisions with working gas near the surface of the targets. This improves the sputtering rate by enhancing the ionization of the plasma on the surface of the target material, indicating the plasma is able to be sustained at a lower pressure than a normal sputtering system. The bombarding ions cause atoms to be sputtered from the target material by momentum transfer between the colliding ions and the target atoms. The atoms of the target are ejected and deposited onto the substrate. A simplified scheme of the magnetron is given in Figure 2.9. Magnetron sputtering has many advantages such as (1) high deposition rates, (2) ease of sputtering any metal, alloy or compound, (3) excellent

coverage of steps and small features, (4) ability to coat heat-sensitive substrates, (5) ease of automation, and (6) excellent uniformity on large-area substrates [22].

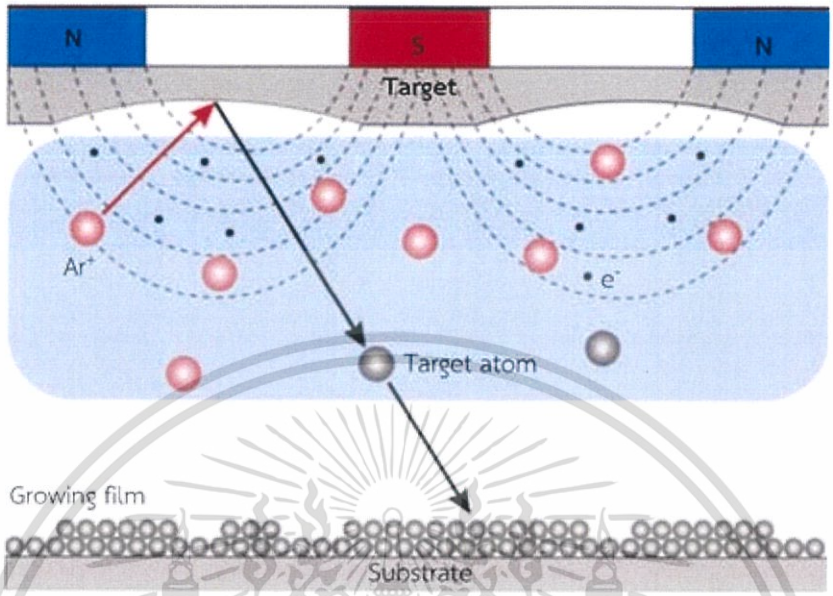

Figure 2.9 Schematic diagram of magnetron sputtering system.

2.6.5 Sputtering targets

For the operation of the sputtering systems, several kinds of equipment are prepared. And one of the most important is the sputtering target. Typically, the sputtering targets are solid slab a variety of size and shape. The target materials can be made of a wide variety of material, including pure metals, alloys, and compounds such as Bi_2Te_3. The composition of the thin films are controlled by the sputtering yield and the area ratio of each element includes the atomic weights of each element. For lab scale, the thin films have obtained, have distributed non-uniformly over the substrate at different substrate positions. A rotating substrate holder is often used to obtain uniform composition over the entire substrate [27].

However, most of the industrial processes have used compound targets due to preferring simplicity and repeatability. However, only a few works have been reported using a Bi_2Te_3 target. Which, there are several unresolved issues such as the phase purity and the control composition of the film which may deviate from that of the compound target. Thus, there is a need for improved understanding of the deposition conditions for Bi_2Te_3 phases from compound targets.

2.6.6 Sputter deposition

The deposition rate is dependent on sputtering yield and the probability of the emitted atom to reach the substrate. The deposition rate is a very important parameter controlling the structure, impurity and physical property of thin films. Sputtering involves many parameters that affect the deposition process and deposition rate such as base pressure, sputtering pressure, sputtering power, target and substrate temperature, etc. They affect the kinetic energy of the impinging particles, are of importance for the properties of the film. The microstructure of the film or its quality which includes surface roughness, adhesion, impurity, the density of the film produced by the sputtering process is a result of the interplay of the above parameters. Contribution of such a large number of parameters makes the process complex but also provides a large degree of control over the film growth process, if optimized properly. Generally, the deposition rate in a magnetron-deposition system is significantly increased. Hence, the prediction of how the deposition rate is affected due to the improvement of sputtering parameters is important. In the case of magnetron sputtering, the method to predict the deposition rate is to calculate the "rate per watt".

2.6.7 Thin Film Growth Process

Thin films growth is a complex process controlled both by thermodynamic driving forces and kinetic mechanisms. In a sputtering process, the sputtered atoms are transported to the surface of the substrate, which atoms diffuse on the substrate surface are called "adatoms". Diffusion of adatoms on the surface depending on the energy of adatoms and interactions at the substrate. Kinetic mechanisms, adatoms form chemical bonds with atoms of the substrate or with other adatoms or release from the surface. Thin film formation is related to the mobility of adatoms during growth. Thermodynamic factors, the adatoms tend to assemble on surfaces into the most stable positions.

When adatoms come into contact with each other, they form small clusters which clusters may also be mobile. If the deposition parameters are such that a cluster collides with other adsorbed species before getting desorbed on the surface of the substrate, it starts growing in size. After reaching a certain critical size, the cluster or nuclei becomes thermodynamically stable. Nucleation occurs when stable clusters of adatoms form, which is called the nucleation stage. The nucleation stage is formed

until a maximum number density is reached. As the growth, the process continues these islands start to coalesce and this stage is called coalescence, and a continuous thin film is formed. Thin film growth process can be classified into three modes and are (1) Volmer–Weber model, (2) Frank–Van der Merwe model and (3) Stranski–Krastanov model [28], shown in Figure 2.10.

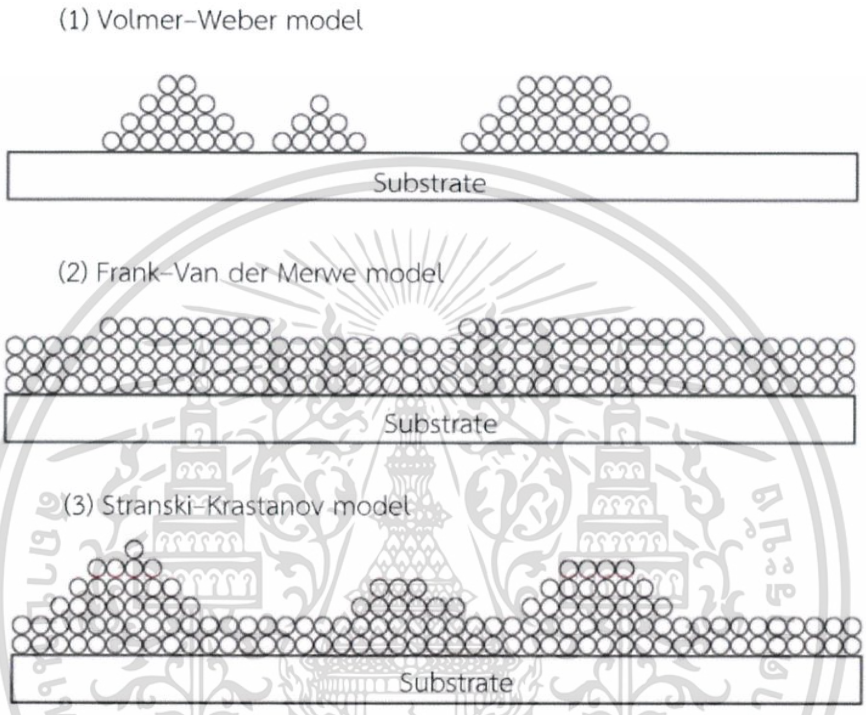

Figure 2.10 Schematic illustration of thin film growth modes.

(1) Volmer–Weber model or mechanism of island growth.

Mechanism of island growth happens when the interaction between the atoms is stronger than the interaction with the substrate surface. In this case, Island or 3-D growth mode is created and formed of discrete on the substrate surface. Finally, the nuclei grow in size until they intersperse with each other to form a continuous film.

(2) Frank–Van der Merwe model or layer by layer growth mechanism.

The layer-by-layer growth mechanism happens when the interaction between adatoms and the substrate surface is stronger than the interaction with different adatoms. The growth of the next layer does not begin until the complete formation of the previous one is finished, so there is a 2-D growth.

(3) Stranski–Krastanov model

This growth mode is a combination of 2-D and 3-D growth modes. When the growth starts as 2-D (layered) and then change to a 3-D (island). After completion of the 2-D layer growth, the 3-D island growth occurs.

During deposition of a polycrystalline film, several fundamental kinetic processes. And finally, when a polycrystalline film has fully coalesced and a continuous film is formed, the film thickness increases by continued deposition. Atoms arriving at the surface of the film can be created new grains on top of existing grains or they can contribute to layer epitaxial growth, which serves as a template with low-energy sites for further grain growth. Island formation and growth leads to impingement of islands to form grain boundaries. The development of grain structure during subsequent film growth is determined largely by surface mobility of adatoms relative to the deposition rate, and by the substrate temperature. Each of these processing conditions affects the diffusivity and mobility in the thin film, which causes defects during film deposition [32]. The resulting, grain shapes are then predominantly equiaxed. The occlusion of slow-growing grains by faster-growing grains may result in the evolution of thickness, grain size, and the surface of the film, shown in Figure 2.10.

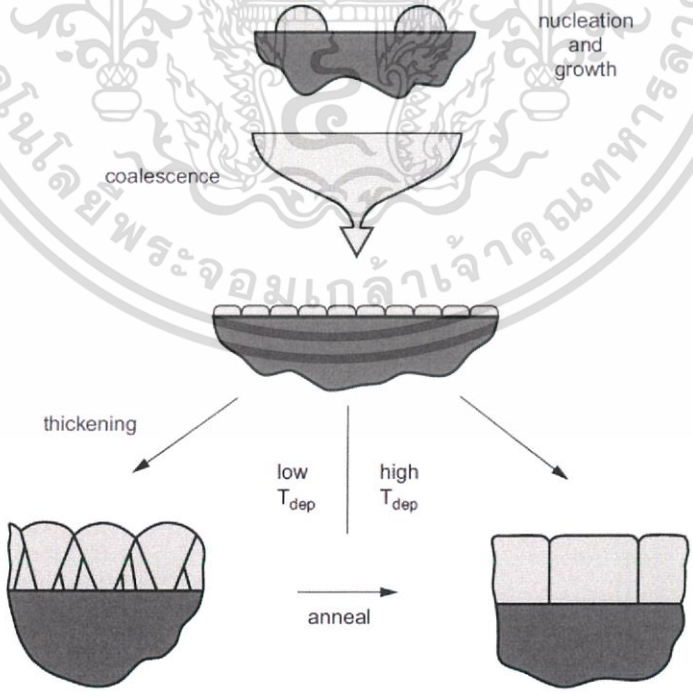

Figure 2.11 Grain growth in a two-dimensional polycrystalline material [32].

Grain coarsening occurring through the motion of grain boundaries is normally referred to as grain growth, as shown in Figure 2.11. The result of such grain boundary migration is shrinkage and elimination of small grains which, in turn, leads to an increase in the average grain size.

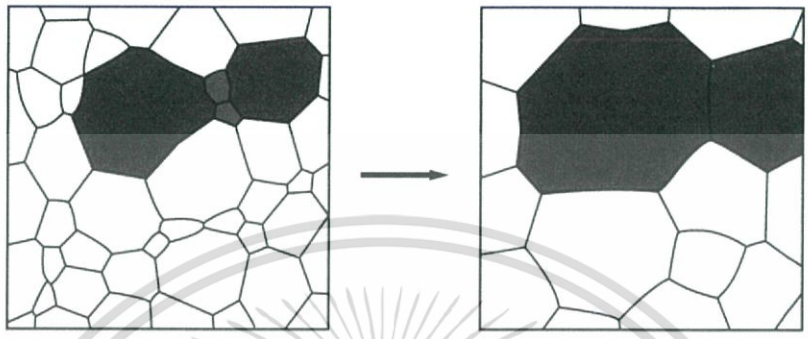

Figure 2.12 Grain boundary in a two-dimensional polycrystalline material [32].

In addition, the structure may be developed during post-deposition processing, for example, due to post-annealing, where grain growth, recrystallization, defect disruption etc. are possible structure-developing processes.

2.6.8 Structural consequences of the growth process [28,32]

Since magnetron sputtering was used to synthesize the thin films in the present studies. The microstructure evolution of thin films is related to the mobility of the adatoms during growth. The energy supply to the atoms is provided by the following mechanism (a) thermal effect, (b) ionic bombarding, and (c) chemical reactions at the substrate, which relevant for sputtering parameters. The main sputtering parameters are substrate temperature, substrate bias voltage, sputtering pressure, the deposition rate, and base pressure. The effects of sputtering parameters have produced the mechanisms in the growth of thin films can be explained by the structure zone model, as defined as three zones, as shown in Figure 2.13. The structure zone model is related to the normalized temperature, when T_s is the temperature of the substrate and T_m is the melting the temperature of the target.

The first zone corresponds to low deposition temperatures, Ts/Tm <0.3.

This zone is formed by small and elongated grains that form a columnar structure with porous morphology and weakly binding grains. The columnar the structure is produced by a low diffusion, low mobility of the atoms adsorbed by the

substrate surface. And the atomic shadow effects, which are produced by varying velocity in the growth of the columns. The various incidence angles at which the atoms arrive at the surface of the substrate.

In the second zone consists of larger columnar grains separated by dense grain boundaries, $0.3 \leq T_s/T_m \leq 0.45$.

The substrate temperature increasing homogeneous which leads to a higher diffusion of the adatoms, which produce a dense structure with a higher degree of binding among the columns and the borders between columns, with borders of the grain beginning to form. Dislocations are primarily located in the boundary regions. Surface or grain-boundary diffusion seems to be dominating parameters, since the columnar grain size increases with T=Tm, in accordance with activation energies for these mass-transport mechanisms.

In the third zone is characterized by bulk diffusion processes such as grain growth and recrystallization, $T_s/T_m > 0.45$.

The volumetric diffusion size has a great influence on the morphology of the film, due to the increase in the diffusion into the grains, which produces growth of the grains, formation of the equiaxed grain and re-crystallization. These effects produce a greater crystalline structure.

In the Thorton model, the T zone as a transitional zone between the first and second zone discussed above was added. The T zone is formed by grains defined by the limits of the low porosity. The surfaces of the T zone are denser and less rough than the two surfaces around them.

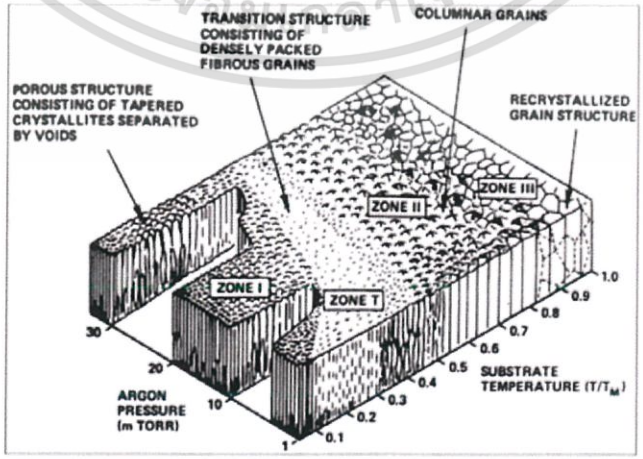

Figure 2.13 Schematic Thornton structure zone diagram [28,32].

2.7 Experimental design

Response surface methodology (RSM) is a statistical design method using mathematical and statistical methods for designing experiments, building models, evaluating the effects of several factors and finding the optimum conditions for target responses. RSM consists of a group of mathematical and statistical techniques used in the study of a functional relationship between a response of interest (y) and the number of associated control (x_1, x_2, x_3,...,x_k) variables denoted.

Generally, a low-degree polynomial model can be used approximate the function of relationship.

$$y = f'(x) + \varepsilon \tag{2.33}$$

Where x is the number of associated control (x_1, x_2, x_3,... ,x_k), $f'(x)$ is a response surface and ε is the noise or error observed in the response (y). The response can be explained graphically, either in the three-dimensional space or as contour plots as shown in Figure 2.14.

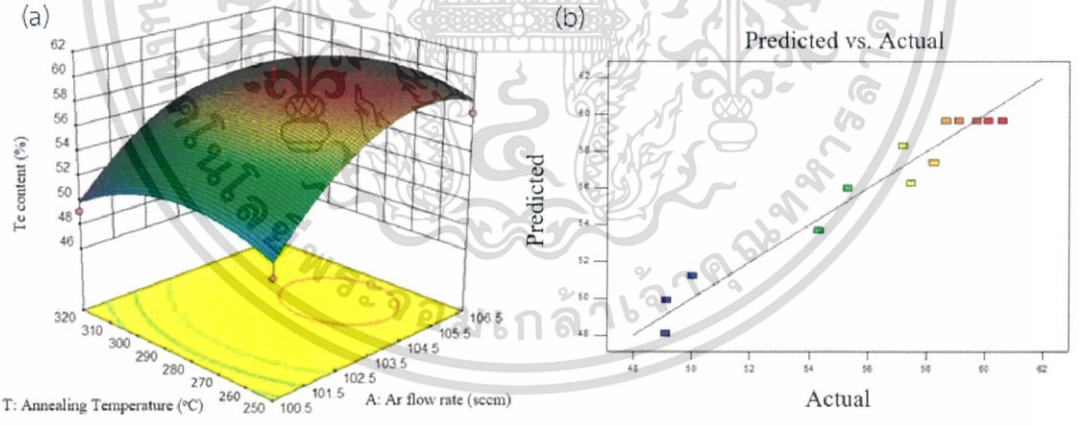

Figure 2.14 (a) Three-dimensional response surface and (b) contour plot of Te content on Bi-Te thin films predicted from the quadratic model

Most of the optimal design of experiments are associated with the mathematical model of the process which experiments are designed only for every unique problem.

A second-order model can be built efficiently with central composite designs (CCD). This design consists of the following three portions [24]:

1. The design 2^k factorial called the factorial portion.
2. An axial portion consisting of 2^k points arranged
3. Central point, n_0.

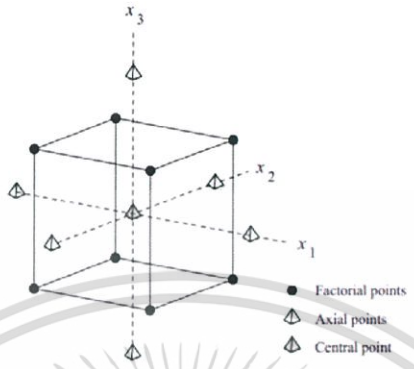

Figure 2.15 Central composite design for 3 design variables at 2 levels [24].

CCD presents a choice to 3N designs in the building of second-order models because the number of experiments is decreased as compared to a full factorial design [Chap3]. This study used response surface methodology (24) based on a central composite design (CCD) to optimize deposition parameters [2].

When the estimated equation is obtained, an experimenter can be examined the normal plot, the main effects, the contour plot, and ANOVA statistics (F-test, t-test, R^2, the adjusted R^2, and lack of fit) to define the adequacy of the fitted model [24].

2.8 Characterization techniques

2.8.1 Field emission scanning electron microscope (FE-SEM) and Energy Dispersive X-Ray Spectrometer (EDS)

The field emission scanning electron microscopy (FE-SEM) is a type of electron microscope that images the sample surface by scanning over it with high-energy beam of electrons. Primary electron beam is generated from Field Emission Source (FES) and it is accelerated in a high electrical field gradient (0.5 to 30 kV). The electron beam is focused by electromagnetic lens to a sharp point. The electromagnetic lenses consists of condenser lens, scan coils, stigmator coils and objective lens. The condenser lens is used to control the diameter of the electron beam. The condenser lens consists mostly out of two parts affects the contrast of Image. The scan coils deflect the electron beam over the sample according to a zig-

zag pattern which the image of the sample on the monitor occurs from this scanning movement. The objective lens is the lowest lens in the column. The objective lens focuses the electron beam on the sample. After that, the electron beam bombards a sample. A large number of signals are emitted such as backscattered electrons, secondary electrons, X-ray and Auger electrons. A detector counts these secondary electrons and sends the signals to an amplifier. The signals are transduced to an image signal that appears on the screen. The difference of the signal reflects surface microstructure morphology of the sample depending on the signals that achieved from the interaction between a primary electron and the sample.

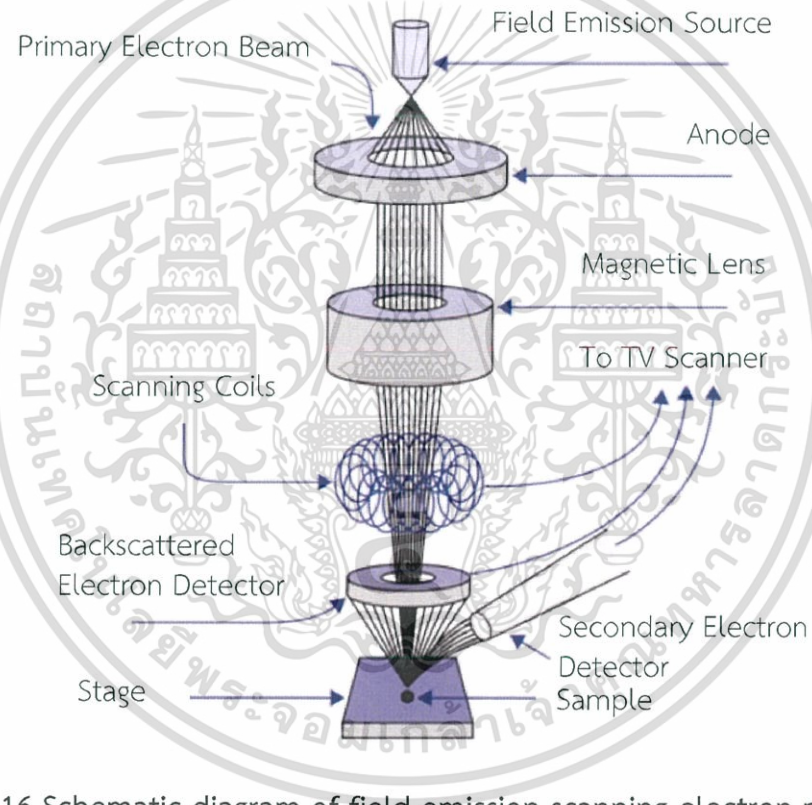

Figure 2.16 Schematic diagram of field emission scanning electron microscope components.

Energy Dispersive X-Ray Spectrometer (EDS) analysis is a technique used for measuring the elemental composition of the Bi-Te films by detecting characteristic X-ray. The bombarding electrons knock against lower shell electrons of the specimen atoms, which knocks electrons out of the atoms of the sample. An electron from higher shell electrons fills a vacancy in lower shell of an atom, results in the emission

of characteristic x-rays that allows for the identification of elements of the sample as shown in Figure 2.17.

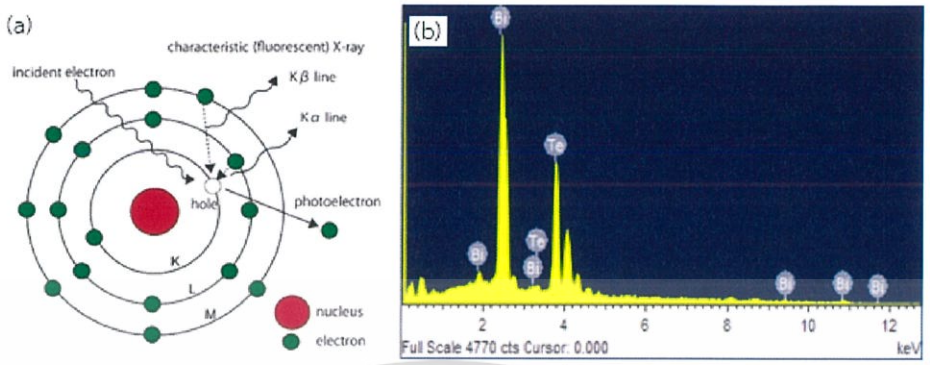

Figure 2.17 (a) EDS Process (b) EDS spectrum of Bi_2Te_3 film

2.8.2 X-Ray Diffractometer (XRD)

X-Ray diffraction (XRD) is a nondestructive analytical technique used for characterization of the structure of a crystalline material and can provide information on crystal structure such as average crystallite size, micro strain and dislocation density and the study of preferred orientation in crystals by diffraction x-rays through the sample. The diffraction pattern can describe the structure of a crystal in terms of lattice plane (hkl) with different reflection planes and inter-planar distance (d_{hkl}) at different angles, as described by Bragg's law,

$$2d \sin\theta = n\lambda \qquad (2.34)$$

Where d is the spacing between the crystal planes, θ is the Bragg angle for which reflections of these planes occurred, n is the order of diffraction and λ is the X-ray's wavelength.

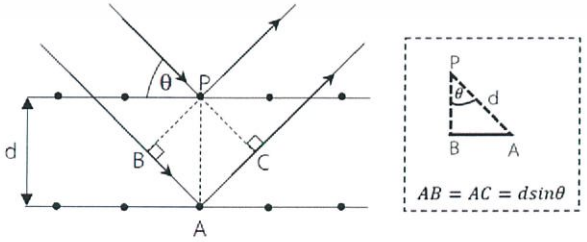

Figure 2.18 Schematic showing X-ray diffraction from crystal planes with inter-planar distance

The crystallite size (D), microstrain (ε), and dislocation density (ρ) of the Bi-Te films have been calculated using the preferred orientation of the XRD peak. The crystallite size (D) of thin films grown on flexible substrates was calculated by Scherrer's formula as shown in equation,

$$D = \frac{k\lambda}{\beta \cos \theta} \tag{2.35}$$

$$\varepsilon = \frac{\beta \cos \theta}{4} \tag{2.36}$$

$$\rho = \frac{1}{D^2} \tag{2.37}$$

where k is the constant usually taken as 0.94, λ is the X-ray radiation wavelength (0.154056 nm), β is the full width at half maximum (FWHM), and θ is the diffraction angle.

Microstrain developed in the film, which is determined from disarrangement of lattice during their deposition and depends on the deposition parameters. The dislocation density is the density of imperfections in the crystal during the growth of film. The microstrain (ε) and the dislocation density (ρ) were evaluated using the equations 2.36 and 2.37, respectively. The crystallite size of the Bi-Te thin film decreased, while the microstrain and dislocation density increased.

2.8.3 Mobility and Carrier concentration measurement

The Hall effect is commonly used techniques to investigate the electrical transport properties of materials, such as carrier concentration (n), conductivity type (n-type or p-type) and carrier mobility (μ) [32,33,34]. When an electric current flow through a sample placed in a magnetic field, a voltage difference (the Hall voltage) will be generated perpendicular to both the current and the magnetic field as result of the Lorentz force. This effect is known as the Hall effect [33,34].

The carrier mobility (μ) can be conveniently determined by use of electrical resistivity measurement technique of film. The electrical resistivity can be measured using either a four-point probe or van der Pauw measurement technique [22]. The van der Pauw method is a commonly used technique in the Hall measurement systems for measuring electrical resistivity [33-36].

The van der Pauw method is a commonly used technique in the Hall measurement systems for measuring electrical resistivity. The main purpose of the

resistivity measurement is to measure the sheet resistance (R_S) . To make a measurement, a voltage is applied between the contacts placed and the current flowing across the opposite place is measured as shown in Figure 2. 19 (a) . Subsequently, a magnetic field is applied in the direction perpendicular to the sample and the Hall voltage (V_H) is measured as shown in Figure 2.19 (b).

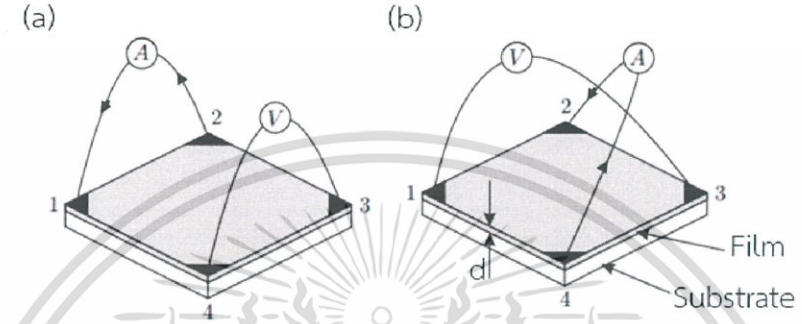

Figure 2.19 Schematic diagram showing for the van der Pauw and Hall measurement [24]

The resistance for each measurement can be found using Ohm's law (V=IR) such as $R_{12,34}=V_{34} / I_{12}$ [32,35]. The van der Pauw method consists of two measurements of resistivity such as one measured along a vertical place ($R_{vertical}$) and one measured along a horizontal place ($R_{horizontal}$).

$$R_{vertical} = \frac{R_{12,34} + R_{34,12} + R_{21,43} + R_{43,21}}{4} \quad (2.38)$$

$$R_{horizontal} = \frac{R_{23,41} + R_{41,23} + R_{32,14} + R_{14,32}}{4} \quad (2.39)$$

The sheet resistance (R_S) can be calculated using the van der Pauw equation [32,33,35]:

$$\exp(-\pi R_A / R_S) + \exp(-\pi R_B / R_S) = 1 \quad (2.40)$$

From the van der Pauw technique can be defined the sheet carrier concentration (n_s) by measuring the Hall voltage (V_H). The Hall voltage can be calculated in terms of the sheet concentration [32,33,35]:

$$n_S = \frac{IB}{qV_H} \tag{2.41}$$

A formula for the majority carrier mobility (μ_s) can be defined in terms of sheet resistance and sheet concentration [32,33,35]:

$$\mu_S = \frac{1}{qn_S R_S} \tag{2.42}$$

In this thesis, Hall voltage was investigated by a Hall Effect measurement System, Ecopia model HMS-3000. The measurements require four ohmic contacts to be placed on the sample, the sample should be uniform and its thickness should be accurate [35].

2.8.4 Electrical resistivity and Seebeck coefficient measurement

Ulvac ZEM - 3 is a commercially usable instrument for simultaneous measurement of both Seebeck coefficient and electrical resistivity of Bi-Te films. Seebeck coefficient measurement is to measure the voltage difference (ΔV) across a sample under a fixed temperature gradient (ΔT) at some fixed temperature (T) based on a static DC method. The Seebeck coefficient is the slope of a voltage versus temperature-difference curve, as defined in Equation 2.27 is actually the ratio of the gradients of V and T. The diagram is shown in Fig. 2.20.

$$S = -\frac{\Delta V}{\Delta T} \tag{2.43}$$

The temperature difference (ΔT) between two ends of the film was varied as 10°C, 20 °C and 30°C.

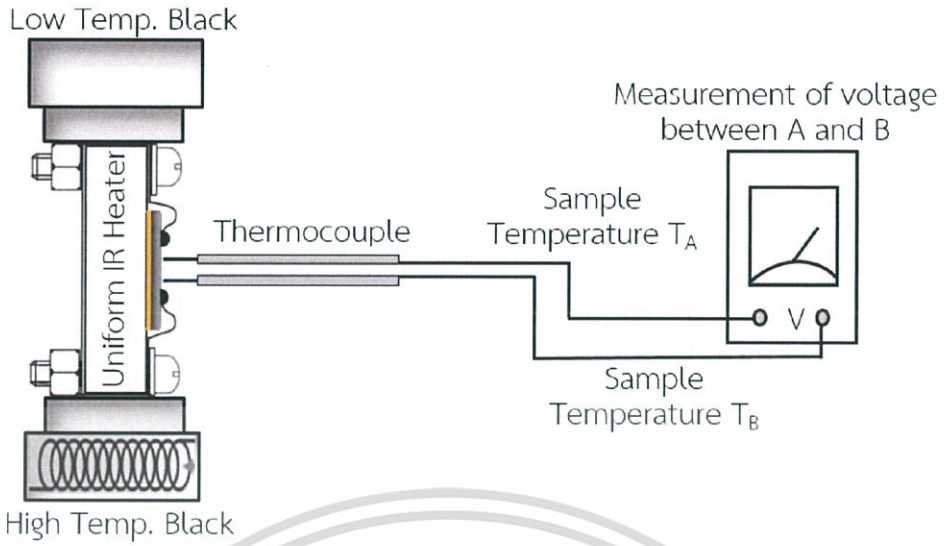

Figure 2.20 Diagram of high temperature Seebeck coefficient measurement.

The electrical resistivity of Bi-Te films is measured via the DC four-terminal method by applying a constant current (I) through the sample and measuring the voltage difference (ΔV) between thermocouples A and B as shown in Figure 2.21.

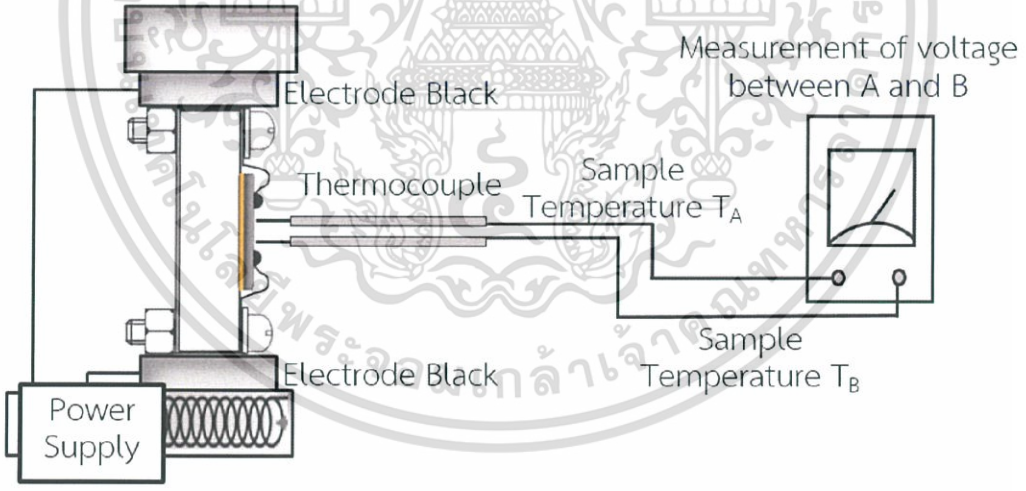

Figure 2.21 Diagram of high temperature electrical resistivity measurement.

Ohm's law is used to calculate the resistance (R) and the resistivity (ρ) of Bi-Te films is calculated by considering the length (L) between the probes and the cross-section area (A) of the specimen, can be defined as

$$V = IR,\ I_{ref} = I_{sample} \tag{2.44}$$

$$R_{sample} = \frac{V_{sample}}{V_{ref}} \times R_{ref} \tag{2.45}$$

$$\rho_{sample} = \frac{R_{sample} \times L_{sample}}{A_{sample}} \tag{2.46}$$

2.9 Literature Reviews

Previously, many researchers have reported the preparation of Bi_2Te_3 films by sputtering with deposition conditions controlled to achieve the stoichiometry of Bi_2Te_3 thin films. Most of research has used co-sputtering and adjusted sputtering powers of Bi and Te targets to control the compositions. However, a control of sputtering parameters using a Bi_2Te_3 target has not been studied yet. It has been reported that there has been a study of the compound targets case. Sun et al. [9] studied the effects of adjusting the Ar working gas pressure and the substrate temperature on the growth and compositions of $FeSb_2$ films by magnetron sputtering. XRD images showed the structures and orientations of thin films as illustrated in Figure 2.22. From EDX results reveal that the Fe:Sb ratios of the three $FeSb_2$ films are about 33:67, 38:62 and 39:61, respectively. They found that the deposition sputtered working pressure and substrate temperature affected the structures, compositions and orientations of thin films.

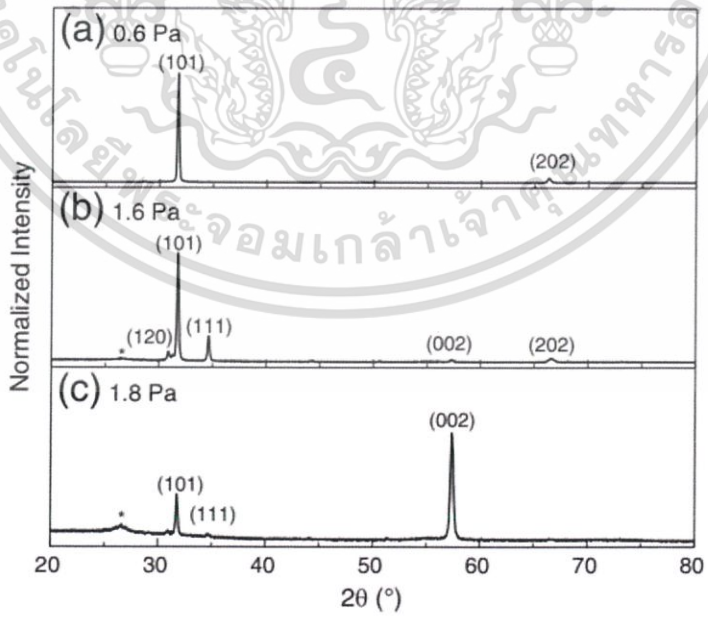

Figure 2.22 Normalized XRD patterns of three $FeSb_2$ films grown at 350 °C with different Ar pressures of (a) 0.6 Pa, (b) 1.6 Pa and (c) 1.8 Pa, respectively.

H. J. Lee et al. [1] studied the electrical resistivity of Bi-Te thin films fabricated by RF magnetron co-sputtering. The electrical resistivity was very dependent on the Te content.

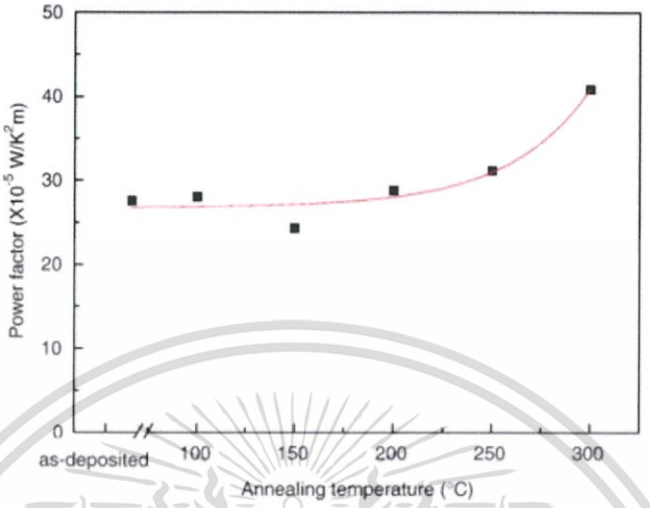

Figure 2.23 Influence of annealing temperature on power factor of films

The films exhibits positive Seebeck coefficients when the Te content was more than 80%. The films with 65% Te content obtained the maximum power factor of 3.7×10^{-4} W/K^{2}m. Z.-k. Cai et al. [5] proposed that the Bi_2Te_3 films were fabricated by co-sputtering-method, followed by annealing method between 250 °C to 450 °C. They reported that at the annealing temperature of 275 °C, the maximum power factor of 3.288×10^{-4} W/K^{2}m was obtained. These results demonstrate that high-performance Bi_2Te_3 thin films can be prepared by DC and RF magnetron co-sputtering with post-annealing. H. Huang et al. [3] proposed the influence of the target composition and annealing temperature (100—300°C) on thermoelectric properties of bismuth telluride films grown via radio frequency magnetron sputtering. Stoichiometric Bi_2Te_3 thin films were deposited using sputtering target with a Te-content of 45 at.%. The power factor of the films measured at room temperature reached the highest value as 4×10^{-4} W/K^{2}m, which was annealed at 300 °C as shown in Figure 2.15.

T. Khumtong et al. [18] studied the influence of the Ar flow rate (50 - 120 sccm) and the pre-heat temperature of the substrate (150 - 450 °C) on the Te content (%Te) of flexible Sb_2Te_3 thin film. They reported that the pre-heat temperature of the substrate affected the structures and compositions of thin films as shown in Figure 2.24.

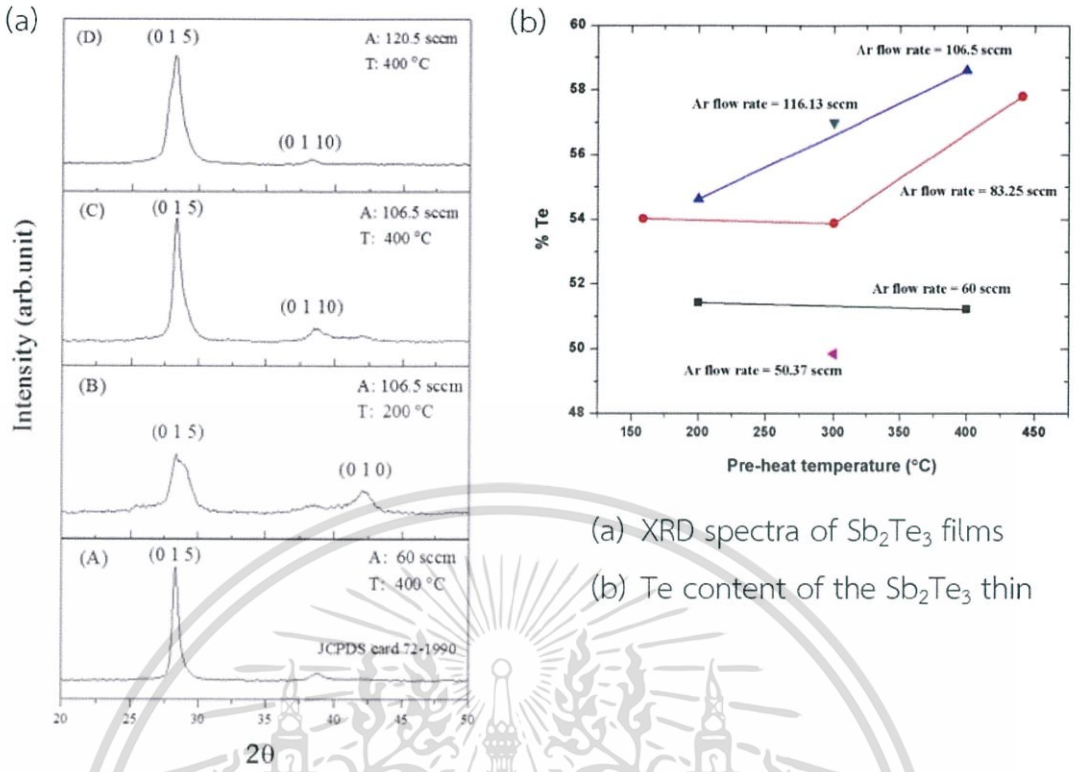

(a) XRD spectra of Sb_2Te_3 films

(b) Te content of the Sb_2Te_3 thin

Figure 2.24 The influence of the pre-heat temperature

Most researchers have studied bismuth telluride films that were prepared by DC or RF magnetron co-sputtering and they would study only one deposition parameter while keeping the other deposition parameters constant because increases in the deposition parameters have an effect on the number and the cost of experiments needed to conduct more research [26]. In this thesis, Bi-Te thin films were deposited using a Bi_2Te_3 target by RF magnetron sputtering but this method is different from a co-sputtering technique. It was difficult to control the stoichiometry of Bi-Te films due to the difference in [Bi] and [Te] sputtering yields [8]. Study of the effects of sputtering parameters, including the Ar gas flow rate (sputtering pressures) and pre-heating temperature and the annealing temperature on chemical composition of [Bi]:[Te]. However, we used a statistical technique to optimize the deposition parameters to achieve the stoichiometric Bi_2Te_3 thin films. An alternative for a study of the effects of deposition parameters, including the Ar gas flow rate and the annealing temperature on the response (Te content) of thin films is response surface methodology (RSM).

Finally, the purpose of this thesis is to understand the key parameters of maximizing thermoelectric power factor in Bi-Te thin films by an in-depth investigating on the chemical composition, structural and thermoelectric properties of thin films.

Chapter 3

Research methodology

This chapter explains the deposition of bismuth-telluride (Bi-Te) films on a polyimide (Kapton®) flexible substrate using magnetron sputtering technique.

3.1 Deposition of Bi-Te thin films

3.1.1 Substrate Preparation

Thin film thermoelectric devices provide the possibility of using flexible substrates and can be applied to diverse fields. Polyimide (Kapton®) has been widely reported with high –performance flexible substrates due to low thermal conductivity (0.12 $Wm^{-1}K^{-1}$), a wide range of temperatures, thermal stability and low coefficient of thermal expansion ($12x10^{-6}\ K^{-1}$). The procedure in preparation of substrate is shown in Figure 3.1. The flexible substrates were attached to a glass slide with a size of 2.5 cm x 7.5 cm as exhibited in Figure 3.1(a). The flexible substrates were cleaned with methanol in an ultrasonic bath for 15 min in order to remove the residual paste from the substrate cases and then the substrates were cleaned with deionized water for 5 min as exhibited in Figure 3.1(b). The flexible substrate was blown and dried with N_2 gas after a final ultrasonic bath as exhibited in Figure 3.1(c).

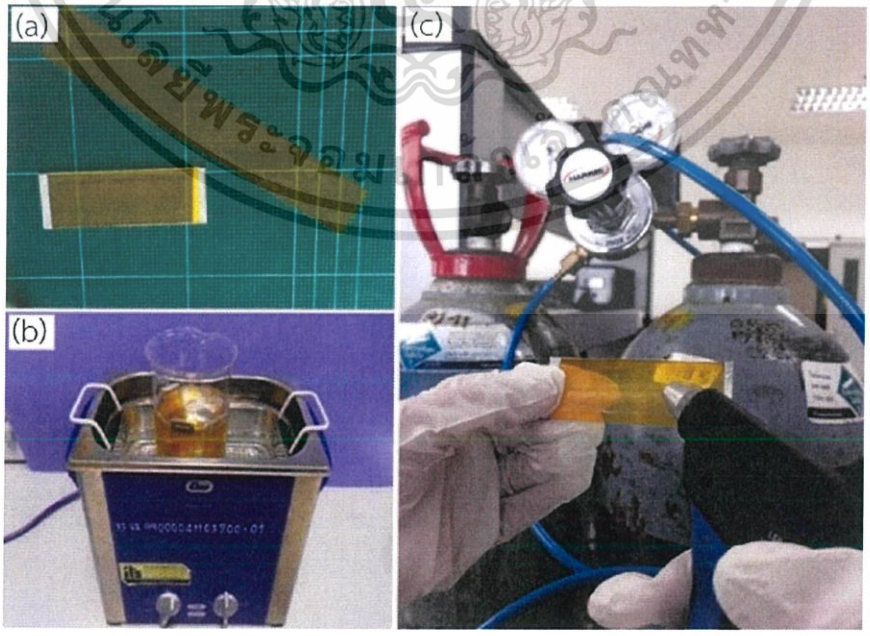

Figure 3.1 Preparation of polyimide flexible substrate.

3.1.2 Thin Film Preparation

Magnetron sputtering system with RF and DC deposition capabilities was used to fabricate the Bi-Te films. The schematic diagram of sputtering system together with its all main components is shown in Figure 3.2. An alloy bismuth telluride target (Bi_2Te_3 purity of 99.9%, Stanford Advanced Materials) with a diameter of 3 inches was used in the sputtering system and the target-substrate distance was maintained at 50 mm.

The base pressure of the vacuum chamber was below 2.7×10^{-5} Pa using the vacuum pump system. The vacuum pump system has the ability to exhaust a vacuum chamber from atmosphere down to the high vacuum, consists of a rotary pump and diffusion pump as shown in Figure 3.3. The rotary pump was used to achieve a rough processing chamber from atmosphere to a medium vacuum, down to about 10^{-2} mbar. The diffusion pump was used to achieve a higher vacuum in 10^{-5}-10^{-6} mbar.

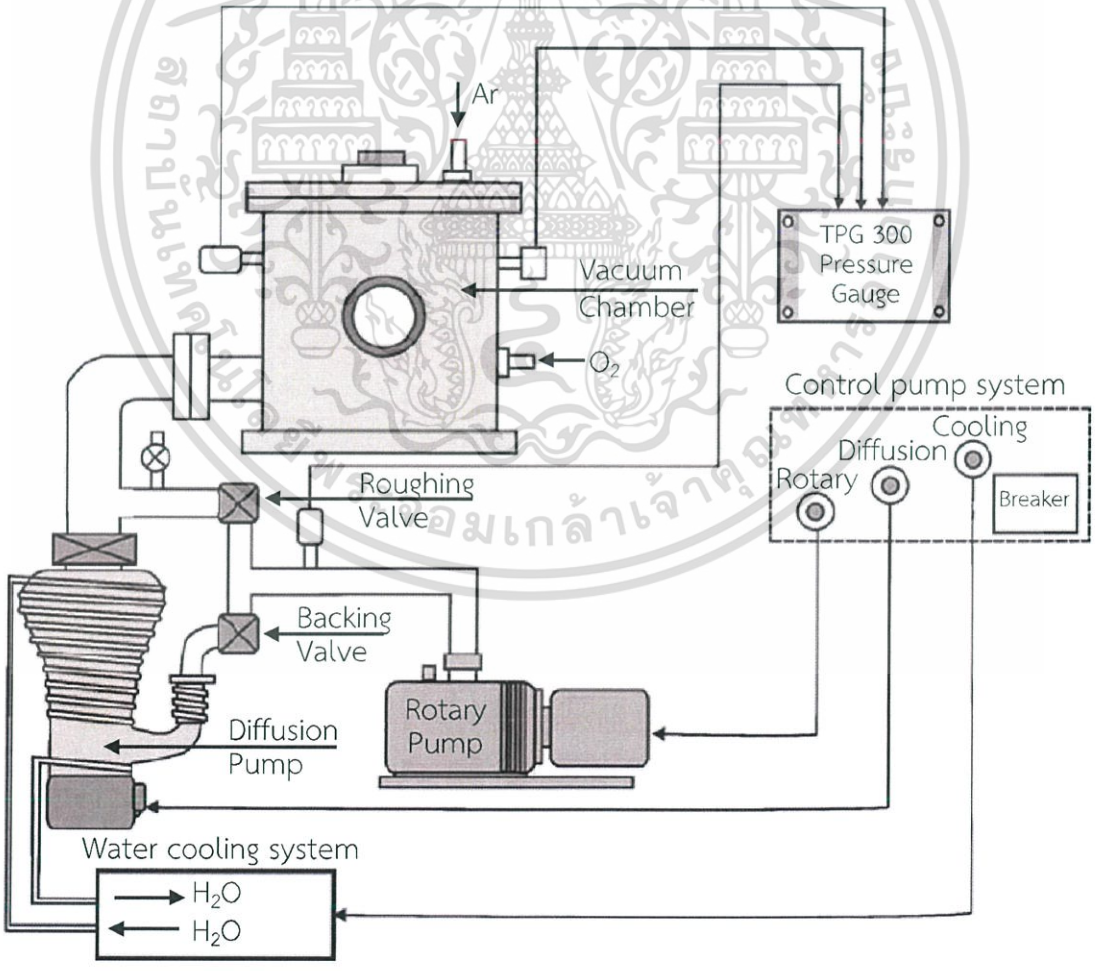

Figure 3.2 Schematic diagram of vacuum system in the sputtering system.

3.1.2.1 Starting the vacuum system

The substrate was put into the sample holder and the magnetron sputtering process sequence is as follows:

1) Switch on the main power (No. 1).
2) Switch on the rotary pump (No. 2).
3) Open the chamber-roughing valve (No. 3) and observe the pressure. When the gauge shows a pressure of 6×10^{-1} mbar or less, close the roughing valve.
4) Open the backing valve (No. 4), returning the vacuum system to stand-by. When the pressure in the chamber drops to below 2×10^{-3} mbar, open the diffusion pump (No. 5).
5) Switch on the water cooling system (No. 6). The water provides cooling for the diffusion pump.
6) After 45 min, the diffusion pump should be warmed up. The vacuum system will then be on stand-by for pumping the chamber.
7) Open the high vacuum (No. 7). When the pressure in the chamber drops to below 2.7×10^{-5} mbar the system is ready to begin the magnetron sputtering process (base pressure).
8) For Bi-Te thin films were prepared using RF sputtering. Set the RF power at 45 W (No. 8).
9) Set the sputtering pressure (Ar gas flow rate) in the chamber to that desired.
10) Pre-sputtered for 10 minutes before deposition with the shutter for the sputter gun closed.
11) Open the shutter and start the deposition process on the specified time.
12) Close the shutter to stop the deposition process.
13) Turn off the power supply, shut off the Ar gas flow.
14) Switch off the diffusion pump (No. 9) leave the diffusion pump cools down about 10 minutes, then switch off the high vacuum (No. 10) leave about 30 minutes.
15) Turn off the water cooling system.
16) Open air in the chamber (No. 11) and remove the sample from the sample holder.
17) Bi-Te thin films were prepared using DC sputtering. Set the DC power at 45 W (No.12) and then follow steps 9 to 16, respectively.

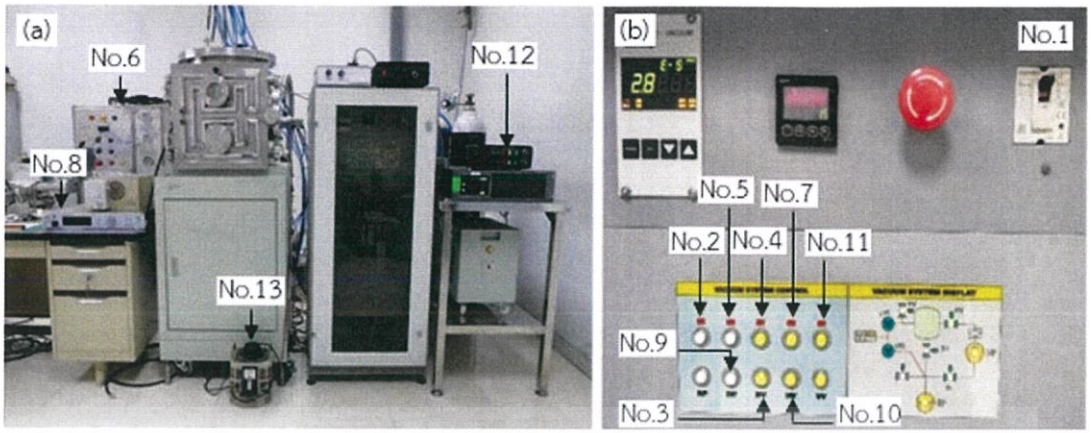

Figure 3.3 (a) schematic diagram of sputtering system (b) monitor of operating system

3.1.2.2 Pre-heating substrate process

In the experiment, for studying the influence of pre-heating substrate on the chemical composition, the structural and the thermoelectric properties of Bi-Te thin films on flexible substrates prepared by RF and DC magnetron sputtering. Temperatures were in the range of 150°C to 400°C and a common heating time of 1 h was used, a sequence is as follows:

1) Substrates were prepared and loaded into the sample holder.
2) Set the base pressure in the chamber to that obtained to below 2.7×10^{-5} mbar in step 1 to 7.
3) The substrate was heated by a halogen lamp (No. 13) and then beginning deposition process.

3.1.2.3 Annealing temperature process

In the experiment, for studying the effect of annealing temperature on the chemical composition, the structural and the thermoelectric properties of Bi-Te thin films on flexible substrates. Temperatures in the range of 250°C to 320°C were investigated and a common annealing time of 1 h was used, a sequence is as follows:

1) After the deposition process, the samples were annealed in a N_2 atmosphere.
2) Set the base pressure in the chamber to follow step 1 to 7.
3) And then, set the N_2 atmosphere in the chamber to about 6×10^{-3} mbar.
4) Set the annealing temperatures by a halogen lamp.

3.2 Effect of sputtering parameters on Bi-Te thin films

In this work, the Bi-Te thin films were deposited on flexible substrates using a Bi_2Te_3 target. RF and DC magnetron sputtering techniques were used. This thesis focuses on the study of the effects of sputtering parameters, including the Ar gas flow rate (sputtering pressure) , the annealing temperature and pre- heating substrate on chemical composition of [Bi]:[Te], following objectives:

1) To study the synthesis of Bi-Te thin films deposited by RF magnetron sputtering process and the investigation of the effect of sputtering pressures on chemical composition, structural and thermoelectric properties of Bi-Te thin films on flexible substrates.

Table 3.1 Conditions used for the deposition of Bi-Te films by RF magnetron sputtering with different sputtering pressures.

Object	Specification
Target	Bi_2Te_3 purity (99.9%)
Substrate	Polyimide
Base pressure	$2.7x10^{-5}$ mbar
Sputtering pressure	0.6 - 1.6 Pa
RF Power	45 W
Deposition time	30 min.

2) To study the synthesis of Bi-Te thin films deposited by RF magnetron sputtering process and RSM was used for a statistical study of the effects of Ar gas flow rate (sputtering pressure) and annealing temperature on chemical composition, structural and thermoelectric properties of Bi-Te thin films on flexible substrates.

Table 3.2 Conditions used for the deposition of Bi-Te films by RF magnetron sputtering with different Ar gas flow rates and annealing temperature.

Object	Specification
Target	Bi_2Te_3 purity (99.9%)
Substrate	Polyimide
Base pressure	$2.7x10^{-5}$ mbar
Ar gas flow rate	100.5-106.5 sccm
Annealing temperature	250-320 °C

Object	Specification
RF Power	45 W
Deposition time	30 min.

3) To study the influences of pre-heating substrate on chemical composition, structural and thermoelectric properties of Bi-Te thin films on flexible substrates prepared by RF and DC magnetron sputtering. Comparison of the thermoelectric properties of flexible Bi-Te deposited by RF and DC magnetron sputtering have been studied.

Table 3.3 Conditions used for the deposition of Bi-Te films by RF and DC magnetron sputtering with different pre-heating temperature.

Object	Specification	
Target	Bi_2Te_3 purity (99.9%)	
Substrate	Polyimide	
Base pressure	$2.7x10^{-5}$ mbar	
Sputtering pressure	$1.4x10^{-2}$ mbar (1.4 Pa)	
Pre-heating substrate	150-350 °C	
Supply	RF	DC
Power	45 W	45 W
Deposition time	30 min	5 min
Thickness	1.3 μm	1.3 μm

3.3 Characterization of Bi-Te thin films

The surface microstructure morphology and composition of the Bi-Te films were investigated by field emission scanning electron microscopy (FE-SEM, JSM-7001F) and energy dispersive spectroscopy (EDS), respectively. The crystalline structure was measured by grazing incidence X-rays diffraction (Bruker AXS D8 Discover). Mobility and carrier concentration were obtained by the Van der Pauw method with a Hall effects measurement system (Ecopia, HMS3000). Finally, the Seebeck coefficient and electrical conductivity were concurrently measured at room temperature and up to 300 °C by ZEM-3 (ULVAC-RIKO).

3.3.1 Field emission scanning electron microscopy (FE-SEM) and Energy Dispersive X-rays Spectrometer (EDS)

Electrons are emitted from a field emission source and accelerated in a high electrical field gradient. The electron beam is focused and deflected to a narrow scan beam that bombards the sample, resulting in both improved spatial resolution and minimized sample charging and damage. The resolution of a scanning electron microscope is about 1.2 nm at 30 kV. The accelerating voltage is changeable in a range from 0.5 to 30 kV.

The sample is scanned by an electron beam. The electrons interact with atoms in the sample, resulting to secondary electrons, X-rays and backscattered electrons are ejected from the sample. After that, the detector catch the secondary electrons produces an electronic signal and transform to the image, as shown in Figure 3.4.

The X-rays detector is attached to the FE-SEM equipment, which the sample is bombarded with a 100-200 keV electron beam. In this works, the surface morphology of the Bi-Te films was investigated by a scanning electron microscope (FE-SEM) model JSM-7001F operating at 15 kV. The element compositions of all thin film samples were investigated by a JOEL electron probe microanalyzer (EPMA) model INCA PentaFETx3 equipped with a field emission scanning electron microscope as shown in Figure 3.4 (b). The sample was cleaved with a size of 8 mm x 8 mm and attached to the sample holder. The average element compositions were measured with an accuracy of ±2% in 3 different locations on each sample using EDX analysis.

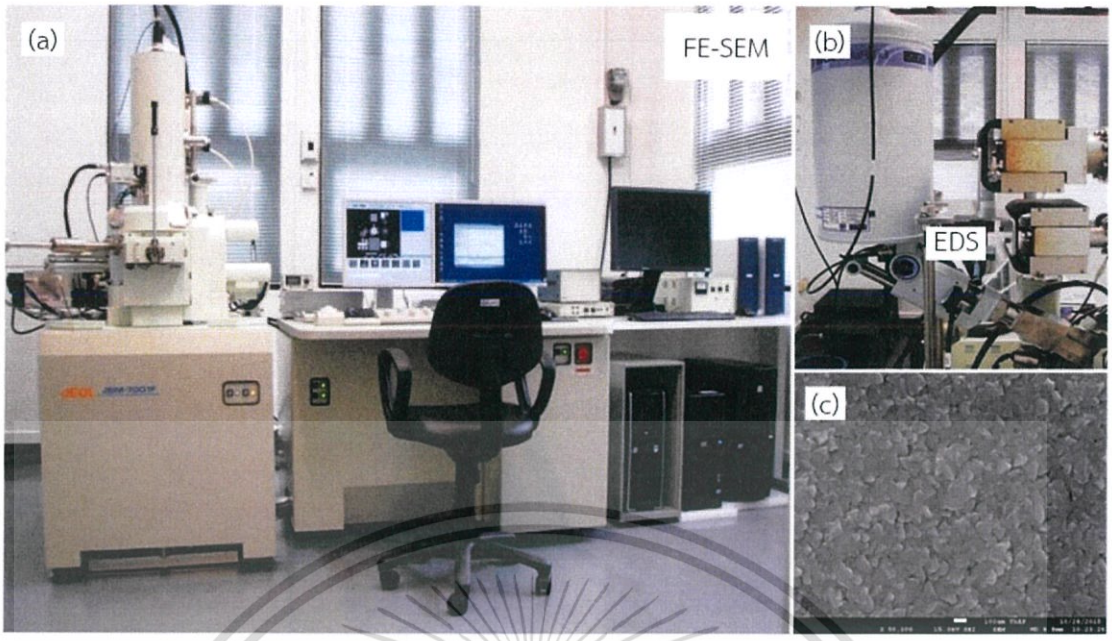

Figure 3.4 (a) FE-SEM model JSM-7001F (b) EDS model INCA PentaFETx3 (c) FE-SEM surface images of Bi-Te thin film

3.3.2 X-rays Diffraction (XRD)

X- rays interact with the atoms in a crystal of film, which produces a diffraction pattern of X- rays at specific angles from each set of lattice planes in a film as shown in Figure 3.5. The unit cell structure of film can be determined by analyzing the diffracted X-rays beams in correspondence with the Bragg's law.

In this works, the crystalline structure was measured by grazing incidence X-rays diffraction technic (D8 DISCOVER- Bruker AXS). A power of 40 kV and 40 mA was used for X-rays source, which produced K–alpha radiation from copper $(\mathrm{Cu} - \mathrm{K}_{\alpha})$. The data collection was performed in a range of angle (2θ) from 20° to 70° with a step width of 0.02°/s. The sample was cleaved with a size of 1 cm x 1 cm and attached to the sample holder. The XRD pattern was compared to Powder Diffraction File (PDF) by the Joint Committee on Powder Diffraction Standard, (JCPDS). The JCPDS card used are 44-0667, 72-2036 and 08-0027 for Bismuth Telluride.

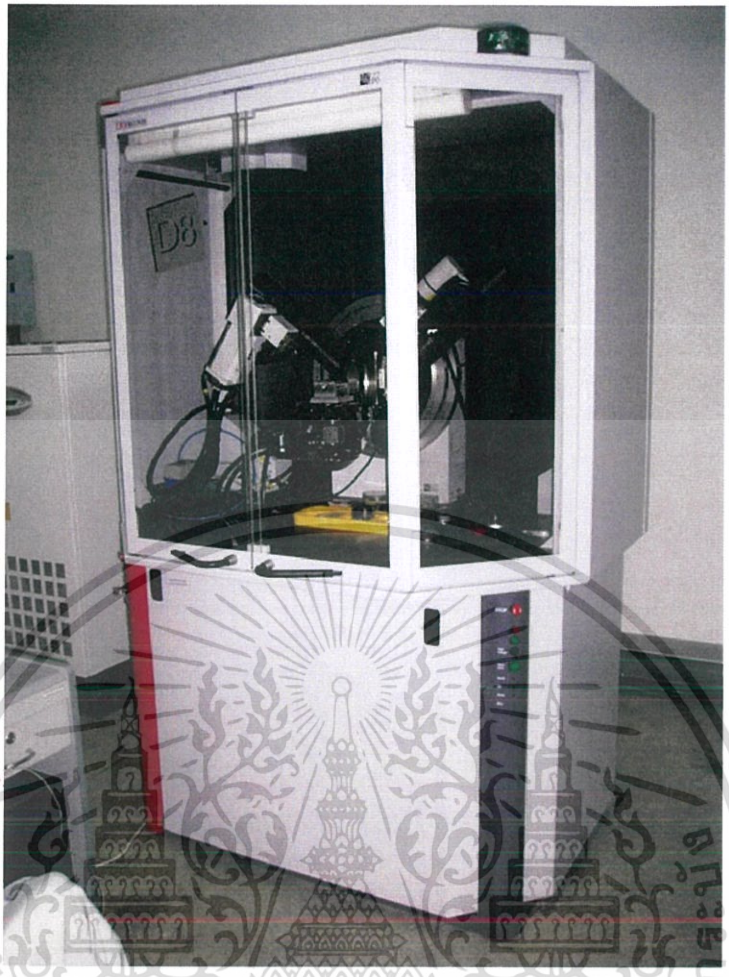

Figure 3.5 A Bruker-AXS D8 Vario Advance-UNLV

3.3.3 Ecopia HMS-3000

The mobility and carrier concentration of the films were measured at room temperature using Hall measurement system model Ecopia HMS-3000, operating in the Van der Pauw sample geometry as shown in Figure 3.6 (a).

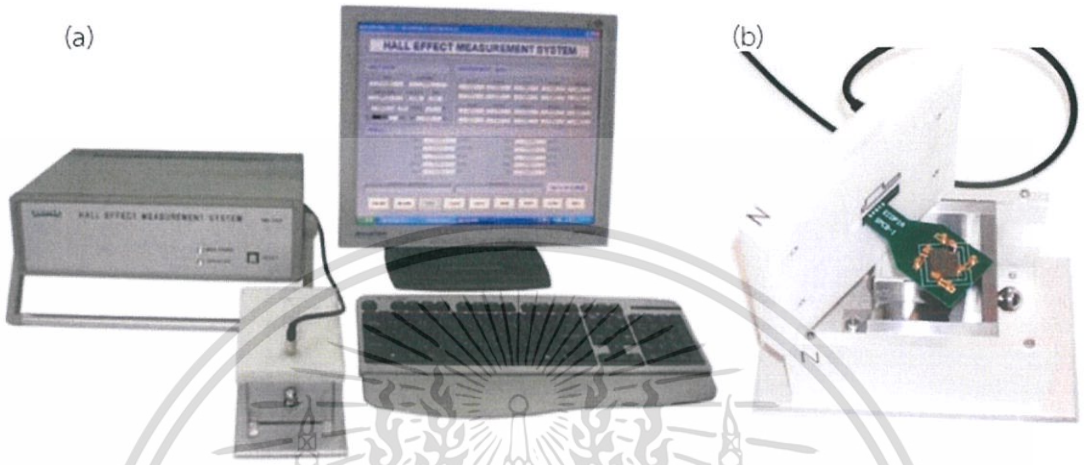

Figure 3.6 (a) Ecopia HMS-3000 (b) Sample mounting parts of HMS-3000 system.

In this works, the mobility and carrier concentration were measured using Hall measurement system with a magnetic field of 0.55 Tesla. The sample was cleaved with a size of 8 mm x 8 mm and attached to the sample holder as shown in Figure 3.5 (b). The software of HMS-3000 was run on the computer and automatically calculating the carrier concentration, mobility, and resistivity of the sample.

3.3.4 Ulvac ZEM-3

The commercial equipment (ZEM-3, Ulvac, Inc.) was used to measure the electric resistivity and Seebeck coefficient of the samples. All measurements were controlled by a computer and automatic measurement at a specified temperature for different temperatures. The estimated accuracy of the measured Seebeck coefficient and electrical resistivity were ±5%. The sample was attached to the sample holder with a size of 3 mm x 12 mm as exhibited in Figure 3.7.

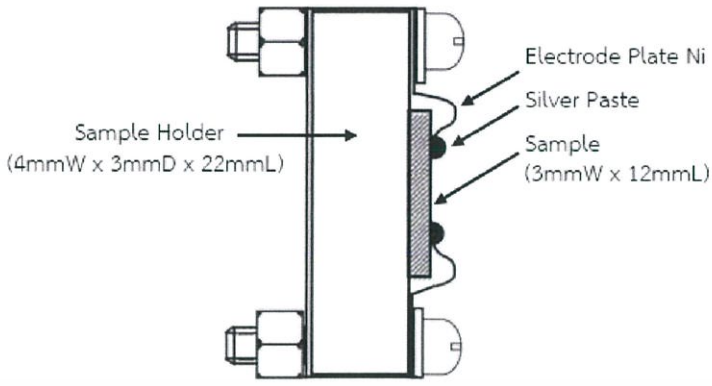

Figure 3.7 Diagram of the thin film attachment

In this works, the electric resistivity and Seebeck coefficient of the Bi-Te films were measured at room temperature (25°C) and applied temperature range of 50°C to 300°C.

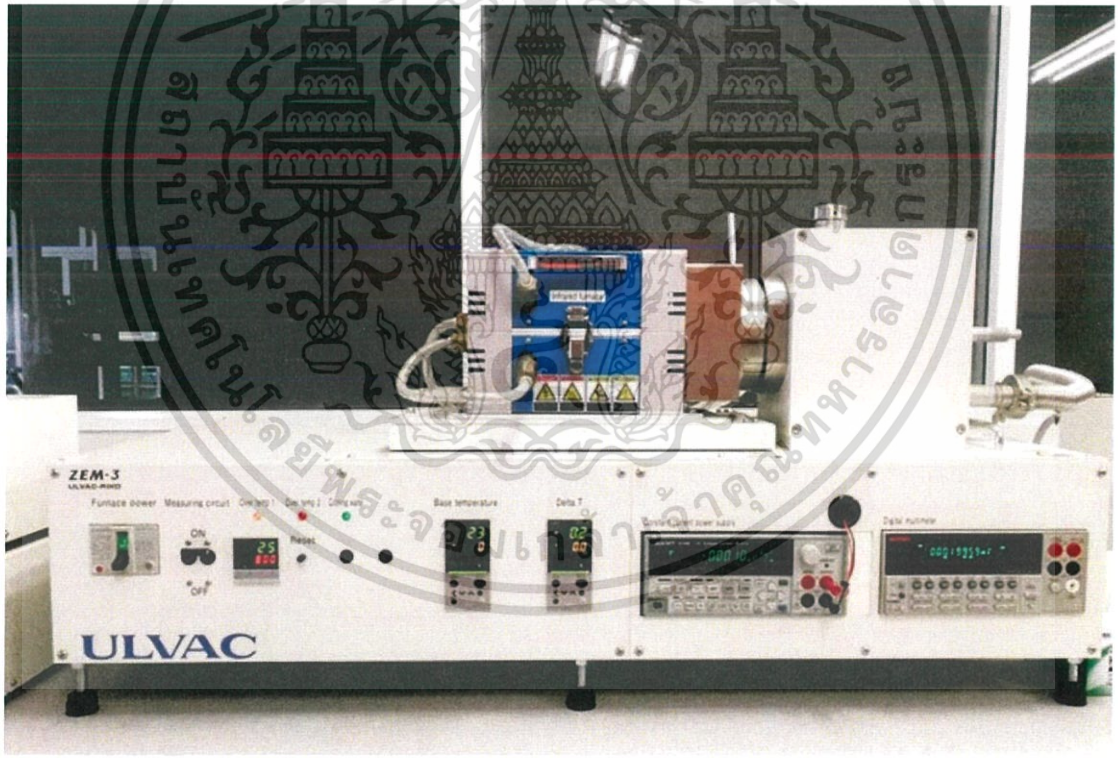

Figure 3.8 Ulvac ZEM-3

Chapter 4

Main Results and Discussion

This chapter explains the characterization of Bismuth-telluride (Bi-Te) films deposited under the various conditions of sputtering parameters, including sputtering pressures (0.6–1.6 Pa), annealing temperature (250–320 °C) and pre-heating temperature (150–400 °C).

4.1 The effect of sputtering pressures on Bi-Te thin films deposited by RF magnetron sputtering process.

4.1.1 Compositional analysis

The effects of deposition pressure on the Te content of thin films were investigated. Fig. 4.1 shows the %Te content of thin films under the different sputtering pressures of 0.6, 0.8, 1.0, 1.2, 1.4 and 1.6 Pa. These average element compositions were measured by EDS in three different areas.

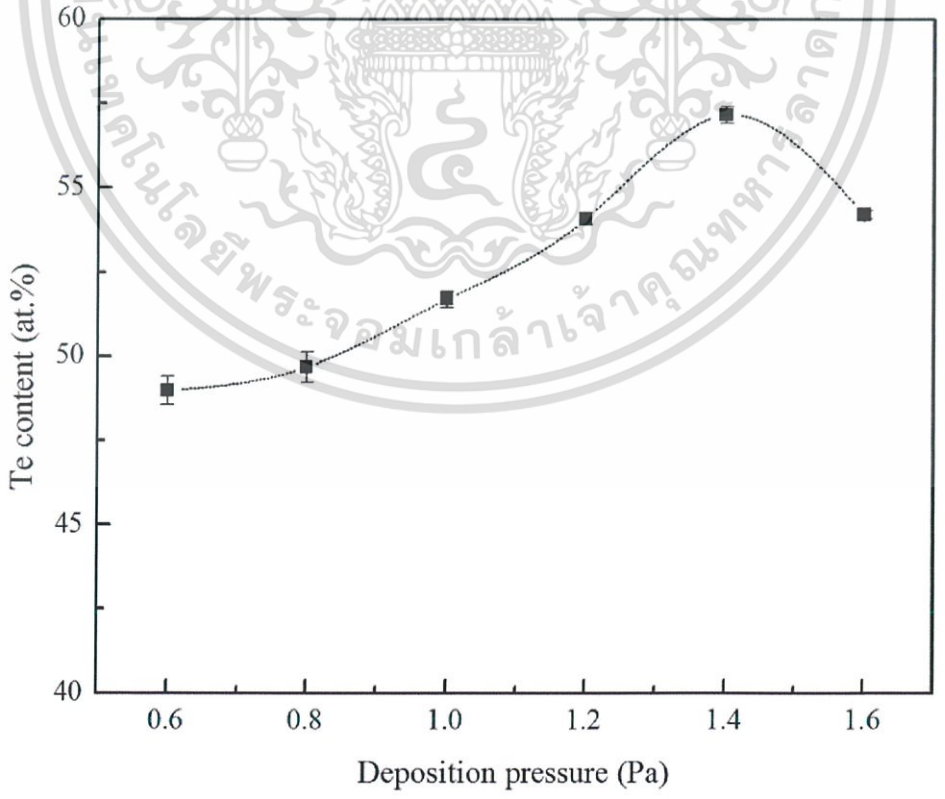

Figure 4.1 Te content (at.%) of the Bi-Te thin films.

It was found that all the deposited thin films were deficient in their Te element. This result indicated that sputtering pressure alone could not control the stoichiometric composition of Bi_2Te_3 thin films. In general, good thermoelectric properties of Bi-Te thin films depend on stoichiometric Bi_2Te_3 thin films ([Bi]:[Te] = 40:60) [2,7]. It can be seen in Fig. 4.1 that the deposited thin films at 0.6 Pa were non-stoichiometric Bi_2Te_3 thin films, with the chemical composition of Te content lower than 60 at.%. The Te content was poor due to the sputtering yields of Te being lower than Bi [2,8], as shown in Fig. 4.2(A).

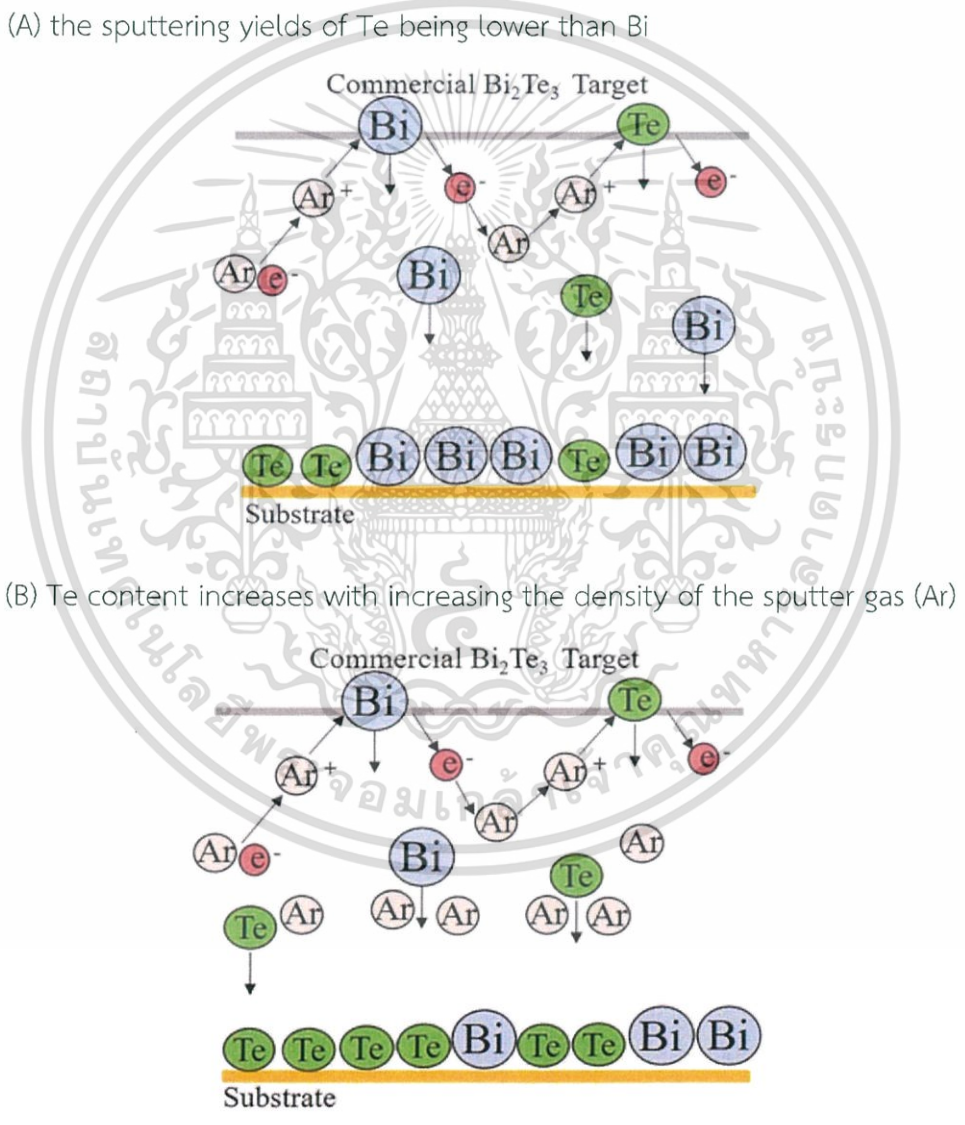

Figure 4.2 Schematic representation of deposition effects on Te content: (A) the sputtering yields of Te being lower than Bi, (B) Te content increases with increasing the density of the sputter gas (Ar).

When the sputtering pressures increased from 0.8 to 1.4 Pa, the Te content of thin films increased from 49 to 57 at.%. The increase of Te content is due to the density of the sputter-gas (Ar) also increases the collision probability between sputtered particles [10]. In this work, the sputtering target composition consisted of bismuth (Bi) and tellurium (Te) elements as Bi_2Te_3. Typically, the atomic mass of the Bi element is larger than Te. When the sputter-gas pressure increases, the sputter-gas ions (Ar^+) are reflected as neutral atoms [10]. Thus, the Bi elements were obstructed by the Ar gas increase, thereby affecting the composition and film structure as shown in Fig. 4.2 (B). However, the Te content of the thin film decreased at 54 at.%Te as the sputtering pressure increased from 1.6 Pa. The decrease of Te content may be both Bi and Te elements were obstructed when Ar gas pressure is relatively high.

4.1.2 Surface morphology and crystallinity

Three selected samples with various Te contents and Ar gas pressures: (A) 49 at.%Te (P=0.8 Pa), (B) 54 at.%Te (P=1.6 Pa) and (C) 57 at.%Te (P=1.4 Pa) were measured for surface morphology, crystal and chemical structures using FE-SEM and XRD. Fig. 4.3 shows the surface morphology of Bi-Te thin films from various sputtering pressures and Te contents. As shown in Fig. 4.3(A), the Bi-Te thin film with the sputtering pressure of 0.8 Pa has a smooth surface. As the sputtering pressure increases, it was found that grain boundary clearly affects the surface diffusion of the adatoms, as shown in Fig. 4.3(B) and (C). Normally, the collision probability between sputtered particles and gas particles is intensified while the increase of sputtering pressure causes the mean free path of sputtered particle to be reduced. Particles with lower kinetic energy have insufficient surface mobility to aggregate and grow [10,11].

(A) 49 at.%Te (P=0.8 Pa)

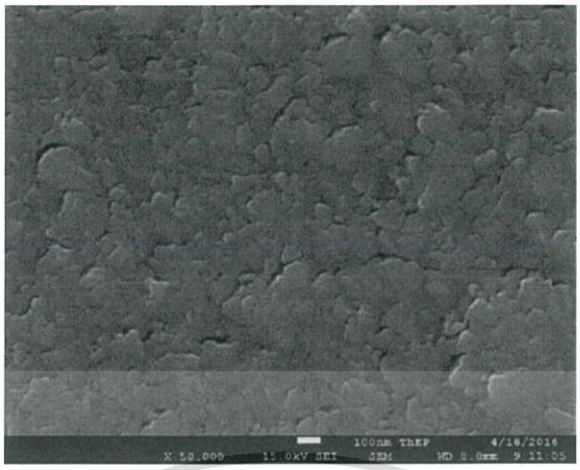

(B) 54 at.%Te (P=1.6 Pa)

(C) 57 at.%Te (P=1.4 Pa)

Figure 4.3 Top view FE-SEM images of the Bi-Te thin films at various Te contents and Ar gas pressures: (A) 49 at.%Te (P=0.8 Pa), (B) 54 at.%Te (P=1.6 Pa) and (C) 57 at.%Te (P=1.4 Pa)

Figure 4.4 shows the XRD patterns of the Bi-Te films with various sputtering pressures and Te contents. As seen from Fig. 4.4(A), the thin film has a peak corresponding to the (014), (108) and (0012) planes in the BiTe phase (JCPDS card 44-0667), located at 27.568°, 38.040° and 45.285°.

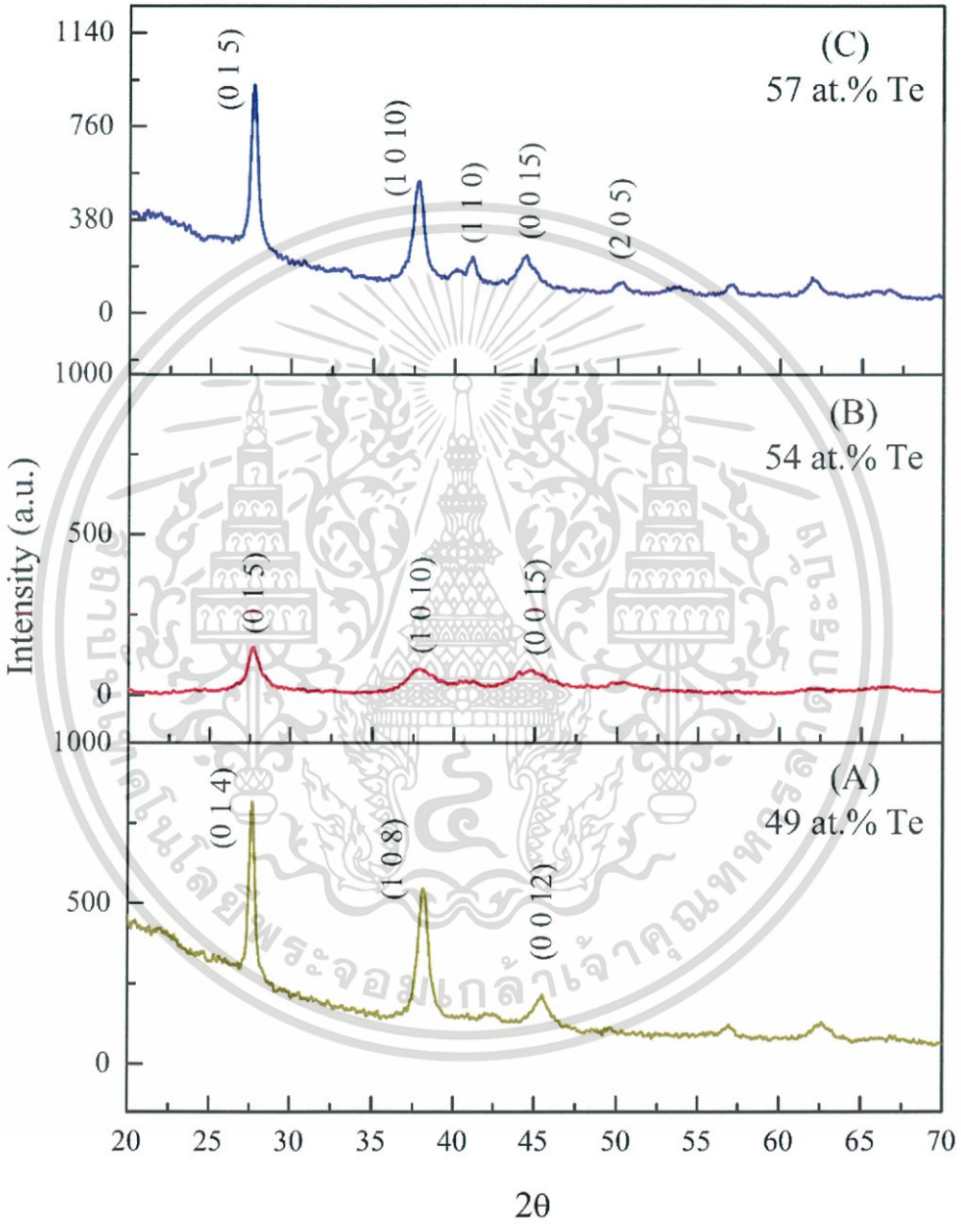

Figure 4.4 XRD patterns of the Bi-Te thin films according at various Te contents and Ar gas pressures: (A) 49 at.%Te (P=0.8 Pa), (B) 54 at.%Te (P=1.6 Pa) and (C) 57 at.%Te (P=1.4 Pa)

The peak positions clearly change from the BiTe phase to the peak of (015), (1010) and (110) planes in Bi_2Te_3 phase (JCPDS card 72-2036), located at 27.663°,37.822° and 40.827°, as shown in Fig. 4.4(C), when the Te content of the film increases from 49 to 57 at.%. It was found that the intensities of other small peaks improve, such as (0015) and (205), located at 45.563° and 50.039°, when the Te content of the film increased to a nearly stoichiometric ratio.

The crystallite size (D) of thin films grown on flexible substrates was calculated by the Scherrer's formula as shown in equation (4.1),

$$D = \frac{k\lambda}{\beta \cos \theta} \tag{4.1}$$

where k is the constant usually taken as 0.94, λ is the X-ray radiation wavelength (0.154056 nm), β is the full width at half maximum (FWHM), and θ is the diffraction angle.

For real polycrystalline materials, the intensity profile tends to be broader because of two main imperfections: Scattering from small coherent domains (Scherrer, 1918), and internal micro-strain associated with variations in the d-spacing of the scattering crystals (Stokes and Wilson, 1944) [36]. Microstrain developed in the film, which is determined from the disarrangement of lattice during their deposition causes variation in shapes and positions for the diffracted lines [12,36]. The dislocation density is the density of imperfections in the crystal during the growth of film. The formation of nano-crystallites is caused by annihilation and recombination of the dislocation [12,13,37]. The microstrain (ε) and the dislocation density (ρ) were evaluated using the equations (4.2) and (4.3), respectively.

$$\varepsilon = \frac{\beta \cos \theta}{4} \tag{4.2}$$

$$\rho = \frac{1}{D^2} \tag{4.3}$$

The crystallite size (D), microstrain (ε), and dislocation density (ρ) of the Bi-Te films have been calculated using the preferred orientation of the XRD peak, and the values are given in Table 4.1. The crystallite size increased from 16.13 nm to

20.08 nm as the sputtering pressure was increased from 0.8 to 1.4 Pa. The width of the diffraction peak decreases as a result of the decrease in lattice micro-strain and the increase in crystallite size according to the results of the film (A) and (D). The strain of the Bi-Te films decreases from 2.24×10^{-3} to 1.80×10^{-3} lines^{-2}m^{-4}, and the dislocation density decreases from 3.84×10^{15} to 2.47×10^{15} lines/m^2. The microstrain increases to 4.11×10^{-3} lines^{-2}m^{-4} at the film (B), is caused by the non-uniform displacements of the atoms with respect to their reference-positions in the lattice, according to the FESEM [36].

Table 4.1 Analysis of the Bi-Te thin films from XRD patterns.

Film	Te content (at.%)	2θ (°)	Crystallite size, D (nm)	Micro-strain, ε (lines^{-2}m^{-4})	Dislocation density, ρ (lines/m^2)
(A)	49	27.57	16.13	2.24×10^{-3}	3.84×10^{15}
(B)	54	27.66	8.81	4.11×10^{-3}	12.87×10^{15}
(C)	57	27.66	20.08	1.80×10^{-3}	2.47×10^{15}

The result shows clearly that microstrain and dislocation density is inversely proportional to crystallite size. The decrease of microstrain and dislocation density with increasing the sputtering pressure led to a decrease in the concentration of lattice imperfections. As sputtering pressure was increased from 1.4 to 1.6 Pa, the crystallite size of the Bi-Te thin film decreased, while the microstrain and dislocation density increased. The result of small crystallite size in the growth direction of the microstrains, stacking faults, dislocations and point defects is caused by the peak broadening. We suggest that sputtering pressure was increased excessively; it affected the formation of the crystal structure of the Bi-Te thin film. With a relatively high sputtering pressure, a higher flux of reflected neutrals will obstruct the growing film. From the XRD, EDS and the FE-SEM results, appropriate sputtering pressure influences the Te content and crystal quality of the Bi-Te thin films.

4.1.3 Electrical and thermoelectric properties

The carrier concentration and mobility, electrical resistivity, Seebeck coefficient, and power factor (PF) of different Te contents thin films with were

measured at room temperature and are summarized in Table 4.2. PF is a property of material that describes its ability to generate more energy from a given temperature difference. It can be calculated by using the Seebeck coefficient and electrical conductivity $(S^2\sigma)$ at a given temperature.

All of the Bi-Te thin films have a negative Seebeck coefficient, indicating that the thin films were affirmed to be n-type semiconductors. The carrier concentration decreases from 10.40×10^{20} to 6.26×10^{20} cm^{-3} with increasing Te content. Therefore, stoichiometry Bi_2Te_3 plays a vital role in reducing the carrier concentration of the films. The absolute value of the Seebeck coefficient increases from 35 to 119 μV/K and, according to theory, the Seebeck coefficient is inversely related to the carrier concentration, given by equation (2.30)

$$S(T)=\frac{\pi^2 k_B^2 T}{3e}\left[\frac{1}{n}\frac{d\,n(E)}{dE}+\frac{1}{\mu}\frac{d\,\mu(E)}{dE}\right]_{E=E_F} \qquad (2.30)$$

Table 4.2 Summary of the electrical and thermoelectric properties of the Bi-Te thin films at room temperature.

Film	Te content (at. %)	Carrier concentration (cm^{-3})	Carrier mobility (cm^2/Vs)	Electrical conductivity (S/m)	Seebeck coefficient (μV/K)	Power factor (W/K^2m)
(A)	49	-10.4×10^{20}	9.50	15.8×10^{4}	-34.6	1.89×10^{-4}
(B)	54	-8.93×10^{20}	3.93	5.61×10^{4}	-58.2	1.90×10^{-4}
(C)	57	-6.26×10^{20}	6.73	6.74×10^{4}	-118.6	9.49×10^{-4}

In this work, the carrier concentration of the BiTe structure (49 at.%Te) was greater than in the Bi_2Te_3 structure (57 %at.Te), and this result corresponds to research of Caha et.al [17] revealed that the free carrier concentration in BiTe is about one order of magnitude larger than Bi_2Te_3. The carrier mobility of 9.50 cm^2/Vs occurs at film (A), decreases to 3.93 cm^2/Vs at film (B) and changes to 6.73 cm^2/Vs at film (C). According to the XRD analyses, we observed a decrease of the carrier mobility of the Bi-Te thin films at 54 at.%Te as result of poor crystalline quality of the Bi-Te films, as shown in the XRD results.

Generally, carrier mobility in the thin film is limited, owing to the scattering mechanisms at the grain boundaries and in-grain scattering processes [11,18,19]. The FE-SEM results showed that the large grain boundaries of the Bi-Te thin films at 54 at.%Te affected the motion of charge carriers due to grain boundary behavior being similar to barriers to charge carrier [1]. It can be induced that the reduced carrier mobility of Bi-Te thin films depends on grain size and grain boundary. In general, electrical conductivity (σ) depends on both carrier concentration (n) and mobility (μ), as shown in equation (2.7)

$$\sigma = ne\mu_e \tag{2.7}$$

The highest electrical conductivity of film (A) 49 at.%Te (P=0.8 Pa) was obtained because the film has both the highest carrier concentration and the highest mobility. In addition, the electrical conductivity decreases when the Te content of the thin films increases, corresponding to Lee et al. work [6]. Compared to other previous works, the carrier concentration was the same order of magnitude as found in the works of Yuan et al. (-9.5×10^{20} cm^{-3}) [1] and Lee et al. (-3.91×10^{20} cm^{-3}) [6]. However, the mobility was lower than Yuan et al. (12.1 cm^2/Vs) [1], who prepared the bismuth telluride thin films with substrate heating at 350°C. It may indicate improvement of crystallization of the films.

In this work, the highest power factor at room temperature was approximately 9.49×10^{-4} W/K^2m for the Bi-Te thin film at 57 at.%Te without the annealing process. Yuan et al. [1] reported that the bismuth telluride thin films were fabricated by RF magnetron sputtering with oriented layered structure. The power factor at room temperature was obtained at 8.8×10^{-4} W/K^2m. Caiet al. [2] reported that the best Bi_2Te_3 thin film was prepared by a co-sputtering technique with post-annealing. The n-type Bi_2Te_3 thin film had a high power factor of 8.21×10^{-4} W/K^2m with the annealing temperature of 450°C. These results indicated that the value of power factor was close to previous reports.

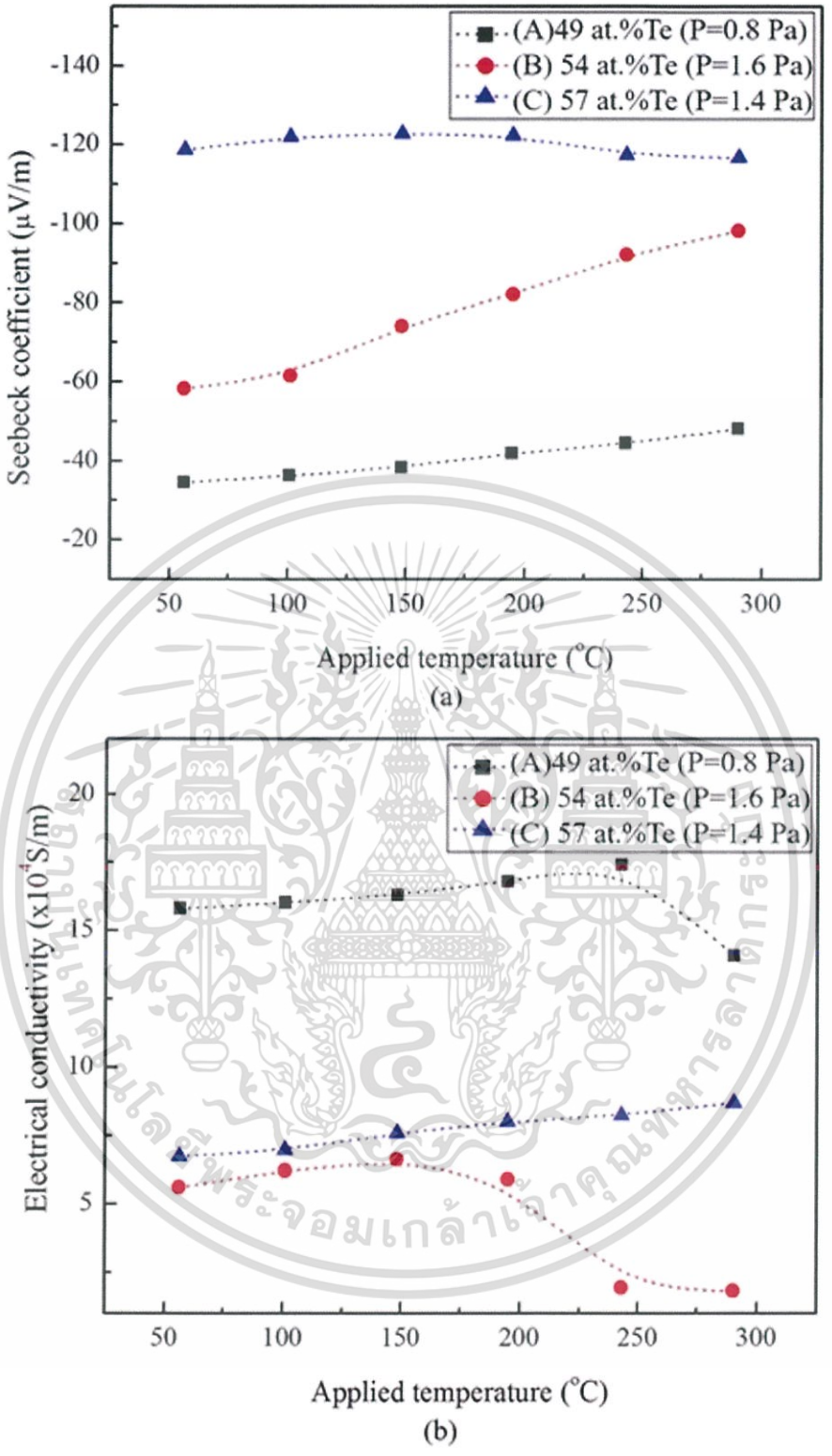

Figure 4.5 Effect of applied temperature on (A) Seebeck coefficient, (B) electrical conductivity of Bi-Te thin film according to different Te contents and Ar gas pressures.

Figure 4.5(A) shows the effect of applied temperature (ranging from 50 to 300 °C) on the Seebeck coefficient of different Te contents thin films. The maximum Seebeck coefficient absolute value, 122 μV/K for the Bi-Te thin film at 57 at.%Te (nearly stoichiometric Bi_2Te_3) is obtained with the applied temperature of 195°C. According to equation (4), S directly depends on the measuring temperature (T) and inversely depends on the carrier concentration (n). Nevertheless, the Seebeck coefficient depends on film thickness [20] and dislocation density [21].

In this work, the thickness of films does not significantly affect the Seebeck coefficient due to all of the Bi-Te thin films being approximately 1.3 m. Watling et al. [21] investigated the effect of dislocation density on the Seebeck coefficient, and the results indicated that S directly depends on dislocation density. Reconsidering Table 4.1, dislocation density values of films (A) 49 at.%, (B) 54 at.% and (C) 57 at.% were 3.84×10^{15}, 12.84×10^{15} and 2.47×10^{15} lines/m^2, respectively. Although the dislocation density value of film (A) 49 at.% is close to that of film (C) 57 at.%, the carrier concentration of film (A) 49 at.% is higher than that of film (C) 57 at.% by about two times, resulting in Seebeck coefficients of film (A) 49 at.% being significantly different from those of film (C) 57 at.%. For film (B) 54 at.%, the dislocation density is the highest, while its Seebeck coefficient is lower than that of film (C) 57 at.%. This result indicates that the carrier concentration affects the Seebeck coefficient more than the dislocation density.

Figure 4.5 (B) shows the effect of the applied temperature on the electrical conductivity of all samples. It was found that the electrical conductivity increases when the applied temperature is below 195 °C, as a result of semiconductor behavior increasing when temperature increases [2]. The electrical conductivity of the film decreases when the applied temperature is above 195 °C. We suggest that this is probably due to the increase of carrier scattering with the carrier concentration increase, corresponding to Cai et al. [2].

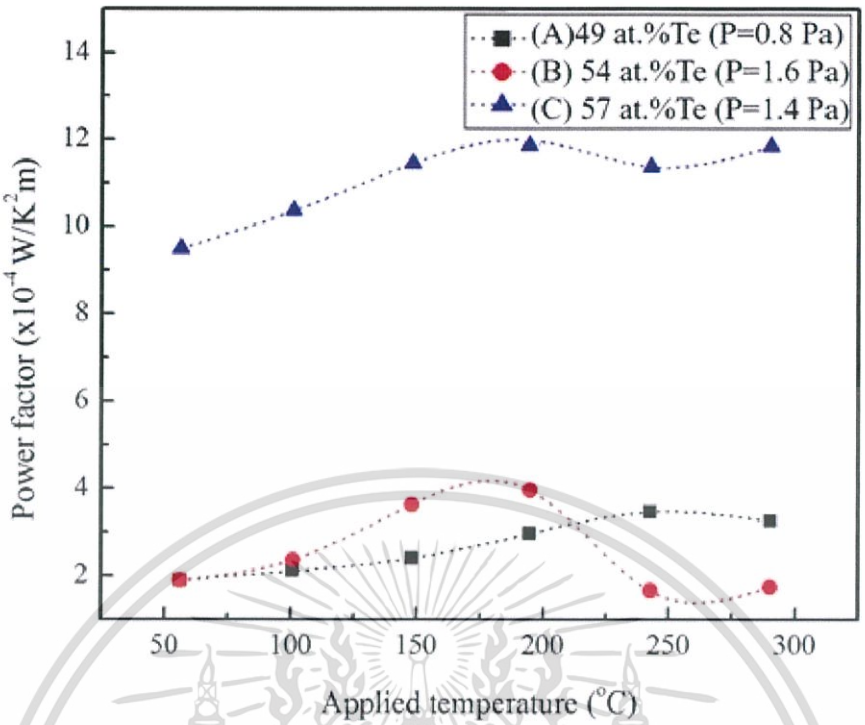

Figure 4.6. Effect of applied temperature on power factor of Bi-Te thin films deposited with different Te contents and Ar gas pressures.

Figure 4.6 shows the power factor (PF) of bismuth telluride films deposited at various conditions. The temperature dependence of PF is strongly dominated by Te content, leading to the highest value of 12.0×10^{-4} W/K^{2}m at 195 °C for the Bi-Te thin film at 57 at.%Te, nearly stoichiometric Bi_2Te_3.

4.2 The effects of the Ar gas flow rate (sputtering pressures) and annealing temperature of Bi-Te thin films were deposited by RF magnetron sputtering process. RSM was used for a statistical study of the effects of deposition parameters.

4.2.1 Model fitting and statistical analysis

Response surface methodology (RSM) based on a central composite design (CCD) was used for model fitting and statistical analysis. The relationship between factors for consideration (Ar flow rate and annealing temperature) and the responses ([Bi]:[Te] content) was analyzed by Design-Expert® Software. Ar flow rates used are 99.3, 100.5, 103.5, 106.5 and 107.5 sccm which are comparable to sputtering pressure

at 0.8, 1.0, 1.3, 1.6 and 1.7 Pa, respectively. The design experiment results of CCD and the responses measurement are given in Table 4.3.

Table 4.3 The design point combinations and the corresponding experimental responses.

Run numbers	Factors		Responses
	Ar flow rate (sccm)	Annealing Temperature (°C)	Te content (at.%)
1	103.5	235	57.49
2	103.5	285	59.12
3	103.5	334	54.33
4	106.5	320	55.31
5	103.5	285	58.66
6	103.5	285	59.74
7	107.7	285	58.24
8	103.5	285	60.61
9	100.5	250	50.02
10	103.5	285	60.11
11	106.5	250	57.2
12	100.5	320	49.12
13	99.3	285	49.10

Statistical analysis is performed by the analysis of variance (ANOVA) using experimental data obtained in Table 4.3. The significance of the model fit of the experimental data was determined by parameters F-test, p-value, R^2 and lack of fit [15]. The F-value is the ratio of the Model Mean Square to the Residual Mean Square and is used as the test statistic for comparing model variance with residual variance [16]. The F-value must be used in combination with the p-value to test the significance of the model.

Generally, the tested models showed the model and the coefficient terms are statistically significant when the p-value is less than 0.05 [14, 16]. The results showed that the quadratic model is suitable to describe the relationship between

experimental factors (Ar flow rate and annealing temperature), Te content and the model, and are significant according to a statistical parameter as shown in Table 4.4. The F-value of the model is 4.12 and p-value is 0.0002, both implying that the quadratic model is significant.

Table 4.4 Te content fit summary.

Source	Sequential p-value	Lack of Fit p-value	F Value	P-Value Prob > F	
Linear	0.0552	0.0024	32.21	0.0024	
2FI	0.8944	0.0018	38.58	0.0018	
Quadratic	0.0002	0.1024	4.12	0.1024	Suggested
Cubic	0.9069	0.0266	11.74	0.0266	Aliased

An analysis of variance (ANOVA) was done to verify the significance of the model selected. The ANOVA results of the quadratic model are presented in Table 4.5. The model equation adequately identified the response with the F-value of 28.72 which implies the model is significant. The p-value of 0.0002 indicates that there is only a 0.02% chance that an F-value this large could occur, due to noise in the experiments [14]. In this case A, A^2 and T^2 are significant, where A is the Ar flow rate and T is the annealing temperature. The lack of fit (p-value= 0.1024) value is not significant relative to pure error. Non-significant lack of fit is good and shows that the model was sufficient for predicting the response (Te content) of thin film.

Table 4.5 ANOVA results in Ar flow rate and annealing temperature.

Source	Sum of squares	DF	Mean square	F value	p-value	
Model	201.68	5	40.34	28.72	0.0002	Significant
A	86.43	1	86.43	61.55	0.0001	
T	6.59	1	6.59	4.69	0.0670	
AT	0.25	1	0.25	0.17	0.6887	
A^2	83.20	1	83.20	59.25	0.0001	
T^2	38.04	1	38.04	27.09	0.0012	
Residual	9.83	7	1.40			
Lack of Fit	7.43	3	2.48	4.12	0.1024	Not significant
Pure Error	2.40	4	0.60			

R^2 = 0.9535, R^2 (Adjusted) = 0.9203.

The relationship between the response and the Ar flow rate and the annealing temperature is given by Eq. (4.1). The regression analysis shows that the determination coefficient (R^2=0. 9535) indicates that the model does not predicts only 4.65% of the total variance, and the adjusted determination coefficient (AdjR^2=0. 9203) is satisfactory to confirm the significance of the fit model. A good fit to the model should yield an R^2 of at least 0.80 [15]. The empirical relationship between the response (Te content), and the Ar flow rate and the annealing temperature in coded units can be expressed as:

$$Te\ content = -4387.27383 + 81.31007A + 1.30610T - 2.35714 \times 10^{-3} AT - 0.38426A^2 - 1.90888 \times 10^{-3} T^2 \quad (4.1)$$

where A is the Ar flow rate and T is the annealing temperature. The graphical representation of the actual response data versus the predicted values is shown in Fig. 4.7 It can be seen that they are in agreement with the actual response data (R^2 = 0.9535) between experimental data and predicted results. The regression equation and R^2 are confirmed to assess the fit of the model.

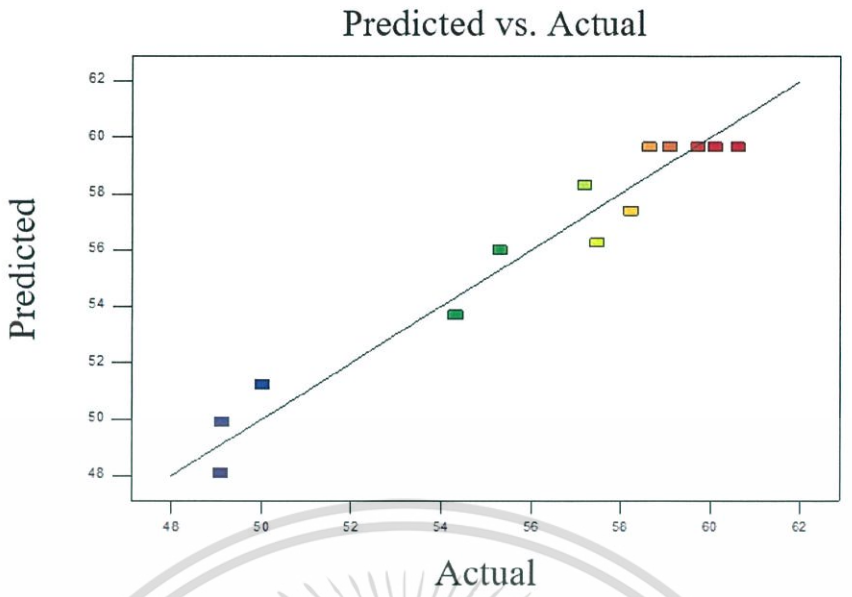

Figure 4.7 The actual response data versus the predicted response data.

4.2.2 Compositional analysis

Response surface plots were formed based on the quadratic model and are shown in Fig. 4.8 (A) and (B). It can be observed that the Te content of Bi-Te thin film tended to decrease with an increase in the annealing temperature (>300 °C) and an Ar flow rate lower than 103.5 sccm. The annealing temperature affects the Te content of Bi-Te thin film because a vapor pressure of Te is lower than Bi which causes the evaporation of Te in the films at high temperature [2]. In addition, when the Ar flow rate increases, it has an effect on the growth rate and the increase of Te content. By increasing the sputter-gas pressure, a higher flux of reflected heavier element (Bi) will eventually hit the growing film and thereby affect the composition and film structure [20]. From Fig. 4.8 (B), the stoichiometric Bi_2Te_3 thin films can be prepared with the terms appropriate for the Ar flow rate (103.5-106.5 sccm or 1.3-1.6 Pa) and the annealing temperature (260-300 °C) under several conditions such as at the Ar flow rates of 103.5 sccm (1.3 Pa) followed by an annealing temperature of 285 °C.

(A) Response surface plots of Te content

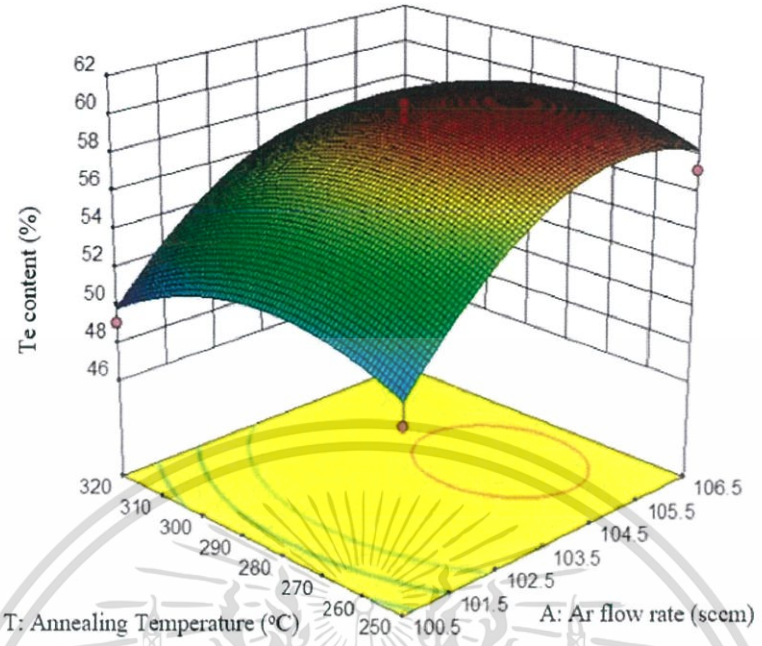

(B) Contour plots

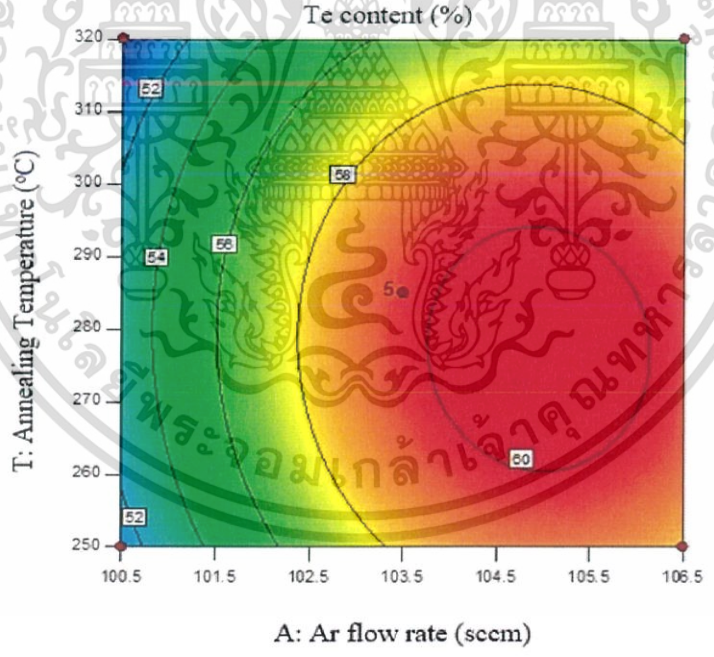

Figure 4.8 (A) Response surface plots of Te content and (B) contour plots on Bi-Te thin films predicted from the quadratic model.

4.2.3 Surface morphology and crystallinity

From Table 4.3, the design point combinations and the corresponding experimental responses can be seen. The selective Bi-Te thin films in Table 4.3 with different Te contents were measured for crystal structure and composition using XRD and EDS, respectively. The selected samples with various Te contents were (A) 49 at. %Te, (B) 54 at. %Te, (C) 57 at. %Te and (D) 60 at. %Te.

Figure 4.9 shows the surface microstructure morphology of the Bi-Te thin films. The grain shape of thin films changes with the Ar flow rate and increasing annealing temperature. The thin film was deposited with annealing temperature of 320 °C and 334 °C, indicated a smoother surface, as shown in Fig. 4.9(A) and (B). It may be the partial fusion of some Bi_2Te_3 grains due to the excessive deposition with an annealing temperature of 300 °C [4]. The thin film was deposited at the Ar flow rate of 103.5 sccm, it was found that the grain boundary is clearer as annealing temperature below 300 °C, when comparing between Fig. 4.9(B) and (D). At high Ar gas flow rate, it was found that the grain boundary is cleares with the arrangement of the non-uniform of the surface, which may be due to the surface diffusion of the adatoms, as shown in Fig. 4.9(B).

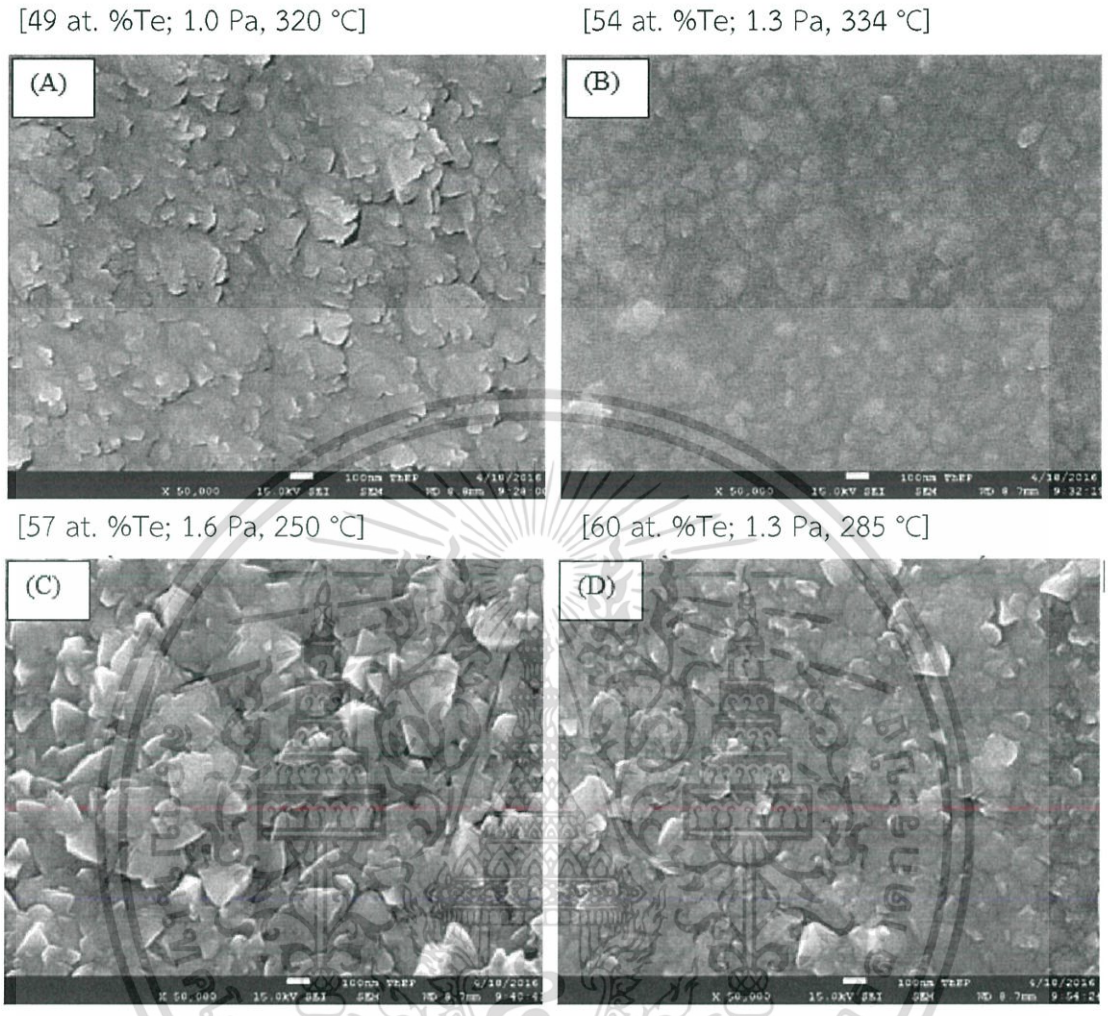

Figure 4.9 Top view of FE-SEM images of the Bi-Te thin films with different Te contents: (A) 49 at. %Te, (B) 54 at. %Te, (C) 57 at. %Te and (D) 60 at. %Te.

Figure 4.10 shows the XRD patterns of the Bi-Te thin films with various contents of Te. Comparing the XRD pattern of the films in Fig. 3 (A) with the JCPDS card no. 44-0667 suggests that the film has a structure corresponding to the (0 1 4), and (1 0 8) planes of Bi-Te. The dominant phase change from Bi-Te to Bi_2Te_3 was observed when the Te-content of thin films increased from 49 at. %Te to 54 at. %Te. When the Te content of the film increased, the peak positions and intensity were clearly changed. Three major diffraction peaks of Bi_2Te_3 (JCPDS card 08-0027) were found to be, located at 17.738°, 27.616° and 38.131°, which are indexed as a reflection from the (0 1 5) and (1 0 1 0) planes of Bi_2Te_3 as shown in Fig. 3 (B)–(D). The intensity

of other small peaks, such as (1 1 0), (0015) and (1 1 1 5), has been improved for stoichiometric Bi_2Te_3 in Fig. 3 (D), as the hexagonal crystal lattice structure belonging to R-3m space group of Bi_2Te_3 films is dominant [3, 5].

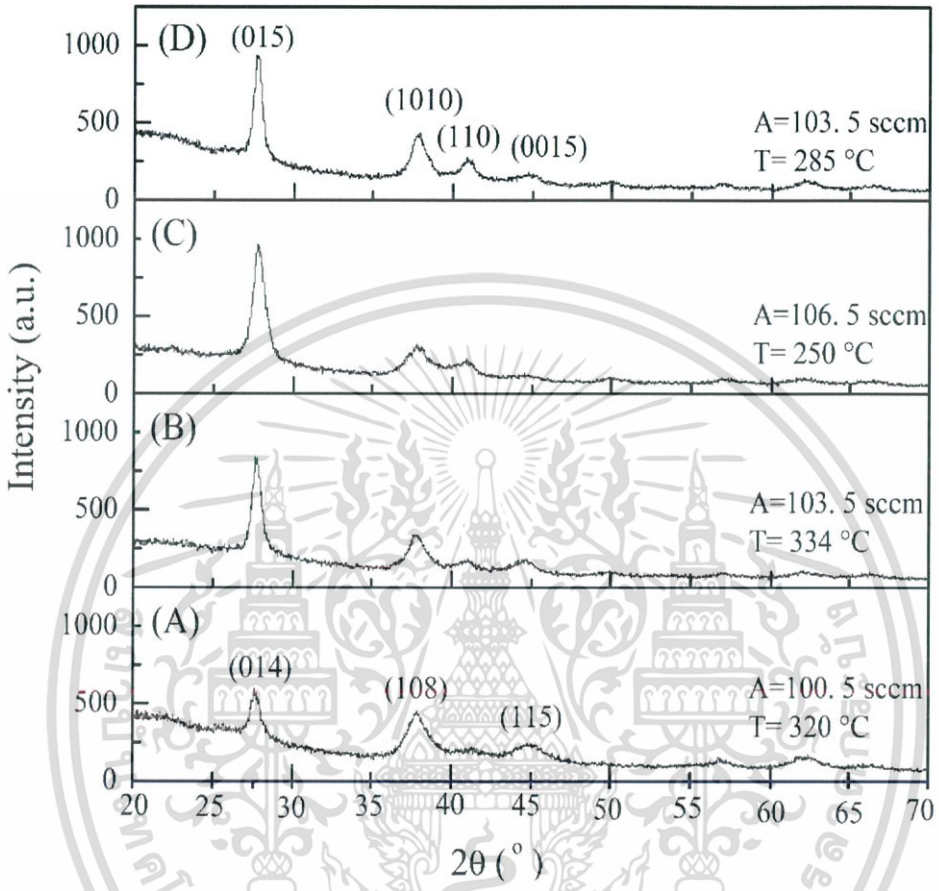

Figure 4.10 XRD patterns of the Bi-Te thin films with different Te contents: (A) 49 at. %Te, (B) 54 at. %Te, (C) 57 at. %Te and (D) 60 at. %Te

The crystallite size (D) of the Bi-Te thin films was calculated by the Scherrer equation, using a diffraction peak with (0 1 5) plane, , where k is the constant usually taken as 0.9, is the wavelength of X-ray radiation (0.154056 nm), is the full width at half maximum (FWHM), and is the diffraction angle [17]. The crystallite size of the films at 54 at. %Te, 57 at. %Te and 60 at. %Te were equal to 14, 10 and 16 nm, respectively, and are shown in Fig. 3 (B)-(D). It was found that the crystallite size of the thin film at 54 at. %Te was higher than the thin film at 57 at. %Te, due to the thin films that were deposited at the Ar flow rates of 103.5 sccm and an annealing temperature of 334 °C and deposited at the Ar flow rates of 106.5 sccm and annealing

temperature of 250 °C. Generally, when the flow rate of the gas increases, the density of the gas in the chamber also increases, which results in the mean free path of sputtered particle reduction. The collision probability between sputtered particles and gas molecules was increased, causing the energy of the particles and mobility for surface diffusion to decrease, and this led to a small crystallite size [18-20]. It can be observed that the crystallite size of the thin film at 54 at. %Te is smaller than the thin film at 60 at. %Te the thin films, the thin films were deposited at the same Ar flow rates of 103.5 sccm followed by different annealing temperatures. It was indicated that the crystalline quality of the films was enhanced after annealing at a suitable temperature and the defects reduced after annealing [5]. The parameters of the Ar flow rates and the annealing temperature affect the crystallite size of the thin film, but the crystallite size of the thin film is of little value compared to other research (~100-200 nm) [4-5].

4.2.4 Electrical and thermoelectric properties

The Seebeck coefficient (S) and electrical conductivity (σ) of different Te contents thin films were measured at room temperature, as shown in Fig. 4.11 (A). All the samples have negative values of Seebeck coefficient, indicating that the films were on an n-type semiconductor [1]. The absolute value of the Seebeck coefficient of thin film at 49 at. %Te is higher than 54 at. %Te. This may be due to the partial fusion of grain size at a high annealing temperature, which agrees with FE-SEM results. After that, the absolute value of the Seebeck coefficient increases from 53 to 95 μV/K, whereas electrical conductivity decreases from 4.5×10^4 to 2.1×10^4 S/m, along with the Te content increasing to 3.1×10^4 S/m for the stoichiometric film.

The electrical conductivity of thin films increases due to the crystallite size of the thin film at 60 at. %Te, higher than the thin film at 57 at. %Te, the density of defects in polycrystalline films reduced affect to the decrease scattering in the films. However, it is well known that the stoichiometric Bi_2Te_3 thin films have high electron mobility and a high Seebeck coefficient (as noted in previous section). In this work, stoichiometric thin films can be obtained, but their thermoelectric properties are restricted, which might be due to the fact that the polycrystallite size of thin films is quite small. Fig. 4.11 (B) shows the effect of Te content on power factors ($S^2\sigma$) of Bi-

Te thin films. The maximum power factor was obtained at 28×10^{-5} W/ K^2m for stoichiometric film.

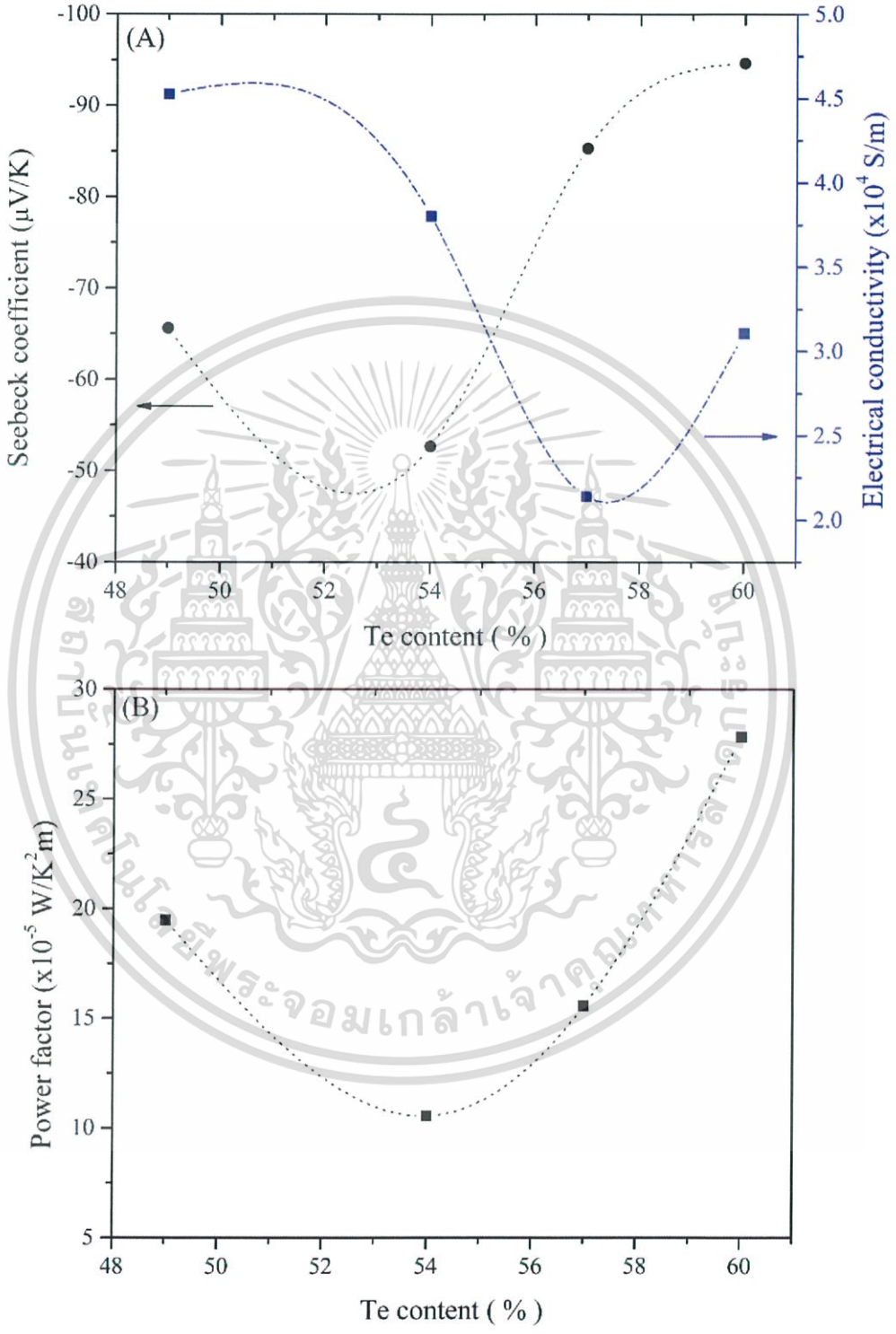

Figure 4.11 The effect of Te content on (A) Seebeck coefficient and electrical conductivity (B) power factor of the Bi-Te thin film at room temperature

Figure 4.12 shows the effect of the annealing temperature on the Seebeck coefficient, electrical conductivity and power factor of stoichiometric Bi_2Te_3 thin films in the range from 50 to 300 °C.

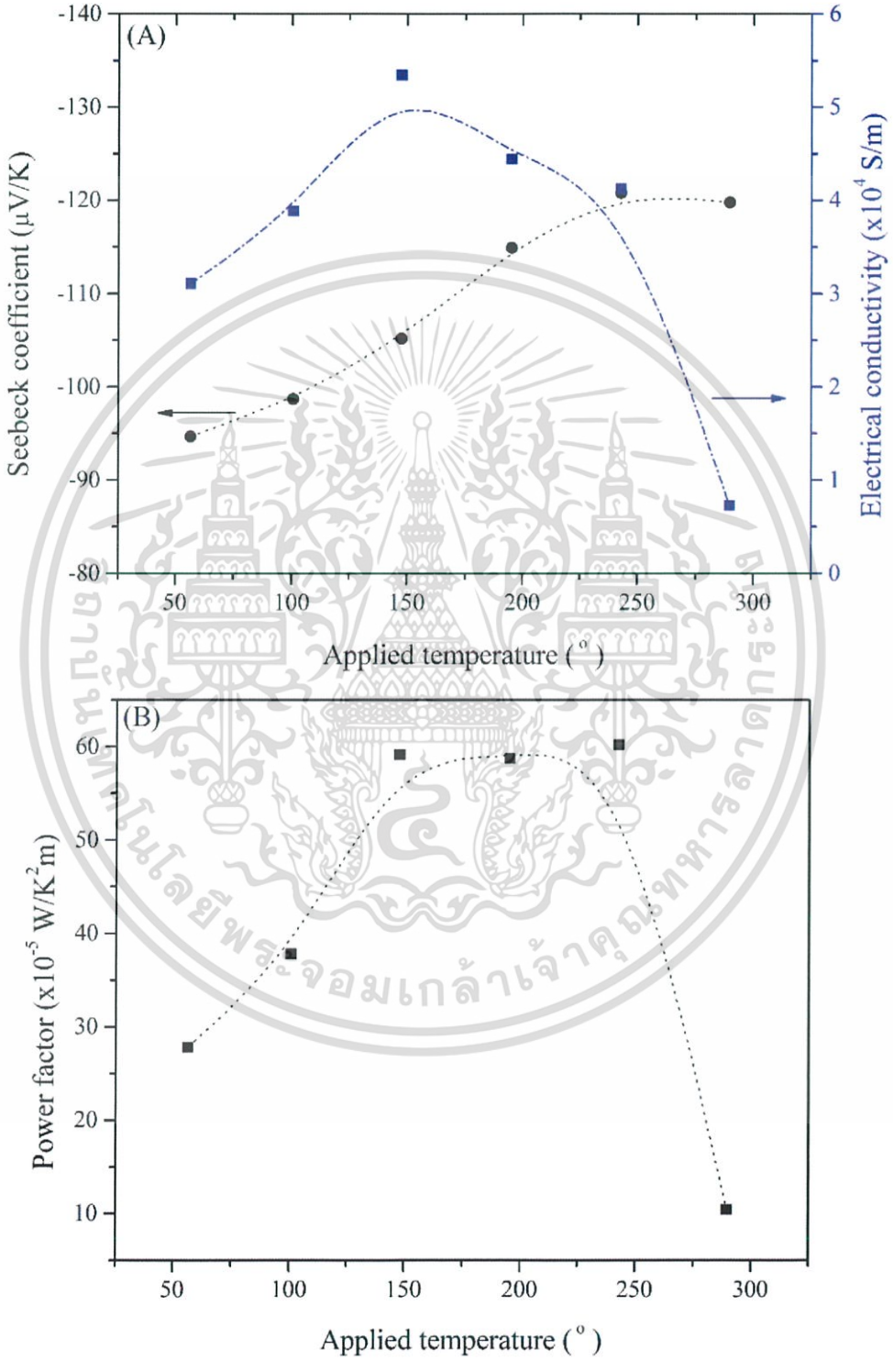

Figure 4.12 The effect of applied temperature on (A) Seebeck coefficient and electrical conductivity (B) power factor of the stoichiometric Bi_2Te_3 thin film

As shown in Fig. 4.12 (A), the absolute value of the Seebeck coefficient increases as the applied temperature increases. The maximum absolute value of the Seebeck coefficient, 121 μV/K, is achieved with the applied temperature of 243 °C. When the applied temperature is above 150 °C, the electrical conductivity of the film decreases with the increase in temperature, because it is probably due to the increase of carrier scattering with the carrier density increase.

The maximum power factor of 61×10^{-5} W/K^{2}m is obtained at the temperature of 243 °C, as shown in Fig. 4.12 (B).

4.3 The influence of pre-heating temperature of Bi-Te thin films were prepared by RF and DC magnetron sputtering.

4.3.1 Compositional analysis

Energy-dispersive X-ray spectroscopy (EDS) provides chemical composition of the deposited Bi-Te films, as shown in Fig. 4.13

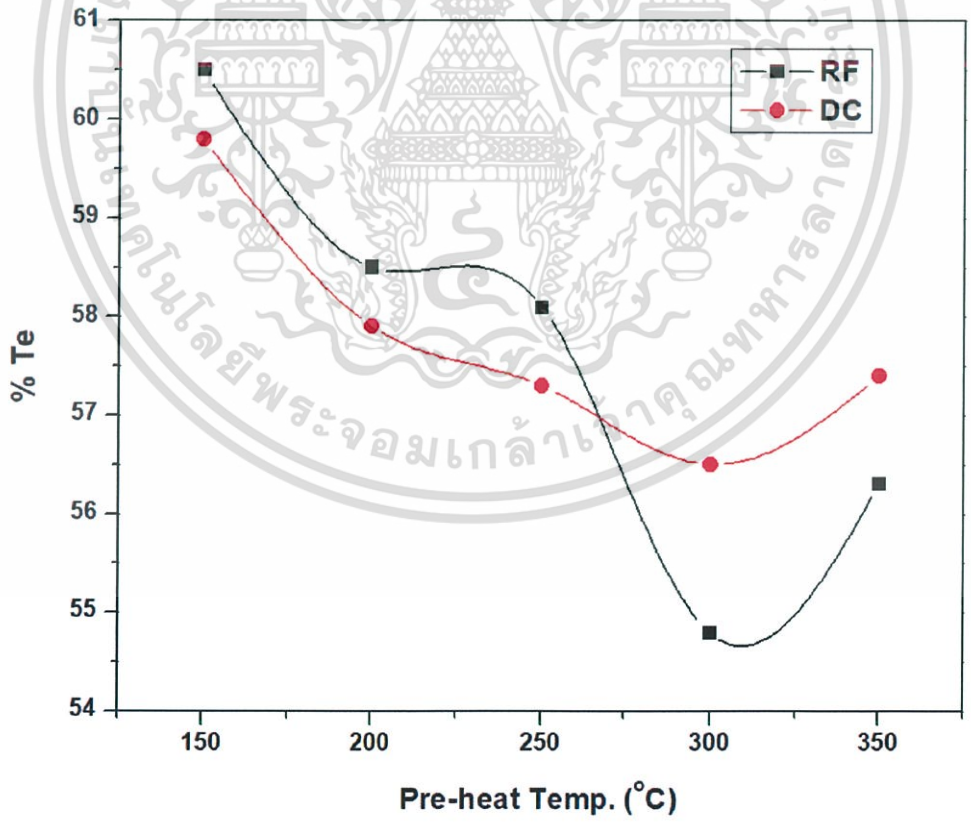

Figure 4.13 Te content in the Bi-Te thin film deposited using DC and RF magnetron sputtering at different preheating temperatures.

It can be seen that both DC and RF magnetron sputtering exhibit a similar behavior of decreasing %Te with increasing pre-heating temperature. The Te content decreased with increasing pre-heating temperature up to 300 °C and increased with increasing pre-heating temperature at 350 °C. This is considered to result from the Te atom evaporation, which caused the concentration of % Te to decrease in the temperature range up to 300 °C.

However, at the higher temperature range, the % Te values clearly increase when the pre-heating temperature increases from 300 to 350 °C. This can be explained by the re- deposition of Te accumulated in the plasma during high substrate temperature, as explained in our previous work [1]. While the substrate temperature gradually decreases, the Te-enriched plasma re-deposits on the substrate.

4.3.2 Surface morphology and crystallinity

Figure 4.14 shows the XRD patterns of the selected samples with pre-heating temperatures of 150 and 350 °C deposited using DC and RF magnetron sputtering. The films have a peak corresponding to the (015) and (0015) planes of the Bi_2Te_3 phase (JCPDS card 72-2036).

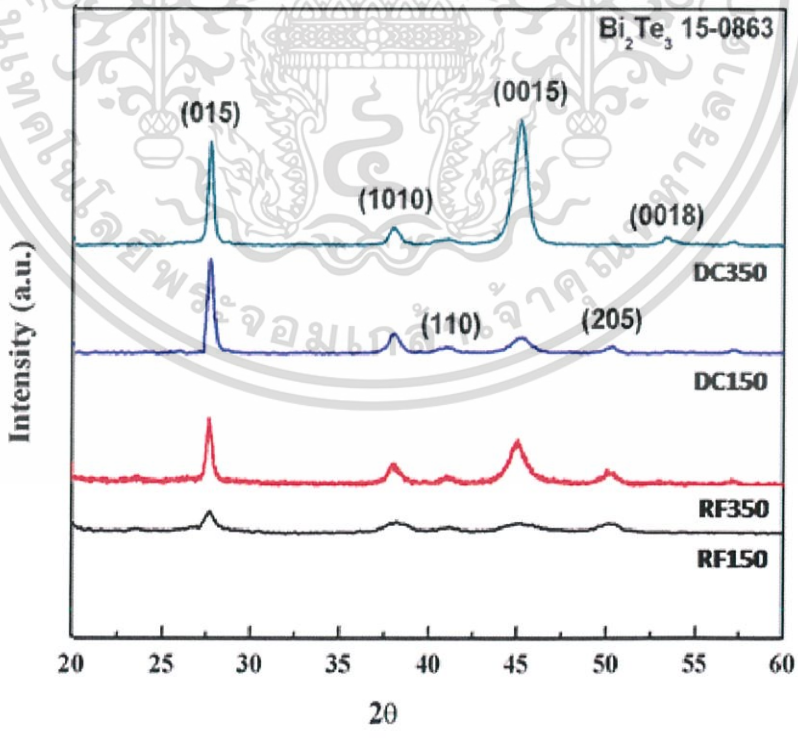

Figure 4.14 XRD patterns of the Bi-Te thin film with a different type of plasma excitation and pre-heating temperature.

In addition, the intensity of diffraction peaks is stronger at the elevated pre-heating temperature, and the crystallinity of Bi-Te films is improved. The thermal can help the diffusion of atoms increases and the dislocated atomic occupancies and enhances the coalescence of adjacent grains, which leads to the improved crystallinity of the films.

It is interesting to note that the samples with a pre-heating temperature at 350 °C (DC350 and RF350) show an increase in preferred orientation of (006) and (0015) planes, as seen in Fig. 4.14 This result is consistent with the works of Shang et al. [10] and Zhang et al. [11] who indicated the requirement of increased substrate temperature to enhance the orientation of the (00l) planes.

In this work, the different orientations of Bi-Te thin films can be contributed using DC and RF magnetron sputtering techniques with the pre- heating temperature. The difference between DC and RF magnetron sputtering affects ion bombardment on the sputtering target and electron accumulation on its substrate and target. DC sputtering directly transfers kinetic energy to sputtered atoms, and the mobility of adatoms is higher than that during the RF sputtering at the same sputtering power [14]. The increase of sputtered atom energy is a factor that enhances (00l). Another factor is that adatoms obtain enough energy to overcome the diffusion barrier to from (00l) textures at high pre-heating temperature.

Table 4.6 XRD analysis of the Bi-Te thin films.

Sample	Grain size (nm)	
	(015)	(0015)
RF150	11.5	N/A
RF350	19.7	12.1
DC150	24.9	N/A
DC350	27.6	24.5

Table 4.6 shows the XRD analysis of the Bi-Te thin films. The grain size (D) of thin films grown on flexible substrates was calculated using Scherrer's formula. The intensity ratio of the sum of all of the c-axis oriented peaks, $\Sigma\{00l\}$, to the sum of all the peaks, $\Sigma\{hkl\}$, were estimated from 0.38 to 0.60. The highly (00l) oriented Bi_2Te_3

thin films have been successfully deposited using the DC magnetron co-sputtering method with post annealing at 350 °C [11].

4.3.3 Electrical and thermoelectric properties

Table 4.7 shows the electrical properties of the Bi-Te thin films, such as carrier density, carrier mobility and electrical conductivity at room temperature. The carrier density was determined at the Te content (%Te) that leads to the defects in the films. The carrier density decreases from 5.70×10^{20} to 4.16×10^{20} cm^{-3} with the Te content increase from 56.3 to 60.5. Thus, the increase of carrier density may be ascribed to the deviations from the stoichiometric composition. The non-stoichiometric films enhance the carrier density of the Bi-Te films [1].

Table 4.7 Summary of the electrical properties of the Bi-Te thin films at room temperature.

Sample	%Te	Carrier density (cm^{-3})	Carrier mobility (cm^2/Vs)	Electrical conductivity (S/cm)
RF150	60.5	4.16×10^{20}	3.17	2.12×10^{2}
RF350	56.3	5.70×10^{20}	5.06	4.61×10^{2}
DC150	59.8	4.51×10^{20}	8.39	6.06×10^{2}
DC350	57.4	5.40×10^{20}	13.04	11.27×10^{2}

The carrier mobility of the Bi-Te thin films is 3.17 to 13.04 cm^2/Vs and correspond to the increase of grain sizes and (00l) orientation. It is surprising that the carrier mobility of more than 10 cm^2/Vs was obtained using only the DC sputtering technique and pre-heating treatment. The sample deposited via RF magnetron sputtering exhibited lower carrier mobility than that deposited via DC magnetron sputtering. In addition, the mobility of the DC350 thin film was similar to Deng et al. (12.1 cm^2/Vs) [15], who prepared the bismuth telluride thin films using substrate heating at 350 ° C. In general, the large crystal sizes have long effective mean free path of carriers and cause a reduction in grain boundary and scattering centre. In addition, the (00l) textured microstructure can benefit the carrier transport along the

ab- plane and provide a high in- plane carrier mobility. Electrical conductivity is determined via carrier concentration and mobility, as described using the following relationship:

$$\sigma = ne\mu_e \tag{2.7}$$

The carrier mobility plays an important role in the electrical conductivity of the Bi-Te thin films. The increase of electrical conductivity from 2.12×10^2 to 11.27×10^2 S/cm is related to the increase of carrier mobility. However, the carrier density slightly affects the electrical conductivity. In addition, the electrical conductivity of the films deposited using DC sputtering is much higher (approximately three-times higher) than using RF sputtering. The increase in electrical conductivity was due to the enhanced crystal size and (00l) texture in the films. The electrical conductivity of the DC350 thin film is comparable with those of hot-pressed or SPS sintered n-type Bi_2Te_3-based bulk alloys [16,17].

Subsequently, temperature dependence of electrical conductivity of the Bi-Te films was determined for the in- plane electrical transport properties, as shown in Fig. 4.15 The result shows that electrical conductivity of the sample deposited via DC sputtering is higher than the sample deposited via RF sputtering over the entire temperature range. The electrical conductivity of all samples increased with increasing temperature from 50 to 200 °C, indicating a typical semiconductor-like behaviour.

In contrast, for the temperature above 200 °C, the electrical conductivity values gradually decreased with increasing temperature. This is probably due to the increase of carrier scattering with the carrier density increase. In this work, the DC350 sample had the highest electrical conductivity of 1.4×10^5 S/m at the measured temperature of 200 °C.

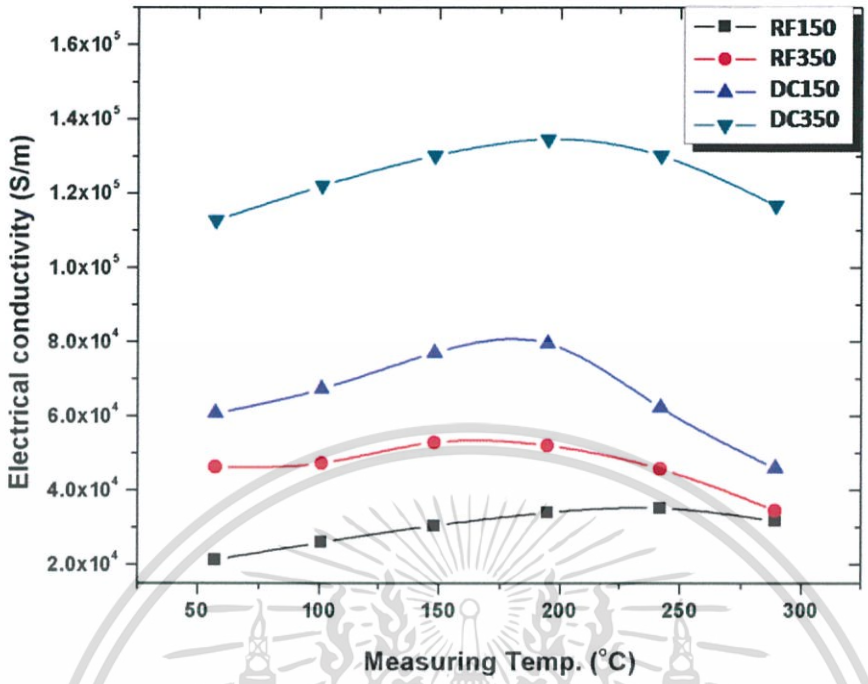

Figure 4.15 Electrical conductivity of Bi-Te films as a function of temperature.

Figure 4.16 shows the temperature-dependence Seebeck coefficient of the Bi-Te thin films measured from 50 to 285 °C. The Seebeck coefficient of all samples exhibit negative values, indicating an n-type semiconductor for which electrons are the majority carriers. It can be seen that all of the films exhibit an identical behaviour of temperature-dependent Seebeck coefficient. The Seebeck coefficient increases with increasing temperature, which can be well explained by the behaviours of heavily doped degenerate semiconductor regimes. The highest Seebeck coefficient was observed on the DC350 samples, and the Seebeck coefficient was in the range of 90-180 μV/K.

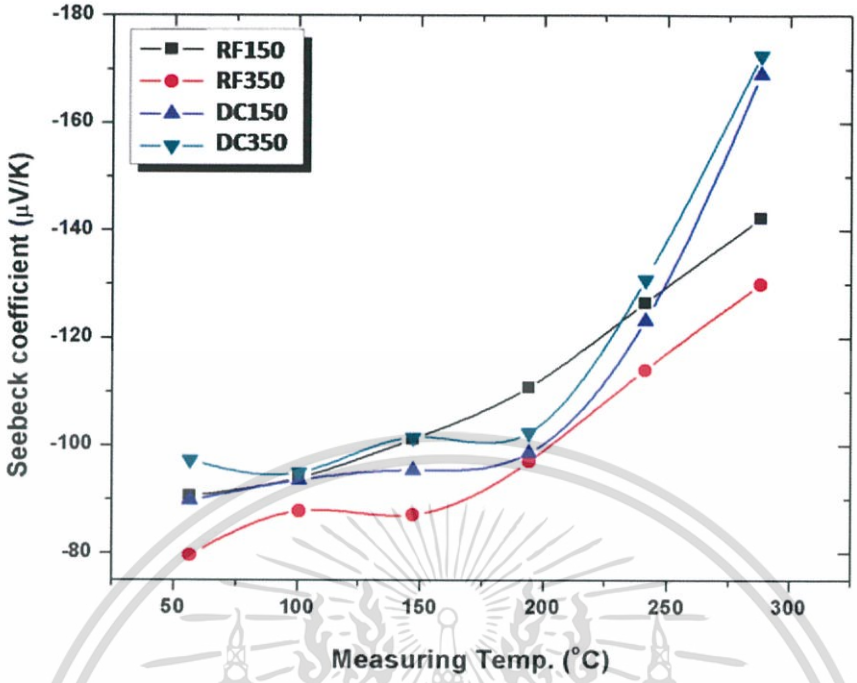

Figure 4.16 Seebeck coefficient of the Bi-Te films as a function of temperature.

The in-plane temperature-dependent power factors of Bi-Te films are shown in Fig. 4.17 The power factor values of both DC and RF films increase with increasing temperature. This was due to the increase of electrical conductivity and Seebeck coefficient with the temperature increase.

The highest power factor of 3.5×10^{-3} W/m.K^2 was obtained for the DC350 sample at the temperature of 285°C. In comparison with the previous works by Kim et al. [6, 18], Huanget al. [7], and Bourgault et al. [19] [power factor was below 1.2×10^{-3} W/(m.K2)], our results show the highest power factor. The films deposited using DC magnetron sputtering exhibit better thermoelectric performance than those deposited using RF magnetron sputtering. Generally, the stoichiometric Bi_2Te_3 film has good thermoelectric properties. Although, the RF150 and DC150 films have a nearly stoichiometric composition, the power factor of the films is less than 1.25×10^{-3} W/m.K^2 in the temperature range of 50–285°C.

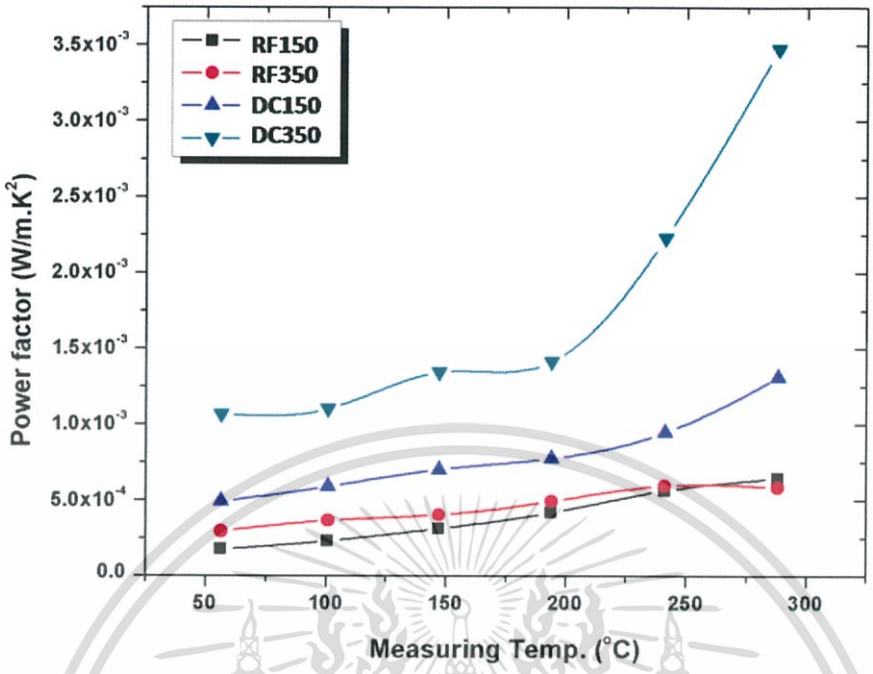

Figure 4.17 Power factor of the Bi-Te films as a function of temperature.

Therefore, the stoichiometric composition and the (00l) - preferred orientation of the films are required for the best thermoelectric application. From our results, the DC magnetron sputtering process is the candidate for obtaining highly (00l) oriented Bi_2Te_3 films with a stoichiometric composition, which may also be favourable for the improvement of thermoelectric properties.

Chapter 5
Conclusion

In this thesis, the flexible Bi-Te thin films were fabricated using an RF and DC magnetron sputtering techniques and controlled sputtering parameters using a Bi2Te3 target. Study of the effects of sputtering parameters, including the Ar gas flow rate (sputtering pressures) and pre-heating temperature and the annealing temperature on chemical composition of [Bi]:[Te]. In this thesis, we have discussed to assess and understand the key parameters and conditions that give the best power factor for Bi-Te thin films deposited by magnetron sputtering. Our finding can then be divided into three parts as follows.

5.1 The effect of sputtering pressures on chemical composition, structural and thermoelectric properties of Bi-Te thin films on flexible substrates.

The effects of various sputtering pressures were significant for controlling compositions and improving thermoelectric properties of Bi-Te thin films. The Te content and the crystal structure of Bi-Te thin film increased with increasing sputtering pressure, and the thermoelectric performance was excellent at 1.4 Pa for nearly stoichiometric Bi_2Te_3.

We found that the best power factor at room temperature was approximately 9.49×10^{-4} W/K^{2}m for the Bi-Te thin film, the sputtering pressure at 1.4 Pa. The maximum power factor, 12.0×10^{-4} W/K^{2}m for the Bi-Te thin film at 57 at.%Te, was obtained with the applied temperature of 195 °C without an annealing process.

5.2 The effect of sputtering pressures and annealing temperature on chemical composition, structural and thermoelectric properties of Bi-Te thin films on flexible substrates.

In this study, the effect of the argon gas flow rate and the annealing temperature on the [Bi]:[Te] content was analyzed by RSM. These results have indicated that the RSM has been used to optimize deposition conditions and predict the value of response ([Bi]:[Te] content) of thin films. The quadratic model which has been developed from the optimization study is accurate in [Bi]:[Te] content prediction from the relationship equation.

$$\text{Te content} = -4387.27383 + 81.31007A + 1.30610T - 2.35714\times10^{-3}AT$$
$$- 0.38426A^{2} - 1.90888\times10^{-3}T^{2}$$

The model determines that optimized deposition conditions can be achieved for stoichiometric Bi_2Te_3 thin films, such as at the Ar flow rates of 103.5 sccm (1.3 Pa) followed by an annealing temperature of 285 °C. The XRD and FE-SEM results indicate that the stoichiometric Bi_2Te_3 thin film with improved crystalline quality was achieved. We found that the maximum Seebeck coefficient and the power factor of the thin films measured at room temperature achieved -95 μV/K and 28×10^{-5} W/K^{2}m, respectively. Less electrical conductivity is 3.1×10^{4} S/m, dependence on the crystalline quality of the thin films. This might be caused its crystal defects from the poor crystalline quality at room temperature. The influence of the post-annealing temperature on the thermoelectric properties of stoichiometric Bi_2Te_3 thin film shows that the absolute value of the Seebeck coefficient, the electrical conductivity and the power factor increases as the temperature increases.

The maximum power factor, 6.1×10^{-4} W/K^{2}m for stoichiometric thin films, was obtained with the applied temperature of 243 °C. Although stoichiometric thin films can be obtained, their thermoelectric properties are restricted, possibly due to the polycrystallite size of thin films being quite small, and improvement in the thermoelectric performance is expected to be achieved with stoichiometry and a high polycrystallinte size of thin films by additionally controlling various sputtering parameters, such as the temperature of substrate and the annealing duration.

5.3 The influence of pre-heating temperature on chemical composition, structural and thermoelectric properties of Bi- Te thin films on flexible substrates prepared by RF and DC magnetron sputtering.

In summary, the Bi-Te thin films deposited using DC and RF magnetron sputtering with different pre-heating temperatures were compared. The energy of sputtered atoms using different ion bombardments and substrate temperatures were the key parameters for controlling the crystal quality and orientation. The increase of grain size and (00*l*)-oriented Bi_2Te_3 films were also favourable for the improvement of thermoelectric properties.

The best thermoelectric performance of the Bi_2Te_3 film was achieved using the DC magnetron sputtering deposition. We found that the largest power factor at room temperature was approximately $10x10^{-4}$ W/K^2m at 103.5 sccm (1.3 Pa) for the Bi-Te thin film, the pre-heating temperature of 350 °C. The maximum power factor, 35×10^{-4} W/K^2m for stoichiometric thin films, was obtained with the applied temperature of 285 °C.

However, the DC magnetron sputtering with a pre-heating temperature of 350 °C resulted in films with a non-stoichiometric composition. Further studies of the DC magnetron sputtering process are necessary to achieve both the highly (00*l*) oriented Bi_2Te_3 films and the stoichiometric composition.

References

[1] X. Zhang, L.-D. Zhao, Journal of Materiomics. 1, 92 (2015)

[2] P. Nuthongkum, A. Sakulkalavek, R. Sakdanuphab, J. Electron Mater. 46 (5), 2900 (2017)

[3] H. Huang, L. Wei-ling, T. Shan-tung, Thin Solid Films. 517, 3731 (2009)

[4] C. Zhao-kun, F. Ping, Z. Zhuang-hao, L. Peng-juan, C. Tian-bao, C. Xing-min, L. Jing-ting, L. Guang-xing, Z. Dong-ping , Appl. Surf. Sci. 280 ,225 (2013)

[5] H.J. Lee, S. Hyun, H.S. Park, S.W. Han, Microelectron. Eng. 88, 593 (2011)

[6] X. Wang, H. He, N. Wang, L. Miao, Appl. Surf. Sci. 276, 539 (2013)

[7] Z.H.Zheng, P. Fan, T.B. Chen, Z.K.Cai, P.J. Liu, G.X. Liang, D.P. Zhang, X.M.Cai, Thin Solid Films. 520, 5245 (2012)

[8] P. Nuthongkum, A. Sakulkalavek, R. Sakdanuphab, J. Electron Mater. 46(11), 6444(2017)

[9] L.M. Goncalves, C. Couto, P. Alpuim, A.G. Rolo, F. Völklein, J.H. Correia, Thin Solid Films. 518, 2816 (2010)

[10] L.M. Goncalves, P. Alpuim, G.Min, D.M. Rowe, C. Couto, J.H. Correia, J. vacuum. 82, 1499 (2008)

[11] R.S. Makala, K. Jagannadham, B.C. Sales, J. Appl. Phys. 94, 3907 (2003)

[12] A. Dauscher, A. Thomy, H. Scherrer, Thin Solid Films. 280, 61 (1996)

[13] H.J. Lee, H.S. Park, S.W. Han, J.Y. Kim, Thermochim Acta. 542, 57 (2012)

[14] X. Wang, H. He, N. Wang, L. Miao, Appl. Surf. Sci. 276, 539 (2013)

[15] K. Dong-Ho, E. Byon, L. Gun-Hwan, S. Cho, Thin Solid Films. 510,148 (2006)

[16] S. Swann, Phys. Technol. 19 (1988)

[17] Y. Deng, L. Hui-min, Y. Wang, Z. Zhi-wei, M. Tan, C. Jiao-lin, J. Alloys Compd. 509, 5683 (2011)

[18] T. Khumtong, A. Sakulkalavek, R. Sakdanuphab, Journal of Alloys and Compounds 715, 65 (2017)

[19] H. Julian Goldsmid. Introduction to Thermoelectricity. Springer Series in materials science. 2009

[20] D. M. Rowe. Thermoelectrics handbook macro to nano. Taylor & Francis Group.2006

[21] A.Sakulkalavek, R.Sakdanuphab, Mat. Sci.Semicon. Proc.56, 313 (2016)

[22] S. Swann. Magnetron sputtering. Phys. Tech. 1,(1988)

[23] M. Rull-Bravo, A. Moure, J.F. Fernández, M. Martín-González. Skutterudites as thermoelectric material: revisited. Journal of RSC Advances. 5(52), 41653-41667, (2015).

[24] Jesús Prado-Gonjal, Paz Vaqueiro, Chris Nuttall, Robert Potter, Anthony V. Powell. Journal of Alloys and Compounds 695,3598-3604 (2017)

[25] Rafay Uz Zaman Shams, Thermoelectric Properties of Materials Based on Double Filled Type-I Clathrates, Anthony V. Powell. Thesis University of Waterloo (2015)

[26] G. S. Nolas, J. L. Cohn, G. A. Slack, S. B. Schujman. Semiconducting Ge clathrates: Promising candidates for thermoelectric applications. Journal of applied physics letters and Compounds 73,2 (1998)

[27] Zhigang Zeng, Penghui Yang, Zhiyu Hu. Journal of Applied Surface Science. 268, 472–476(2013)

[28] O. Caha, A. Dubroka, J. Humlicek, V. Holy', H. Steiner, M. Ul-Hassan, J. Sanchez-Barriga, O. Rader,T. N. Stanislavchuk, A. A. Sirenko, G. Bauer, G. Springholz. Journal of Cryst. Growth Des. 13, 3365–3373(2013)

[29] Waruna Dissanayaka Wijesooriyage, Electrochemical Deposition and Characterization of Thermoelectric Thin Films of $(Bi_xSb_{1-x})_2Te_3$. Thesis Chelmers University of Technology (2011).

[30] E. Ya. Atall, E. S. Itskevich, S. A. Mashkov, S. V. Popova, F. Vereshchagin. Journal of Soviet Physics- Solid State. 10-1, 62-65(1967)

[31] Niloufar Ghafouri, Bismuth Telluride and Antimony Telluride Based Co-evaporated Thermoelectric Thin Films: Technology, Characterization, and Optimization. Thesis University of Michigan (2012).

[32] Rudolf Kinder, Miroslav Mikol´a˘sek, Daniel Donoval, Jaroslav Kov´a˘c, Marek Tlaczala. Journal of Electrical Engeneerig. 64-2, 106–111, (2013)

[33] Akbar Sadaf, Defect ferromagnetism in ZnO and SnO2 induced by non-magnetic dopants. Thesis University of Groningen (2017).

[34] James John Mudd. Photoelectron Spectroscopy Investigation of CdO. Thesis University of Warwick (2014).

[35] Radomir Džakula, Slavica Savić, Goran Stojanović. Processing and Application of Ceramics. 2-1,33–37(2008).

[36] A.R. Bushroa, R.G. Rahbari, H.H. Masjuki, M.R. Muhamad. Journal of vacuum 86 1107,(2012).

[37] Yusheng Zhao, Jianzhong Zhang. Journal of Appl. Cryst. 41, 1095, (2008).

Appendix

Figure 1. Image of a fabricated Bi_2Te_3 thermoelectric on a flexible polyimide substrate.

In the experiment, for studying the influence of pre-heating substrate. Temperatures were in the range of 150°C to 400°C and a common heating time of 1 h was used. It found that the temperature in the chamber was decreased during the sputtering process. The temperature versus time curve diagram to show the temperature in the chamber during the sputtering process, shown in the figure 2.

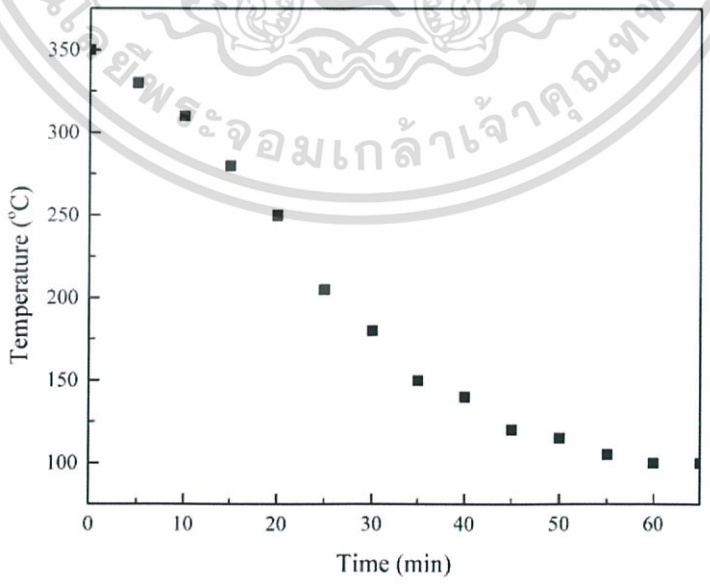

Figure 2. The temperature in the chamber during the sputtering process.

AUTHOR BIOGRAPHY

Miss Pilaipon Nuthongkum

DATE OF BIRTH 8 May 1984

ADDRESS Department of Applied Physics, Faculty of Science and Technology, Rajabhat Rajanagarindra University, Chachoengsao 24000, Thailand

EUCATION Bachelor degree of Science in Physics, Faculty of Science, Prince of Songkla University, Songkla, Thailand (2006).

Master of Science in Nuclear technology, Faculty of Engineering, Chulalongkorn University, Bangkok, Thailand (2008).

PUBLICATION:

1. P. Nuthongkum, A. Sakulkalavek, R. Sakdanuphab, RSM Base Study of the Effect of Argon Gas Flow Rate and Annealing Temperature on the [Bi]:[Te] Ratio and Thermoelectric Properties of Flexible Bi-Te Thin Film.J. Electron Mater. 46 (5), 2900 (2017) [IF:1.566,2017]

2. P. Nuthongkum, A. Sakulkalavek, R. Sakdanuphab, [Bi]:[Te] Control, Structural and Thermoelectric Properties of Flexible Bi_xTe_y Thin Films Prepared by RF Magnetron Sputtering at Different Sputtering Pressures.J. Electron Mater. 46(11), 6444(2017) [IF:1.566,2017]

Journal of ELECTRONIC MATERIALS, Vol. 46, No. 5, 2017
DOI: 10.1007/s11664-016-5024-1

RSM Base Study of the Effect of Argon Gas Flow Rate and Annealing Temperature on the [Bi]:[Te] Ratio and Thermoelectric Properties of Flexible Bi-Te Thin Film

PILAIPON NUTHONGKUM,[1,3] APARPORN SAKULKALAVEK,[1,4] and RACHSAK SAKDANUPHAB[2]

1.—Faculty of Science, King Mongkut's Institute of Technology Ladkrabang, Chalongkrung Rd. Ladkrabang, Bangkok 10520, Thailand. 2.—College of Advanced Manufacturing Innovation, King Mongkut's Institute of Technology Ladkrabang, Chalongkrung Rd. Ladkrabang, Bangkok 10520, Thailand. 3.—e-mail: miss.pilaipon@gmail.com. 4.—e-mail: ksrachsa@kmitl.ac.th

Bismuth telluride (Bi-Te) thin films coated on a flexible substrate were prepared by RF (radio frequency) magnetron sputtering technique. A response surface methodology based on a central composite design was used to optimize deposition parameters, including the amount of Ar gas flow rate (100.5–106.5 sccm) in the sputtering process and the annealing temperature (250–320°C) for stoichiometric Bi_2Te_3 thin films. The mathematical model was validated and proven to be statistically sufficient and accurate in predicting a response (Te content). The stoichiometric Bi_2Te_3 thin films can be prepared on terms appropriate to the Ar flow rate and annealing temperature under several conditions, such as at the Ar flow rate of 103.5 sccm followed by an annealing temperature of 285°C. The characterization of the crystal structure and surface morphology of selected samples with different [Bi]:[Te] content were analyzed by x-ray diffraction (XRD) and a field emission scanning electron microscope, respectively. The XRD spectra showed Bi-Te and Bi_2Te_3 structures that corresponded with the ratio of [Bi]:[Te]. The Seebeck coefficient and electrical conductivity were simultaneously measured at room temperature and up to 300°C by a direct current four-terminal method. The maximum power factor of the stoichiometric Bi_2Te_3 thin film was 61×10^{-5} W/K^{2}m at 243°C.

Key words: Flexible Bi_2Te_3, RSM, thermoelectric, RF sputtering

INTRODUCTION

Thermoelectric materials are of interest since they can be transformed at different temperatures into electric voltage and vice versa.[1] A thermoelectric module has several advantages over competing technologies, such as low maintenance requirements, a long operating lifetime, scalability and possible miniaturization.[2–5] The thermoelectric figure-of-merit (ZT), used to characterize the performance of a thermoelectric material, is defined as $ZT = S^2/\sigma T/\kappa$, where S is the Seebeck coefficient, σ is electrical conductivity, κ is thermal conductivity and T is temperature. A large value of ZT means higher thermoelectric conversion efficiency, which requires a high power factor ($S^2\sigma$) along with low thermal conductivity.[1–5] Bismuth telluride (Bi_2Te_3) is one of the most interesting thermoelectric materials with a high ZT, and it is known to have an excellent thermoelectric performance at room temperature.[1–6] Bi-Te has been developed in the form of thin films because thin film material has an efficiency per unit area higher than bulk materials and low dimensional materials.[5] Thin film thermoelectric devices provide the possibility of using flexible substrates and can be applied to diverse fields.[12] Polyimide (Kapton®) has been widely reported with

(Received June 6, 2016; accepted October 3, 2016; published online October 21, 2016)

high-performance flexible substrates due to low thermal conductivity ($0.12\ Wm^{-1}\ K^{-1}$), a wide range of temperatures, thermal stability and a low coefficient of thermal expansion ($12 \times 10^{-6}\ K^{-1}$).[7–9] Thermoelectric films have been prepared using different deposition methods, such as co-evaporation,[7,8] pulsed laser deposition[10,11] and RF magnetron sputtering.[2–6,12] The RF magnetron sputtering method was selected due to the possibility of large-scale fabrication of high-quality films.[3,5] In the sputtering process, tellurium (Te) exhibits lower sputtering yield than bismuth (Bi),[2,3,5] so it is difficult to obtain stoichiometric Bi_2Te_3 thin films. The separate evaporator sources or sputter targets are needed in composition control. The good thermoelectric properties of Bi_2Te_3 thin films must have a stoichiometric composition [2:3].[2–6] The stoichiometric Bi_2Te_3 thin films have a high electron mobility and a high Seebeck coefficient.[6] The stoichiometry of Bi_2Te_3 thin films has been prepared by controlling various sputtering parameters, such as working pressure,[2,10] sputtering power,[4,6] the temperature of the substrate[2,10] and the post-annealing process.[3–6] Previously, many researchers have reported the preparation of Bi_2Te_3 films by sputtering with deposition conditions controlled to achieve the stoichiometry of Bi_2Te_3 thin films; for example, Lee et al. studied the electrical resistivity of Bi-Te thin films fabricated by RF magnetron co-sputtering. The electrical resistivity was very dependent on the Te content. The films exhibits positive Seebeck coefficients when the Te content was more than 80%. The films with 65% Te content obtained the maximum power factor of $3.7 \times 10^{-4}\ W/K^2m$.[1] Huang et al. proposed the influence of the target composition and annealing temperature (100–250°C) on the thermoelectric properties of bismuth telluride films grown via radio frequency (RF) magnetron sputtering. Stoichiometric Bi_2Te_3 thin films were deposited using a sputtering target with a Te-content of 45 at.%. The power factor of the films measured at room temperature reached the highest value of $4 \times 10^{-4}\ W/K^2m$, which was annealed at 300°C.[3] Wang et al. studied the effects of the annealing temperature (150–350°C) on the thermoelectric properties of Bi_2Te_3 films prepared by co-sputtering. They found that the optimum of the Seebeck coefficient and the power factor was about $-242\ \mu V/K$ and $21\ \mu W/K^2cm$, respectively, obtained at the annealing temperature of 300°C.[4] Cai et al. proposed that the Bi_2Te_3 films were fabricated by a co-sputtering-method, followed by annealing between 250°C and 450°C. They reported that, at the annealing temperature of 275°C, the maximum power factor of $3.288 \times 10^{-4}\ W/K^2m$ was obtained. These results demonstrate that high-performance Bi_2Te_3 thin films can be prepared by DC and RF magnetron co-sputtering with post-annealing.[5] Kim et al. studied Bi-Te thin films that were deposited using RF magnetron co-sputtering. The controlled deposition conditions were the working pressure (8×10^{-2} Pa) and substrate temperature (27–320°C). They reported that the thermoelectric performance had a Bi_2Te_3 crystal structure and a power factor of about $\sim 3 \times 10^{-4}\ W/K^2m$, when the deposition was performed at a substrate temperature below 290°C.[6] Most researchers have studied bismuth telluride films that were prepared by DC or RF magnetron co-sputtering, and studied only one deposition parameter while keeping other deposition parameters constant, because increases in the deposition parameters have an effect on the number and the cost of experiments needed to conduct more research.[13] In this work, Bi-Te thin films were deposited using a Bi_2Te_3 target by RF magnetron sputtering but this method is different from a co-sputtering technique. It was difficult to control the stoichiometry of Bi-Te films due to the difference in [Bi] and [Te] sputtering yields.[3] However, we used a statistical technique to optimize the deposition parameters to achieve the stoichiometric Bi_2Te_3 thin films. An alternative for a study of the effects of the chemical composition of [Bi]:[Te] in various deposition parameters of thin films is RSM, which is a statistical design method using mathematical and statistical methods for designing experiments, building models, evaluating the effects of several factors and finding the optimum conditions for target responses.[13–16] This approach can result in having to do fewer experiments, which therefore reduces the cost, and it has advantages such as making possible improved statistical interpretation of the results, while requiring less time for analysis.[13]

In this study, Bi-Te thin films were deposited on polyimide substrates using an RF magnetron sputtering technique. RSM was used for a statistical study of the effects of deposition parameters, including the Ar gas flow rate (100.5–106.5 sccm), and the annealing temperature (250–320°C) on the response (Te content). Finally, the effects of the Te content on the thermoelectric properties of deposited Bi-Te thin films were studied.

EXPERIMENTAL

Experimental Design

This study used RSM based on a CCD to optimize deposition parameters. The effects of deposition parameters, including the amount of Ar gas flow rate (100.5–106.5 sccm) and the annealing temperature (250–320°C), were analyzed. The effect of the Te content on the response (Te content) is described accordingly to achieve the stoichiometric Bi_2Te_3 thin films. Experimental design and statistical analysis was achieved by the Design-Expert® Software v.9 (Stat-Ease, Minneapolis, USA) and the analysis of variance (ANOVA), respectively.

Preparation of Films

Bismuth-telluride (Bi-Te) thin films were prepared by an RF magnetron sputtering technique

onto a polyimide flexible substrate. The base pressure of the vacuum chamber was below 2.5×10^{-3} Pa and the working pressure was varied from 0.8 to 1.7 Pa by the Ar gas flow rates of 100.5–106.5 sccm. The sputtering target was commercial Bi_2Te_3 (high purity: 99.9%) and the target–substrate distance was maintained at 50 mm. Before the deposition, the substrates were cleaned thoroughly, successively by methanol and acetone for 15 min in an ultrasonic bath. As-deposited films were annealed at different temperatures from 250 to 320°C for 60 min under N_2 atmosphere. The thickness of the Bi-Te films was kept at about 1.5 μm.

Measurements and Characterization

The crystalline structure was measured by grazing incidence XRD (D8 DISCOVER-Bruker AXS). The surface microstructure morphology and composition of the Bi-Te thin films were measured by FE-SEM (JSM-7001F) and EDS, respectively. The Seebeck coefficient and electrical conductivity were simultaneously measured at room temperature and up to 300°C using commercial equipment (ZEM-3; ULVAC-Riko).

RESULTS AND DISCUSSION

Model Fitting and Statistical Analysis

RSM based on CCD was used for model fitting and statistical analysis. The relationship between factors for consideration (Ar flow rate and annealing temperature) and the responses ([Bi]:[Te] content) was analyzed by Design-Expert® Software. The design experiment results of CCD and the responses measurement are given in Table I.

Statistical analysis is performed by ANOVA using experimental data obtained in Table I. The significance of the model fit of the experimental data was determined by parameters F test, p value, R^2 and lack of fit.[15] The F value is the ratio of the Model Mean Square to the Residual Mean Square and is used as the test statistic for comparing model variance with residual variance.[16] The F value must be used in combination with the p value to test the significance of the model. Generally, the tested models showed the model, and the coefficient terms are statistically significant when the p value is <0.05.[14,16] The results showed that the quadratic model is suitable to describe the relationship between experimental factors (Ar flow rate and annealing temperature), Te content and the model, and are significant according to a statistical parameter as shown in Table II. The F value of the model is 4.12 and p value is 0.0002, both implying that the quadratic model is significant.

ANOVA was carried out to verify the significance of the model selected. ANOVA results of the quadratic model are presented in Table III. The model equation adequately identified the response with the F value of 28.72 which implies the model is significant. The p value of 0.0002 indicates that there is only a 0.02% chance that an F value this large could occur, due to noise in the experiments.[14] In this case A, A^2 and T^2 are significant, where A is the Ar flow rate and T is the annealing temperature. The lack of fit (p value = 0.1024) value is not significant relative to pure error. Non-significant lack of fit is good and shows that the model was sufficient for predicting the response (Te content) of thin film.

The relationship between the response and the Ar flow rate and the annealing temperature is given by Eq. 1. The regression analysis shows that the determination coefficient ($R^2 = 0.9535$) indicates that the model predicts only 4.65% of the total variance, and the adjusted determination coefficient ($AdjR^2 = 0.9203$) is satisfactory to confirm the significance of the fit model. A good fit to the model

Table I. Design point combinations and corresponding experimental responses

	Factors		Responses
Run numbers	Ar flow rate (sccm)	Annealing temperature (°C)	Te content (at.%)
1	103.5	235	57.49
2	103.5	285	59.12
3	103.5	334	54.33
4	106.5	320	55.31
5	103.5	285	58.66
6	103.5	285	59.74
7	107.7	285	58.24
8	103.5	285	60.61
9	100.5	250	50.02
10	103.5	285	60.11
11	106.5	250	57.2
12	100.5	320	49.12
13	99.3	285	49.10

Table II. Comparison of ANOVA model results for Ar flow rate and annealing temperature

Source	Sequential *p* value	Lack of fit *p* value	*F* value	*p* value prob > *F*	
Linear	0.0552	0.0024	32.21	0.0024	
2FI	0.8944	0.0018	38.58	0.0018	
Quadratic	0.0002	0.1024	4.12	0.1024	Suggested
Cubic	0.9069	0.0266	11.74	0.0266	Aliased

Table III. ANOVA results for analysis of Ar flow rate and annealing temperature

Source	Sum of squares	*df*	Mean square	*F* value	*p* value	
Model	201.68	5	40.34	28.72	0.0002	Significant
A	86.43	1	86.43	61.55	0.0001	
T	6.59	1	6.59	4.69	0.0670	
AT	0.25	1	0.25	0.17	0.6887	
A^2	83.20	1	83.20	59.25	0.0001	
T^2	38.04	1	38.04	27.09	0.0012	
Residual	9.83	7	1.40			
Lack of fit	7.43	3	2.48	4.12	0.1024	Not significant
Pure error	2.40	4	0.60			

$R^2 = 0.9535$, R^2 (Adjusted) = 0.9203.

should yield an R^2 of at least 0.80.[15] The empirical relationship between the response (Te content), and the Ar flow rate and the annealing temperature in coded units can be expressed as:

$$\text{Te content} = -4387.27383 + 81.31007A + 1.30610T - 2.35714 \times 10^{-3}AT - 0.38426A^2 - 1.90888 \times 10^{-3}T^2 \quad (1)$$

where A is the Ar flow rate and T is the annealing temperature. The graphical representation of the actual response data versus the predicted values is shown in Fig. 1. It can be seen that they are in agreement with the actual response data ($R^2 = 0.9535$) between the experimental data and the predicted results. The regression equation and R^2 are confirmed to assess the fit of the model.

Response surface plots were formed based on the quadratic model and are shown in Fig. 2a and b. It can be observed that the Te content of Bi-Te thin film tended to decrease with an increase in the annealing temperature (>300°C) and an Ar flow rate lower than 103.5 sccm. The annealing temperature affects the Te content of Bi-Te thin film because a vapor pressure of Te is higher than Bi which causes the evaporation of Te in the films at high temperature.[2] In addition, when the Ar flow rate increases, it has an effect on the growth rate and the decrease of Bi content. By increasing the sputter-gas pressure, a higher flux of reflected heavier element (Bi) will eventually hit the growing film and thereby affect the composition and film structure.[20]

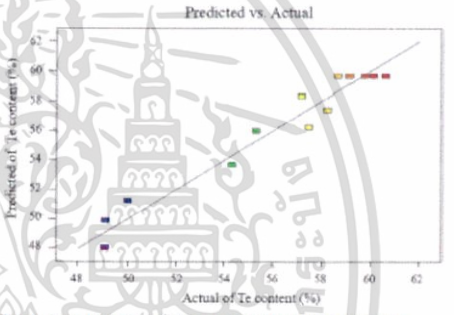

Fig. 1. Actual response data versus predicted response data.

From Fig. 2b, the stoichiometric Bi_2Te_3 thin films can be prepared with the terms appropriate for the Ar flow rate (103.5–106.5 sccm) and the annealing temperature (260–300°C) under several conditions, such as at the Ar flow rates of 103.5 sccm followed by an annealing temperature of 285°C.

Effect of Te Content on Structural and Surface Properties

From Table I, the design point combinations and the corresponding experimental responses can be seen. The selective Bi-Te thin films in Table I with

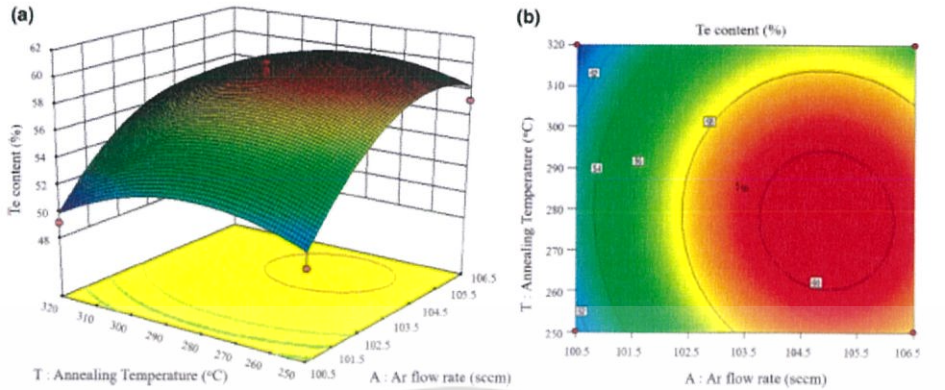

Fig. 2. Response surface curve (a) and contour plots (b) of Te content on Bi-Te thin films predicted from the quadratic model.

different Te content were measured for crystal structure and composition using XRD and EDS, respectively. The selected samples with various Te content were (A) 49 at.%Te, (B) 54 at.%Te, (C) 57 at.%Te and (D) 60 at.%Te.

Figure 3 shows the XRD patterns of the Bi-Te thin films with various content of Te. Comparing the XRD pattern of the films in Fig. 3a with the JCPDS Card No. 44-0667 suggests that the film has a structure corresponding to the (0 0 5), (0 1 4), and (1 0 8) planes of Bi-Te. The dominant phase change from Bi-Te to Bi_2Te_3 was observed when the Te-content of the thin films increased from 49 at.%Te to 54 at.%Te. When the Te content of the film increased, the peak positions and intensity were clearly changed. Three major diffraction peaks of Bi_2Te_3 (JCPDS card 08-0027) were found, located at 17.738°, 27.616°, and 38.131°, which are indexed as a reflection from the (0 0 6), (0 1 5) and (1 0 1 0) planes of Bi_2Te_3 as shown in Fig. 3b–d. The intensity of other small peaks, such as (1 1 0), (0015) and (1 1 1 5), has been improved for stoichiometric Bi_2Te_3 in Fig. 3d, as the hexagonal crystal lattice structure belonging to R-3 m space group of Bi_2Te_3 films is dominant.[3,5]

The crystalline size (D) of the Bi-Te thin films was calculated by the Scherrer equation, using a diffraction peak with (0 1 5) plane, $D = k\lambda/\beta\cos\theta$, where k is the constant usually taken as 0.9, λ is the wavelength of x-ray radiation (0.154056 nm), β is the full width at half maximum (FWHM), and θ is the diffraction angle.[17] The crystalline size of the films at 54 at.%Te, 57 at.%Te and 60 at.%Te were equal to 14 nm, 10 nm and 16 nm, respectively, shown in Fig. 3b, c and d. It was found that the crystalline size of the thin film at 54 at.%Te was higher than the thin film at 57 at.%Te, due to the thin films that were deposited at the Ar flow rates of 103.5 sccm and an annealing temperature of 334°C and

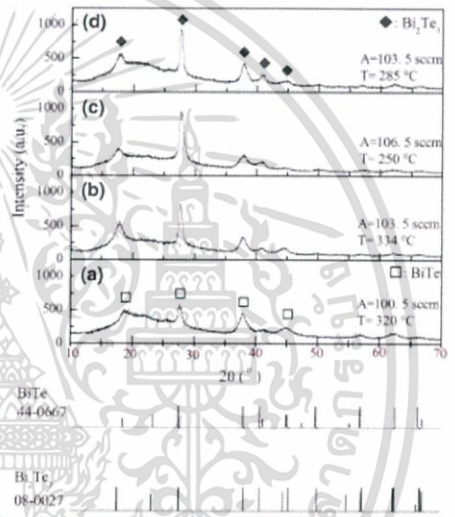

Fig. 3. XRD patterns of the Bi-Te thin films at different Te content: (a) 49 at.%Te, (b) 54 at.%Te, (c) 57 at.%Te and (d) 60 at.%Te.

deposited at the Ar flow rates of 106.5 sccm and annealing temperature of 250°C. Generally, when the flow rate of the gas increases, the density of the gas in the chamber also increases, which results in the mean free path of sputtered particle reduction. The collision probability between sputtered particles and gas molecules was increased, causing the energy of the particles and mobility for surface diffusion to decrease, and this led to a small crystalline size.[18–20] It can be observed that the

crystalline size of the thin film at 54 at.%Te is smaller than the thin film at 60 at.%Te. The thin films were deposited at the same Ar flow rates of 103.5 sccm followed by a different annealing temperature. It was indicated that the crystalline quality of the films was enhanced after annealing at a suitable temperature and the defects reduced after annealing.[5] The parameters of the Ar flow rates and the annealing temperature affect the crystalline size of the thin film, but the crystalline size of the thin film is of little value compared to other research (~100–200 nm).[4,5]

Figure 4 shows the surface microstructure morphology of the Bi-Te thin films. The grain shape of the thin films changes with the Ar flow rate and the annealing temperature increase. The grain shape is consistent with the occurrence of hexagonal crystallite, as shown in Fig. 4c and d, and is consistent with the XRD results. The grain boundary clearly depends on the annealing temperature, and it was found that the increase in annealing temperature contributes to the surface diffusion and agglomeration of the atoms.[3] The thin film was deposited at the Ar flow rate of 103.5 sccm and an annealing temperature of 334°C, and it indicated a smoother surface, as shown in Fig. 4b. This may be due to the partial fusion of some Bi_2Te_3 grains due to the excessive deposition annealing temperature of 300°C.[4]

Thermoelectric Properties at Room Temperature

The Seebeck coefficient (S) and electrical conductivity (σ) of different Te content thin films were measured at room temperature, as shown in Fig. 5a. All the samples have negative values of Seebeck coefficient, indicating that the films were on an n-type semiconductor.[1] The absolute value of the Seebeck coefficient of the thin film at 49 at.%Te is higher than at 54 at.%Te. This may be due to the partial fusion of grain size at a high annealing temperature, which agrees with the FE-SEM results. After that, the absolute value of the Seebeck coefficient increases from 53 to 95 μV/K, whereas electrical conductivity decreases from 4.5×10^4 to 2.1×10^4 S/m, along with the Te content increasing to 3.1×10^4 S/m for the stoichiometric film. The electrical conductivity of thin films increases due to the crystalline size of the thin film at 60 at.%Te, higher than the thin film at 57 at.%Te; the density of defects in polycrystalline films reduced the effect due to the decrease scattering in the films. However, it is well known that the stoichiometric Bi_2Te_3 thin

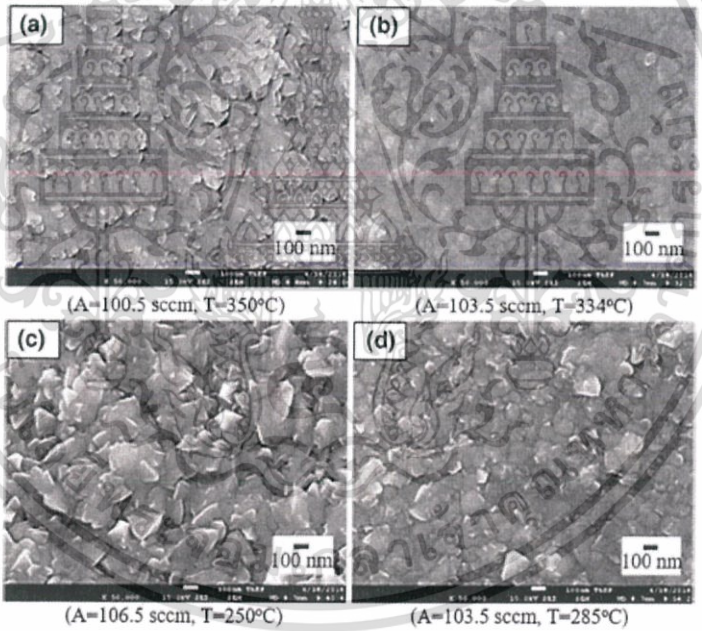

Fig. 4. Top view FE-SEM images of the Bi-Te thin films at different Te content: (a) 49 at.%Te, (b) 54 at.%Te, (c) 57 at.%Te and (d) 60 at.%Te.

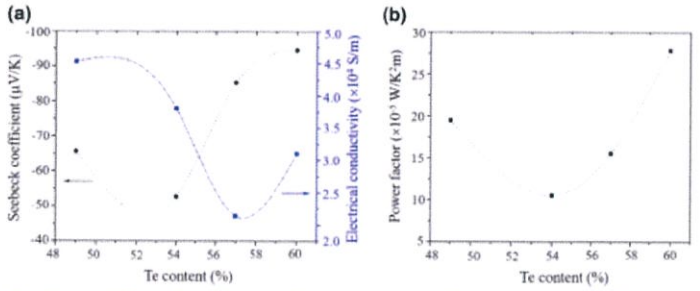

Fig. 5. The effect of Te content on (a) Seebeck coefficient and electrical conductivity, (b) power factor of the Bi-Te thin film at room temperature.

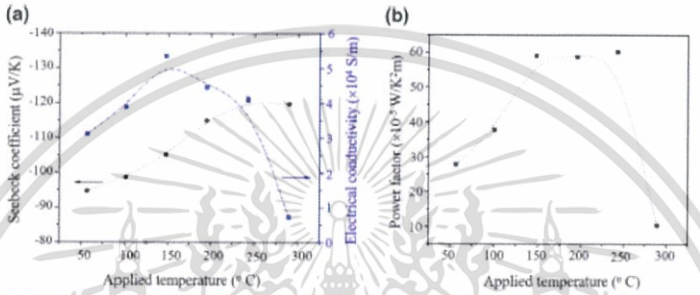

Fig. 6. The effect of applied temperature on (a) Seebeck coefficient and electrical conductivity, (b) power factor of the stoichiometric Bi_2Te_3 thin film.

films have high electron mobility and a high Seebeck coefficient (as already noted). In this work, stoichiometric thin films can be obtained, but their thermoelectric properties are restricted, which might be due to the fact that the polycrystalline size of thin films is quite small.

Figure 5b shows the effect of Te content on the power factors ($S^2\sigma$) of Bi-Te thin films. The maximum power factor was obtained at 28×10^{-5} W/K^{2}m for stoichiometric film. Figure 6 shows the effect of the annealing temperature on the Seebeck coefficient, electrical conductivity and power factor of stoichiometric Bi_2Te_3 thin films in the range from 50°C to 300°C. As shown in Fig. 6a, the absolute value of the Seebeck coefficient increases as the applied temperature increases. The maximum absolute value of the Seebeck coefficient, 121 μV/K, is achieved with the applied temperature of 243°C. When the applied temperature is above 150°C, the electrical conductivity of the film decreases with the increase in temperature, because it will absorb the oxygen in the high-temperature atmosphere of thin films.[5] The maximum power factor of 61×10^{-5} W/K^{2}m is obtained at the temperature of 243°C, as shown in Fig. 6b.

CONCLUSION

In this study, the effect of the argon gas flow rate and the annealing temperature on the [Bi]:[Te] content was analyzed by RSM. These results have indicated that RSM has been used to optimize deposition conditions and predict the value of response ([Bi]:[Te] content) of thin films. The quadratic model which has been developed from the optimization study is accurate in its [Bi]:[Te] content prediction from the relationship equation.

$$\text{Te content} = -4387.27383 + 81.31007A + 1.30610T - 2.35714 \times 10^{-3}AT - 0.38426A^2 - 1.90888 \times 10^{-3}T^2$$

The model determines that optimized deposition conditions can be achieved for stoichiometric Bi_2Te_3 thin films, such as at the Ar flow rates of 103.5 sccm followed by an annealing temperature of 285°C. The XRD and FE-SEM results indicate that a stoichiometric Bi_2Te_3 thin film with improved crystalline quality was achieved. The maximum Seebeck coefficient and the power factor of the thin films

measured at room temperature achieved $-95\ \mu V/K$ and $28 \times 10^{-5}\ W/K^2m$, respectively. Less electrical conductivity is $3.1 \times 10^4\ S/m$, dependent on the crystalline quality of the thin films. This might be caused the crystal defects from the poor crystalline quality at room temperature. The influence of the post-annealing temperature on the thermoelectric properties of stoichiometric Bi_2Te_3 thin film shows that the absolute values of the Seebeck coefficient, the electrical conductivity and the power factor increase as the temperature increases. At the annealing temperature of 243°C, the maximum power factor of $61 \times 10^{-5}\ W/K^2m$ was obtained. Although stoichiometric thin films can be obtained, their thermoelectric properties are restricted, possibly due to the polycrystalline size of thin films being quite small. Improvement in the thermoelectric performance is expected to be achieved with stoichiometry and a high polycrystalline size of thin films by additionally controlling various sputtering parameters, such as the temperature of substrate and the annealing duration.

ACKNOWLEDGEMENT

The author would like to acknowledge the Faculty of Science, King Mongkut's Institute of Technology Ladkrabang for financial support. The author would like to thank the College of Advanced Manufacturing Innovation, King Mongkut's Institute of Technology Ladkrabang for measuring equipment.

REFERENCES

1. H.J. Lee, S. Hyun, H.S. Park, and S.W. Han, *Microelectron. Eng.* 88, 593 (2011).
2. H.J. Lee, H.S. Park, S.W. Han, and J.Y. Kim, *Thermochim. Acta* 542, 57 (2012).
3. H. Huang, L. Wei-ling, and T. Shan-tung, *Thin Solid Films* 517, 3731 (2009).
4. X. Wang, H. He, N. Wang, and L. Miao, *Appl. Surf. Sci.* 276, 539 (2013).
5. C. Zhao-kun, F. Ping, Z. Zhuang-hao, L. Peng-juan, C. Tian-bao, C. Xing-min, L. Jing-ting, L. Guang-xing, and Z. Dong-ping, *Appl. Surf. Sci.* 280, 225 (2013).
6. K. Dong-Ho, E. Byon, L. Gun-Hwan, and S. Cho, *Thin Solid Films* 510, 148 (2006).
7. L.M. Goncalves, C. Couto, P. Alpuim, A.G. Rolo, F. Völklein, and J.H. Correia, *Thin Solid Films* 518, 2816 (2010).
8. L.M. Goncalves, P. Alpuim, G. Min, D.M. Rowe, C. Couto, and J.H. Correia, *J. Vac.* 82, 1499 (2008).
9. T. Jun-Ichi and H. Kido, *J. Ceram. Soc. Jpn.* 123, 298 (2015).
10. R.S. Makala, K. Jagannadham, and B.C. Sales, *J. Appl. Phys.* 94, 3907 (2003).
11. A. Dauscher, A. Thomy, and H. Scherrer, *Thin Solid Films* 280, 61 (1996).
12. Y. Deng, L. Hui-min, Y. Wang, Z. Zhi-wei, M. Tan, and C. Jiao-lin, *J. Alloys Compd.* 509, 5683 (2011).
13. J. Wu, W. Jia-Le, L. Min-Hua, L. Jin-Ping, and W. Dong-Zhi, *Bioresour. Technol.* 101, 8936 (2010).
14. M. Ebrahimi, F. Mahboubi, and M.R. Naimi-Jamal, *Tribol. Int.* 91, 23 (2015).
15. I. Noshadi, N.A.S. Amin, and Richard S. Parnas, *J. Fule* 94, 156–164 (2012).
16. F. Gül Boyaci San, I. Isik-Gulsac, and O. Okur, *J. Energy* 55, 1067 (2013).
17. M. Mamunur Rashid, K.H. Cho, and C. Gwiy-Sang, *Appl. Surf. Sci.* 279, 23 (2013).
18. L. Seon-Hong, E. Yamasue, H. Okumura, and K.N. Ishihara, *Appl. Surf. Sci.* 324, 339 (2015).
19. H. Feng-Hao, W. Na-Fu, T. Yu-Zen, C. Ming-Chieh, C. Yu-Song, and H. Mau-Phon, *Appl. Surf. Sci.* 280, 104 (2013).
20. Y. Sun, E. Zhang, S. Johnsen, M. Sillassen, P. Sun, F. Steglich, J. Bøttiger, and B.B. Iversen, *Thin Solid Films* 519, 5397 (2011).

Journal of ELECTRONIC MATERIALS, Vol. 46, No. 11, 2017
DOI: 10.1007/s11664-017-5671-x

[Bi]:[Te] Control, Structural and Thermoelectric Properties of Flexible Bi_xTe_y Thin Films Prepared by RF Magnetron Sputtering at Different Sputtering Pressures

PILAIPON NUTHONGKUM,[1,4] RACHSAK SAKDANUPHAB,[2] MATI HORPRATHUM,[3] and APARPORN SAKULKALAVEK[1]

1.—Faculty of Science, King Mongkut's Institute of Technology Ladkrabang, Chalongkrung Rd., Ladkrabang, Bangkok 10520, Thailand. 2.—College of Advanced Manufacturing Innovation, King Mongkut's Institute of Technology Ladkrabang, Chalongkrung Rd., Ladkrabang, Bangkok 10520, Thailand. 3.—National Electronics and Computer Technology Center, National Science and Technology Development Agency, Pathum Thani 12120, Thailand. 4.—e-mail: miss.pilaipon@gmail.com

In this work, flexible Bi_xTe_y thin films were prepared by radio frequency (RF) magnetron sputtering using a Bi_2Te_3 target on polyimide substrate. The effects of sputtering pressures, which ranged between 0.6 Pa and 1.6 Pa on the [Bi]:[Te] ratio, and structural and thermoelectric properties were investigated. The [Bi]:[Te] ratio of thin film was determined by energy-dispersive spectrometry (EDS). The EDS spectra show the variation of the [Bi]:[Te] ratio as the sputtering pressure is varied. The film deposited at 1.4 Pa almost has a stoichiometric composition. The selective films with different [Bi]:[Te] ratios and sputtering pressures were characterized by their surface morphologies, crystal and chemical structures by field emission scanning electron microscopy (FE-SEM), x-ray diffraction (XRD) and Raman spectroscopy, respectively. Electrical transport properties, including carrier concentration and mobility, were measured by Hall effect measurements. Seebeck coefficients and electrical conductivities were simultaneously measured by a direct current four-terminal method (ZEM-3). The XRD and Raman spectroscopy results show a difference in microstructure between BiTe and Bi_2Te_3 depending on the [Bi]:[Te] ratio. Electrical conductivity and Seebeck coefficient are related to the crystal and chemical structures. The maximum power factor of the Bi_2Te_3 thin film is 9.5×10^{-4} W/K^2 m at room temperature, and it increases to 12.0×10^{-4} W/K^2 m at 195°C.

Key words: Flexible Bi_2Te_3, RF magnetron sputtering, sputtering pressure, thermoelectric

INTRODUCTION

Bismuth telluride (Bi_2Te_3) is a thermoelectric material that has been widely used due to its high dimensionless figure of merit (ZT) value and high performance at room temperature. The ZT value is the thermoelectric conversion efficiency of thermoelectric materials and is defined as $ZT = S^2\sigma T/\kappa$, where S is the Seebeck coefficient, σ is electrical conductivity, κ is thermal conductivity and T is absolute temperature. The ZT value can be increased when improvements are made to low-dimensional thermoelectric materials.[1,2] Thermoelectric thin film is one of the most important low-dimensional thermoelectric materials, and has been prepared using different deposition methods, such as co-evaporation,[3,4] pulsed laser deposition[5] and RF magnetron sputtering.[1,2,6–8] In addition, research on applying thermoelectric thin film onto flexible substrates has attracted increasing

(Received February 1, 2017; accepted June 30, 2017; published online July 18, 2017)

attention because of its application to multiple devices.[3] The RF magnetron sputtering method was selected due to the possibility of large-scale fabrication of high-quality films.[1,2] Bismuth telluride (Bi_2Te_3) thin films normally require a stoichiometric ratio of [Bi] and [Te] for achieving the best thermoelectric performance. Most of research has used co-sputtering and adjusted sputtering powers of Bi and Te targets to control compositions.[2,6–8] Only a small number of works on the control ratio of [Bi] and [Te] using a Bi_2Te_3 target have been reported. In our previous work,[9] we studied the effects of deposition parameters, including Ar gas flow rate (sputtering pressure) and annealing temperature, on Te content. A commercial Bi_2Te_3 target was used. We found that the composition of thin film was affected by controlling both deposition parameters, and the stoichiometric ratio was achieved at an Ar flow rate of 103.5 sccm following by an annealing temperature of 285°C.

In this work, an in-depth investigation was adopted to analyse the effects of sputtering pressures on the chemical composition, structural and thermoelectric properties of Bi-Te thin films. The Bi-Te thin films were deposited on flexible substrates using a Bi_2Te_3 target and RF magnetron sputtering technique with various sputtering pressures (0.6 Pa, 0.8 Pa, 1.0 Pa, 1.2 Pa, 1.4 Pa and 1.6 Pa).

EXPERIMENT

Bismuth telluride (Bi-Te) thin films were deposited onto a polyimide (Kapton®) flexible substrate using an RF magnetron sputtering technique. Polyimide (Kapton®) was selected due to its thermal stability, low thermal conductivity ($0.12\ Wm^{-1}\ K^{-1}$) and low thermal expansion coefficient ($12 \times 10^{-6}\ K^{-1}$) over a wide range of temperatures.[3,4] The polyimide substrates were ultrasonically cleaned in methanol and deionized water for 15 min and dried with N_2 gas. A commercial bismuth telluride (Bi_2Te_3) sputtering target (high purity: 99.9%) was used and the target-substrate distance was maintained at 50 mm. Before deposition, the base pressure of the deposition chamber was below 2.5×10^{-3} Pa, and presputtering was executed for 10 min to remove any contamination from the target surface. The sputtering pressure varied from 0.6 Pa to 1.6 Pa. The thickness of the Bi-Te films was kept at approximately 1.3 μm. The composition and surface microstructure morphology of the Bi-Te thin films were determined by energy-dispersive spectrometry (EDS) and field emission scanning electron microscopy (FE-SEM, JSM-7001F), respectively. The crystalline structure was characterized by x-ray diffraction (XRD, D8 DISCOVER-Bruker AXS) and Raman spectroscopy (Renishaw InVia spectrometer). Mobility and carrier concentration were obtained by the van der Pauw method with a Hall effects measurement system (Ecopia, HMS3000). Finally, the Seebeck coefficient and electrical conductivity were concurrently measured at room temperature and up to 300°C using a ZEM-3 instrument (ULVAC-RIKO).

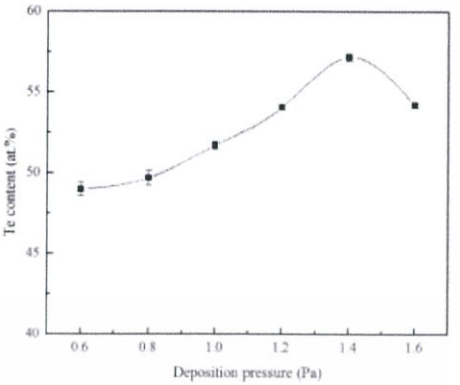

Fig. 1. Te content [atomic percentage (at.%)] of the Bi-Te thin films according to deposition pressure.

RESULTS AND DISCUSSION

Compositional Analysis

The effects of deposition pressure on the Te content of thin films were investigated. Figure 1 shows that the %Te content of thin films under the different sputtering pressures were 0.6 Pa, 0.8 Pa, 1.0 Pa, 1.2 Pa, 1.4 Pa and 1.6 Pa. These average element compositions were measured by EDS in three different areas. It was found that all the deposited thin films were deficient in their Te element. This result indicated that sputtering pressure alone could not control the stoichiometric composition of Bi_2Te_3 thin films. In general, good thermoelectric properties of Bi-Te thin films depend on stoichiometric Bi_2Te_3 thin films ([Bi]:[Te] = 40:60).[2,7]

It can be seen in Fig. 1 that the deposited thin films at 0.6 Pa were non-stoichiometric Bi_2Te_3 thin films, with the chemical composition of Te content lower than 60 at.%. The Te content was poor due to the sputtering yields of Te being lower than Bi,[2,8] as shown in Fig. 2 (A). When the sputtering pressures increased from 0.8 Pa to 1.4 Pa, the Te content of thin films increased from 49 to 57 at.%. The increase of Te content due to the density of the sputter gas (Ar) also increases the collision probability between sputtered particles.[10] In this work, the sputtering target composition consisted of bismuth (Bi) and tellurium (Te) elements as Bi_2Te_3. Typically, the atomic mass of the Bi element is larger than Te. When the sputter gas pressure increases, the sputter gas ions (Ar^+) are reflected as neutral atoms.[10]

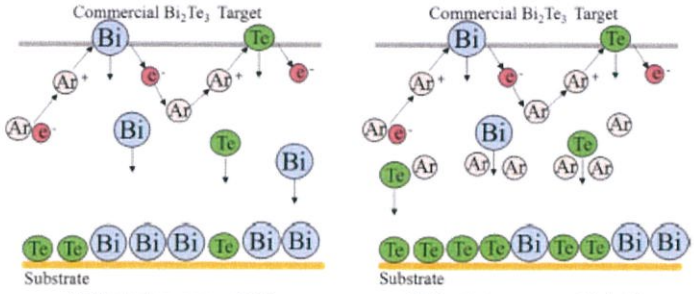

Fig. 2. Schematic representation of deposition effects on Te content: (a) the sputtering yields of Te being lower than Bi, (b) Te content increases with increasing the density of the sputter gas (Ar).

Thus, the Bi elements were obstructed by the Ar gas increase, thereby affecting the composition and film structure as shown in Fig. 2 (B). However, the Te content of the thin film decreased at 54 at.% Te as the sputtering pressure increased from 1.6 Pa. The decrease of Te content may be because both Bi and Te elements were obstructed when Ar gas pressure is relatively high.

Surface Morphology and Crystallinity

Three selected samples with various Te content and Ar gas pressures: (A) 49 at.% Te (P = 0.8 Pa), (B) 54 at.% Te (P = 1.6 Pa) and (C) 57 at.% Te (P = 1.4 Pa) were measured for surface morphology and crystal and chemical structures using FE-SEM, XRD and Raman spectroscopy.

Figure 3 shows the surface morphology of Bi-Te thin films from various sputtering pressures and Te content. As shown in Fig. 3a, the Bi-Te thin film with the sputtering pressure of 0.8 Pa has a smooth surface. As the sputtering pressure increases, it was found that grain boundary clearly affects the agglomeration of the atoms and the surface diffusion of the atoms, as shown in Fig. 3b and c. Normally, the collision probability between sputtered particles and gas particles is intensified while the increase of sputtering pressure causes the mean free path of sputtered particle to be reduced. Particles with lower kinetic energy have insufficient surface mobility to aggregate and grow.[10,11]

Figure 4a shows the XRD patterns of the Bi-Te films with various sputtering pressures and Te contents. As seen from Fig. 4a (A), the thin film has a peak corresponding to the (014), (108) and (0012) planes in the BiTe phase (JCPDS card 44-0667), located at 27.568°, 38.040° and 45.285°. The peak positions clearly change from the BiTe phase to the peak of (015), (1010) and (110) planes in Bi_2Te_3 phase (JCPDS card 72-2036), located at 27.663°, 37.822° and 40.827°, as shown in Fig. 4a (C), when the Te content of the film increases from 49 to 57 at.%. It was found that the intensities of other small peaks improve, such as (0015) and (205), located at 45.563° and 50.039°, when the Te content of the film increased to a nearly stoichiometric ratio.

The crystalline size (D) of thin films grown on flexible substrates was calculated by the Scherrer's formula as shown in Eq. 1,

$$D = k\lambda/\beta\cos\theta \quad (1)$$

where k is the constant usually taken as 0.94, λ is the x-ray radiation wavelength (0.154056 nm), β is the full width at half maximum (FWHM) and θ is the diffraction angle. Microstrain developed in the film, which is determined from disarrangement of lattice during their deposition and depends on the deposition parameters.[12] The dislocation density is the density of imperfections in the crystal during the growth of film.[12,13] The microstrain (ε) and the dislocation density (ρ) were evaluated using the Eqs. 2 and 3, respectively.

$$\varepsilon = (\beta\cos\theta)/4 \quad (2)$$

$$\rho = 1/D^2 \quad (3)$$

The crystalline size (D), microstrain (ε) and dislocation density (ρ) of the Bi-Te films have been calculated using the preferred orientation of the XRD peak, and the values are given in Table I. The crystalline size increased from 16.13 nm to 20.08 nm as the sputtering pressure was increased from 0.8 Pa to 1.4 Pa. Correspondingly, the strain of the Bi-Te films decreases from 2.24×10^{-3} to 1.80×10^{-3} lines^{-2} m^{-4}, and the dislocation density decreases from 3.84×10^{15} to 2.47×10^{15} lines/m^2. The decrease of microstrain and dislocation density from increasing the sputtering pressure led to a decrease in the concentration of lattice imperfections. As sputtering pressure increased from 1.4 Pa to 1.6 Pa, the crystalline size of the Bi-Te thin film decreased, while the microstrain and dislocation density increased. We suggest that sputtering pressure was increased excessively; it

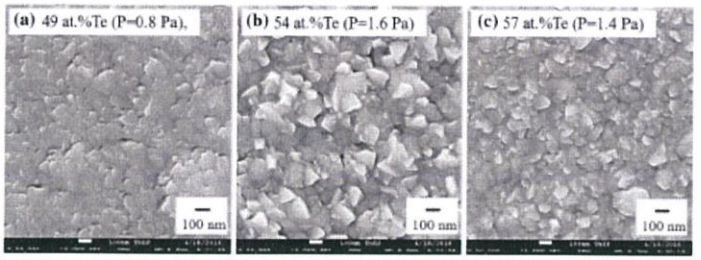

Fig. 3. Top view FE-SEM images of the Bi-Te thin films at various Te contents and Ar gas pressures: (a) 49 at.% Te [pressure (P) = 0.8 Pa], (b) 54 at.% Te (P = 1.6 Pa) and (c) 57 at.% Te (P = 1.4 Pa).

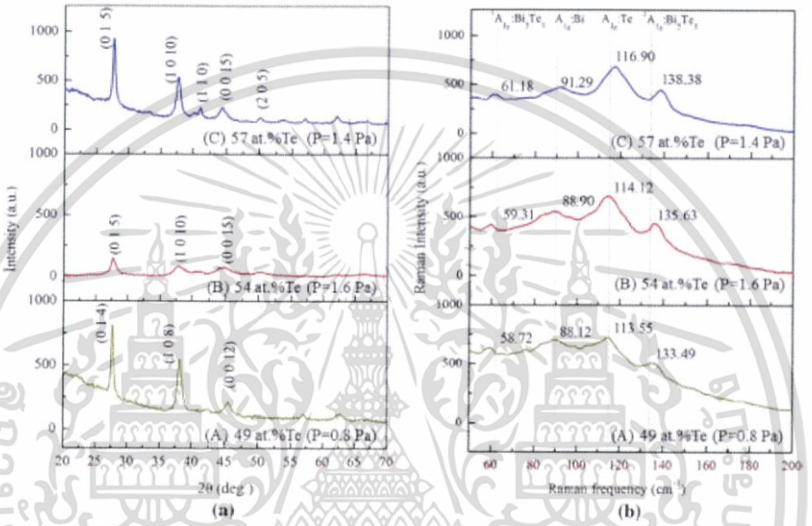

Fig. 4. XRD patterns (a) and Raman spectra (b) of the Bi-Te thin films according at various Te content and Ar gas pressure: (A) 49 at.% Te (P = 0.8 Pa), (B) 54 at.% Te (P = 1.6 Pa) and (C) 57 at.% Te (P = 1.4 Pa).

affected the formation of the crystal structure of the Bi-Te thin film. With a relatively high sputtering pressure, a higher flux of reflected neutrals will obstruct the growing film. From the XRD, EDS and the FE-SEM results, appropriate sputtering pressure influences the Te content and crystal quality of the Bi-Te thin films.

Raman spectra results of the Bi-Te films with various Te contents are shown in Fig. 4b. Bi_2Te_3 has a rhombohedral unit cell belonging to the $D^5_{3d} - R3m$ space group. There are four Raman active modes and the Bi_2Te_3 vibration patterns are predicted at the wave numbers 36.5 cm^{-1}, 62.0 cm^{-1}, 102.3 cm^{-1} and 134.0 cm^{-1}, respectively.[3,14] The peaks analogous to some of the vibrational modes of different phases could have wave numbers too close to each other to be discerned. The observed Raman spectra of Bi_2Te_3 films are $^1A_{1g}$ = 62.0 cm^{-1} and $^2A_{1g}$ = 134.0 cm^{-1}, and when the Te content of the film increased, the Raman spectrum showed an obvious blue shift from 58.72 cm^{-1} to 61.18 cm^{-1} for the $^1A_{1g}$ mode and an obvious blue shift from 133.49 cm^{-1} to 138.38 cm^{-1} for the $^2A_{1g}$ mode. The Raman spectra of films gave clear and strong Te peaks at A_{1g} = 116 cm^{-1} and E_g = 136 cm^{-1}[14] when the Te content of the film increased. Therefore, increasing the Te content of film has a significant effect on these two modes ($^1A_{1g}$, $^2A_{1g}$), thereby inducing a frequency shift. The relative vibration directions for Bi and Te are different for $^1A_{1g}$ and $^2A_{1g}$, which leads to the respective blue shift

Table I. Analysis of results of the Bi-Te thin films from XRD patterns

Film	Te content (at.%)	Sputtering pressure (Pa)	2θ (°)	Crystalline size [D (nm)]	Microstrain [ε (×10^{-3} lines^{-2}/m^4)]	Dislocation density [ρ (×10^{15}lines/m^2)]
(A)	49	0.8	27.57	16.13	2.24	3.84
(B)	54	1.6	27.66	8.81	4.11	12.87
(C)	57	1.4	27.66	20.08	1.80	2.47

Table II. Summary of the electrical and thermoelectric properties of the Bi-Te thin films at room temperature

Film	Te content (at.%)	Carrier concentration (×10^{20} cm^{-3})	Carrier mobility (cm^2/Vs)	Electrical conductivity (×10^4 S/m)	Seebeck coefficient (μV/K)	Power factor (×10^{-4} W/K^2 m)
(A)	49	−10.4	9.50	15.8	−34.6	1.89
(B)	54	−8.93	3.93	5.61	−58.2	1.90
(C)	57	−6.26	6.73	6.74	−118.6	9.49

of the Raman frequencies, which corresponds to the XRD results when the Te content of the film increases to change the structure from a BiTe structure to a Bi_2Te_3 structure.

Electrical and Thermoelectric Properties

The carrier concentration and mobility, electrical resistivity, Seebeck coefficient and power factor (*PF*) of different Te content thin films were measured at room temperature and are summarized in Table II. *PF* is a property of material that describes its ability to generate more energy from a given temperature difference. It can be calculated by using the Seebeck coefficient and electrical conductivity ($S^2\sigma$) at a given temperature.

All of the Bi-Te thin films have a negative Seebeck coefficient, indicating that the thin films were affirmed to be *n*-type semiconductors. The carrier concentration decreases from 10.40×10^{20} cm^{-3} to 6.26×10^{20} cm^{-3} with increasing Te content. Therefore, stoichiometry plays a vital role in reducing the carrier concentration of the Bi_2Te_3 films. The absolute value of the Seebeck coefficient increases from 35 μV/K to 119 μV/K and, according to theory, the Seebeck coefficient is inversely related to the carrier concentration, given by equation[15]:

$$S(T) = \frac{\pi^2 k_B^2 T}{3e}\left[\frac{N(E)}{n} + \left(\frac{\partial \ln \mu(E)}{\partial E}\right)_{E=E_F}\right] \quad (4)$$

where k_B is Boltzmann's constant, e is the electron charge, $N(E)$ is the density of state, n is the carrier concentration and T is the measurement temperature.[15,16] In this work, the carrier concentration of the BiTe structure (49 at.% Te) was greater than in the Bi_2Te_3 structure (57% at. Te), and this result corresponds to research of Caha et al.[17] who revealed that the free carrier concentration in BiTe is about one order of magnitude larger than Bi_2Te_3. The carrier mobility of 9.50 cm^2 V^{-1} s^{-1} occurs at film (A), decreases to 3.93 cm^2 V^{-1} s^{-1} at film (B) and changes to 6.73 cm^2 V^{-1} s^{-1} at film (C). According to the XRD analyses, we observed a decrease of the carrier mobility of the Bi-Te thin films at 54 at.% Te as result of poor crystalline quality of the Bi-Te films, as shown in the XRD results. Generally, carrier mobility in the thin film is limited, owing to the scattering mechanisms at the grain boundaries and in-grain scattering processes.[14,18,19] The FE-SEM results showed that the large grain boundaries of the Bi-Te thin films at 54 at.% Te affected the motion of charge carriers due to grain boundary behaviour being similar to barriers to charge carrier.[1] It can be deduced that the reduced carrier mobility of Bi-Te thin films depends on grain size and grain boundary. In general, electrical conductivity (σ) depends on both carrier concentration (n) and mobility (μ), as shown in Eq. 5

$$\sigma = n\mu q \quad (5)$$

The highest electrical conductivity of film (A) 49 at.% Te (P = 0.8 Pa) was obtained because the film has both the highest carrier concentration and the highest mobility. In addition, the electrical conductivity decreases when the Te content of the thin films increases, corresponding to the work of Lee et al.[6] Compared to other previous works, the

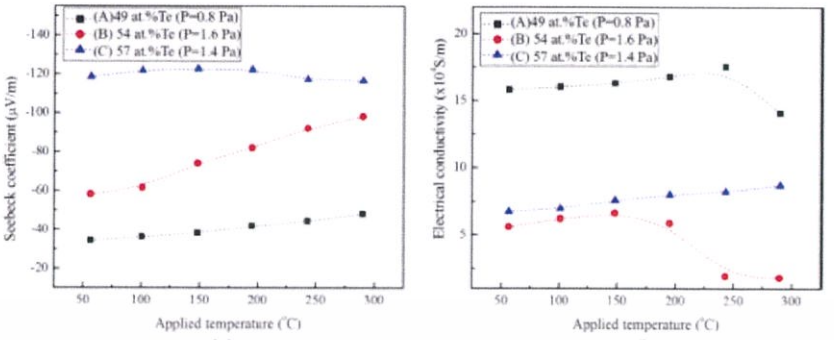

Fig. 5. Effect of applied temperature on (a) Seebeck coefficient, (b) electrical conductivity of Bi-Te thin film according to different Te contents and Ar gas pressures.

carrier concentration was the same order of magnitude as found in the works of Yuan et al.[1] (-9.5×10^{20} cm^{-3}) and Lee et al.[6] (-3.91×10^{20} cm^{-3}). However, the mobility was lower than Yuan et al.[1] (12.1 cm^2/Vs), who prepared the Bi-Te thin films with substrate heating at 350°C. It may indicate improvement of crystallization of the films.

In this work, the highest power factor at room temperature was approximately 9.49×10^{-4} W/K^2m for the Bi-Te thin film at 57 at.% Te without the annealing process. Yuan et al.[1] reported that the Bi-Te thin films were fabricated by RF magnetron sputtering with oriented layered structure. The power factor at room temperature was obtained at 8.8×10^{-4} W/K^2 m. Cai et al.[2] reported that the best Bi_2Te_3 thin film was prepared by a cosputtering technique with postannealing. The *n*-type Bi_2Te_3 thin film had high a power factor of 8.21×10^{-4} W/K^2m with the annealing temperature of 450°C. These results indicated that the value of power factor was close to previous reports. However, the power factor of bismuth telluride thin film was lower than that of bulk material. Shanyu et al.[19] reported the high-performance $Bi_2(Te_{1-x}\ Se_x)_3$ materials using a commercial zone-melting technique, with a Seebeck coefficient of -209 μV/K and highest power factor of $\sim 40 \times 10^{-4}$ W/K^2 m at room temperature.

Figure 5a shows the effect of applied temperature (ranging from 50°C to 300°C) on the Seebeck coefficient of different Te content thin films. The maximum Seebeck coefficient absolute value, 122 μV/K for the Bi-Te thin film at 57 at.% Te (nearly stoichiometric Bi_2Te_3), is obtained with the applied temperature of 195°C. According to Eq. 4, *S* directly depends on the measuring temperature (*T*) and inversely depends on the carrier concentration (*n*). Nevertheless, the Seebeck coefficient depends on film thickness[20] and dislocation density.[21] In this work, the thickness of films does not significantly affect the Seebeck coefficient due to all of the Bi-Te thin films being approximately 1.3 μm. Watling et al.[21] investigated the effect of dislocation density on the Seebeck coefficient, and the results indicated that *S* directly depends on dislocation density. Reconsidering Table I, dislocation density values of films (A) 49 at.%, (B) 54 at.% and (C) 57 at.% were 3.84×10^{15} lines/m^2, 12.84×10^{15} lines/m^2 and 2.47×10^{15} lines/m^2, respectively. Although the dislocation density value of film (A) 49 at.% is close to that of film (C) 57 at.%, the carrier concentration of film (A) 49 at.% is higher than that of film (C) 57 at.% by about two times, resulting in Seebeck coefficients of film (A) 49 at.% being significantly different from those of film (C) 57 at.%. For film (B) 54 at.%, the dislocation density is the highest, while its Seebeck coefficient is lower than that of film (C) 57 at.%. This result indicates that the carrier concentration affects the Seebeck coefficient more than the dislocation density.

Figure 5b shows the effect of the applied temperature on the electrical conductivity of all samples. It was found that the electrical conductivity increases when the applied temperature is below 195°C, as a result of semiconductor behaviour increasing when temperature increases.[2] The electrical conductivity of the film decreases when the applied temperature is above 195°C. We suggest that the Bi-Te thin film absorbs oxygen at higher applied temperature, corresponding to Cai et al.[2]

Figure 6 shows the *PF* of bismuth telluride films deposited at various conditions. The temperature dependence of *PF* is strongly dominated by the Te content, leading to the highest value of 12.0×10^{-4} W/K^2 m at 195°C for the Bi-Te thin film at 57 at.% Te, nearly stoichiometric Bi_2Te_3.

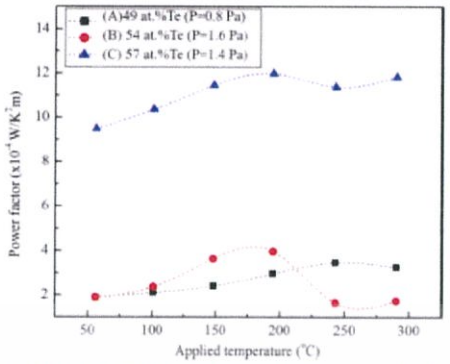

Fig. 6. Effect of applied temperature on the power factor of Bi-Te thin films deposited with different Te contents and Ar gas pressures.

CONCLUSIONS

Flexible Bi-Te thin films were fabricated using an RF magnetron sputtering technique and controlled sputtering parameters using a Bi_2Te_3 target. The effects of various sputtering pressures were significant for controlling compositions and improving thermoelectric properties of Bi-Te thin films. The Te content and the crystal structure of Bi-Te thin film increased with increased sputtering pressure, and the thermoelectric performance was excellent at 1.4 Pa for nearly stoichiometric Bi_2Te_3. The maximum power factor, 12.0×10^{-4} W/K^2 m for the Bi-Te thin film at 57 at.% Te, was obtained with the applied temperature of 195°C without an annealing process.

ACKNOWLEDGEMENTS

The author would like to acknowledge the Faculty of Science, King Mongkut's Institute of Technology Ladkrabang for financial support.

REFERENCES

1. Y. Deng, H.-M. Liang, Y. Wang, Z.-W. Zhang, M. Tan, and J.-L. Cui, *J. Alloys Compd.* 509, 5683 (2011).
2. C. Zhao-kun, F. Ping, Z. Zhuang-hao, L. Peng-juan, C. Tian-bao, C. Xing-min, L. Jing-ting, L. Guang-xing, and Z. Dong-ping, *Appl. Surf. Sci.* 280, 225 (2013).
3. L.M. Goncalves, C. Couto, P. Alpuim, A.G. Rolo, F. Völklein, and J.H. Correia, *Thin Solid Films* 518, 2816 (2010).
4. L.M. Goncalves, P. Alpuim, G. Min, D.M. Rowe, C. Couto, and J.H. Correia, *J. Vac.* 82, 1499 (2008).
5. A. LiBassi, A. Bailini, C.S. Casari, F. Donati, A. Mantegazza, M. Passoni, V. Russo, and C.E. Bottani, *J. Appl. Phys.* 105, 124307 (2009).
6. H.J. Lee, S. Hyun, H.S. Park, and S.W. Han, *Microelectron. Eng.* 88, 593 (2011).
7. X. Wang, H. He, N. Wang, and L. Miao, *Appl. Surf. Sci.* 276, 539 (2013).
8. Z.H. Zheng, P. Fan, T.B. Chen, Z.K. Cai, P.J. Liu, G.X. Liang, D.P. Zhang, and X.M. Cai, *Thin Solid Films* 520, 5245 (2012).
9. P. Nuthongkum, A. Sakulkalavek, and R. Sakdanuphab, *J. Electron. Mater.* 46, 2900 (2017).
10. Y. Sun, E. Zhang, S. Johnsen, M. Sillassen, P. Sun, F. Steglich, J. Bottiger, and B.B. Iversen, *Thin Solid Films* 519, 5397 (2011).
11. H. Feng-Hao, W. Na-Fu, T. Yu-Zen, C. Ming-Chieh, C. Yu-Song, and H. Mau-Phon, *Appl. Surf. Sci.* 280, 104 (2013).
12. R. Sathyamoorthy and J. Dheepa, *J. Phys. Chem. Solids* 68, 111 (2007).
13. T. Khumtong, P. Sukwisute, A. Sakulkalavek, and R. Sakdanuphab, *J. Electron. Mater.* 46, 3166 (2017).
14. V. Russo, A. Bailini, M. Zamboni, M. Passoni, C. Conti, C.S. Casari, A. LiBassi, and C.E. Bottani, *J. Raman Spectrosc.* 39, 205 (2008).
15. A. Sakulkalavek and R. Sakdanuphab, *Mat. Sci. Semicon. Proc.* 56, 313 (2016).
16. M. Cutler and N.F. Mott, *Phys. Rev.* 181, 1336 (1969).
17. O. Caha, A. Dubroka, J. Humlíček, V. Holý, H. Steiner, M. Ul-Hassan, J. Sánchez-Barriga, O. Rader, T.N. Stanislavchuk, A.A. Sirenko, G. Bauer, and G. Springholz, *Cryst. Growth Des.* 13, 3365 (2013).
18. H. Yue, A. Wu, Y. Feng, X. Zhang, and T. Li, *Thin Solid Films* 519, 5577 (2011).
19. S. Wang, G. Tan, W. Xie, G. Zheng, H. Li, J. Yang, and X. Tang, *J. Mater. Chem.* 22, 20943 (2012).
20. Z. Zeng, P. Yang, and Z. Hu, *Appl. Surf. Sci.* 268, 472 (2013).
21. J.R. Watling and D.J. Paul, *J. Appl. Phys.* 110, 114508 (2011).